STATE UNIVERSITY OF PONTA GROSSA
POSTGRADUATE PROGRAM IN SANITARY AND ENVIRONMENTAL ENGINEERING

CAROLINA KRATSCH SGARBOSSA

USE OF SOLAR ENERGY FOR ELECTRIC POWER GENERATION AND WATER HEATING IN SUSTAINABLE BUILDINGS IN THE STATE OF PARANA-BRAZIL CONSIDERING FUTURE SCENARIOS OF GLOBAL CLIMATE CHANGE

PONTA GROSSA
2019

CAROLINA KRATSCH SGARBOSSA

USE OF SOLAR ENERGY FOR ELECTRIC POWER GENERATION AND WATER HEATING IN SUSTAINABLE BUILDINGS IN THE STATE OF PARANA-BRAZIL CONSIDERING FUTURE SCENARIOS OF GLOBAL CLIMATE CHANGE

Thesis presented to the Postgraduate Program in Sanitary and Environmental Engineering of the State University of Ponta Grossa, as a requirement to obtain Master's degree.

Supervisor: Dr. Jorim Sousa das Virgens Filho

PONTA GROSSA

2019

Sgarbossa, Carolina Kratsch
S523 Use of solar energy for electric power generation and water heating in sustainable buildings in the state of Parana-Brazil considering future scenarios of global climate change / Carolina Kratsch Sgarbossa. Ponta Grossa, 2019.
113 f.

Thesis (Postgraduate Program in Sanitary and Environmental Engineering), State University of Ponta Grossa.

Supervisor: Prof. Dr. Jorim Sousa das Virgens Filho.

1. Global solar radiation. 2. Solar energy. 3. Climate changes. I. Virgens Filho, Jorim Sousa. II. State University of Ponta Grossa – Postgraduate Program in Sanitary and Environmental Engineering. IV. T.

CDD : 621.473

Ficha catalográfica elaborada por Maria Luzia F. Bertholino dos Santos– CRB9/986

CERTIFICADO DE APROVAÇÃO

Título da Dissertação: **"Use of Solar Energy for Electric Power Generation and Water Heating in Sustainable Buildings in the State of Parana-Brazil Considering Future Scenarios of Global Climate Change"**

Nome: **Carolina Kratsch Sgarbossa**

Orientador: **Prof. Dr. Jorim Sousa das Virgens Filho**

Aprovado pela Comissão Examinadora:

Prof. Dr. Jorim Sousa das Virgens Filho
Universidade Estadual de Ponta Grossa - UEPG

Prof. Dr. Emad Habib
University of Louisiana at Lafayette

Prof. Dr. Gustavo Castilho Beruski
Faculdade de Ensino Superior Santa Bárbara - FAESB

Ponta Grossa, 19 de março de 2019.

A cloud does not know why it moves in such a direction and at such a speed.
It feels only an impulse that leads her to this or that direction.
But the sky knows the motifs and the designs behind all the clouds, and you will also know, when you rise up enough to see beyond the horizons.
(Richard Bach)

ABSTRACT

The Sun is the primordial and indispensable component for the maintenance of life on Earth because it is the main source of energy of the planet. Considering the geographical position of Brazil and its mainland, Brazilian cities present great potential for the use of solar energy as a source of renewable energy, which provides a reduction of impacts to the environment caused by the exploitation of natural resources. Buildings are responsible for half of the country's electricity consumption and in addition, regional changes caused by climate change can also influence the generation and final energy consumption, since most of the risks and consequences of these changes are concentrated in urban areas. With this prelude as a motivation, this research aimed to estimate the potential of photovoltaic solar energy and solar energy for heating water in buildings in the State of Paraná, considering scenarios of climate change. Thus, four empirical models of solar radiation estimation were evaluated from air temperature data. Since the performance of the models was evaluated through the appropriate statistical indices, two of these presented the best results for localities in Paraná. In order to estimate the electric energy produced by the photovoltaic system, as well as by the solar heating system for a hypothetical single family dwelling in present and future conditions, impacted by climatic changes, daily climatological data of global solar radiation and air temperature were used, as well as modeling for systems. For the simulation of future climate scenarios, the model PGECLIMA_R was used, which is a computational tool for stochastic generation of daily climate data. In the evaluation of the results, statistical methods such as Analysis of Variance (ANOVA) were used, with comparison of means (Tukey test) and Kruskal-Wallis test, multiple comparison by Dunn method. The results pointed to annual indices of 98% service of the photovoltaic system scaled in all the analyzed locations. In the evaluation of the performance of the solar heating system, which estimates by the F-Chart method the annual solar fraction or percentage of energy demand that is covered by the system, based on the monthly average solar radiation incidence, it was verified that all localities present annual values of solar fraction between 82.4% and 129.8%, values considered very good for this purpose. Therefore, in view of the results found, it was concluded that the State of Paraná has favorable climatic conditions for the installation of solar energy systems, both photovoltaic and solar water heating, even taking into account possible changes in the the end of the 21st century.

Key-words: Global solar radiation; Solar energy; Climate changes.

RESUMO

O Sol é o componente primordial e imprescindível para a manutenção da vida na Terra, pois é a principal fonte de energia do planeta. Tendo em vista a posição geográfica do Brasil e sua continentalidade, as cidades brasileiras apresentam um grande potencial para a utilização da energia solar, como fonte de energia renovável, que proporciona reduções de impactos ao meio ambiente, ocasionados pela exploração de recursos naturais. As edificações são responsáveis por metade do consumo de energia elétrica país. Além disso, as alterações regionais provocadas pelas mudanças climáticas também podem influenciar na geração e no consumo final de energia, visto que a maior parte dos riscos e consequências destas mudanças estão concentrados em áreas urbanas. Tendo este prelúdio como motivação, esta pesquisa teve como objetivo geral estimar o potencial de energia solar fotovoltaica e de energia solar para aquecimento de água em edificações, no Estado do Paraná, considerando cenários de mudanças climáticas. Para tanto, foram avaliados quatro modelos empíricos de estimativa de radiação solar a partir de dados de temperatura do ar. Uma vez que, o desempenho dos modelos foi avaliado por meio dos índices estatísticos apropriados, constatou-se que dois desses apresentaram os melhores resultados para localidades paranaenses. Para estimar a energia elétrica produzida pelo sistema fotovoltaico, bem como pelo sistema de aquecimento solar para uma residência unifamiliar hipotética em condições atuais e futuras, impactadas por mudanças climáticas, foram utilizados dados climatológicos diários de radiação solar global e de temperatura do ar, bem como modelagens específicas para dimensionamento dos sistemas. Para a simulação dos cenários climáticos futuros foi utilizado o modelo PGECLIMA_R que é uma ferramenta computacional para geração estocástica de dados meteorológicos diários. Na avaliação dos resultados obtidos foram utilizados métodos estatísticos como Análise de Variância (ANOVA), com comparação de médias (teste de Tukey) e teste de Kruskal-Wwallis, comparação múltipla pelo método de Dunn. Os resultados apontaram para índices anuais de 98% de atendimento do sistema fotovoltaico dimensionado em todas as localidades analisadas. Na avaliação do desempenho do sistema de aquecimento solar, o qual estima pelo método F-Chart a fração solar anual ou porcentagem da demanda energética que é coberta pelo sistema, com base na média mensal de incidência de radiação solar, verificou-se que todas as localidades apresentam valores anuais de fração solar entre 82,4% e 129,8%, valores estes considerados muito bons para esta finalidade. Portanto, diante dos resultados encontrados, chegou-se à conclusão que o Estado do Paraná possui condições climáticas favoráveis para a instalação dos sistemas de aproveitamento de energia solar, tanto fotovoltaico quanto para aquecimento solar de água, mesmo levando-se em consideração possíveis alterações do clima até o final do século XXI.

Palavras-chave: Radiação solar global; Energia solar; Mudanças climáticas.

LIST OF FIGURES

LIST OF TABELS

SUMMARY

INTRODUCTION

Energy is essential for all living beings, and the Sun is the fundamental element for life on Earth because it is the main source of energy on the planet, besides being responsible for the origin of life. The search for renewable energy sources in order to reduce the impacts to the environment through the exploration of natural resources that can be reestablished in a human time scale is emphasized. Among the most widespread sources are wind, biomass, oceanic and solar energy.

The buildings are responsible for half of the electricity consumption in Brazil. Thus, using the solar resource is to exploit the energy of the environment not only for the nutritional interest of the species, but also to look for technological applications for human life that can be integrated to the buildings with the purpose of reducing the electricity generation of the network public.

In addition, regional changes caused by climate change can also influence the generation and final consumption of energy, since most of the risks of these changes are concentrated in urban areas. With economic and population growth, combined with the heat of climate change, consider increasing the use of energy to cool urban environments, as the increase in temperature will directly affect the thermal comfort of buildings.

Within this context, it is expected that the measures that impose on urban builders technologies that exploit the solar resource in the generation of electric energy and in the heating of water, namely photovoltaic solar energy and photothermal solar energy will be broadly extended.

In view of the above, this research aimed to estimate the potential of photovoltaic solar energy and solar water heating for buildings, in the State of Paraná, considering scenarios of climate change. In order to reach the general objective, three articles were elaborated on this theme, which are presented in the form of chapters.

The first chapter refers to the first article, whose main objective was to evaluate the performance of four empirical models to estimate the global solar radiation from air temperature data compared to observed historical data. The second article, related to chapter 2, had as its main objective to estimate the photovoltaic solar energy production for single-family dwellings in future scenarios of possible climatic changes. The chapter 3 refers to the third article, which aimed to

estimate the solar fraction obtained through solar heating systems for single-family homes, in scenarios of possible climatic changes projected towards the end of the 21st century.

LITERATURE REVIEW

SOLAR RADIATION

According to Martinazzo (2004), life on Earth is possible by the combination of factors that together allow the planet to have sufficient energy and in the right measure for the functioning of all physical and biological phenomena. This energy is the solar radiation and comes from the nearest star called the Sun. Solar radiation keeps the earth's surface at a comfortable temperature, as well as supplies the necessary energy to the planet.

The total power radiated by the Sun is known as luminosity and is of the order of 3.85×10^{26}W, while the intensity radiated by the Sun is about 6.42×10^{7} W/m². Irradiance is the amount of radiant solar energy that reaches a unit of surface area in a unit of time (KREITH and KREIDER, 1978).

Of the total energy incident on the atmosphere, only part of it reaches the Earth surface. Direct solar radiation undergoes scattering, absorption and reflection as it crosses the Earth's atmosphere. Solar radiation that is spread by nitrogen, oxygen and water molecules gives rise to diffuse radiation. It is emphasized that the clouds also represent a diminutive factor of the radiation that reaches the ground, because they have great capacity of reflection and absorption (MARTINAZZO, 2004). Sunshine, or hours of sunshine, that is, the number of hours without direct solar radiation being intercepted by clouds, is used to estimate global solar radiation because of its importance in the amount of solar radiation reaching the surface. Direct radiation is the solar radiation received from the Sun except the portion that is scattered, absorbed or reflected by the atmospheric components, called diffuse radiation.

Global solar radiation is the sum of direct and diffuse radiation on a surface. The most common measure of solar radiation is global solar radiation on a horizontal surface, and can be measured by instruments such as actinographs and pyranometers. Actinograph is composed of sensors based on the differential

expansion of a bimetallic pair that are connected to a feather that, when they expand, record the instantaneous value of solar radiation. Its accuracy lies in the range of 15 to 20%. The pyranometer when tilted measures the overall radiation in the inclined plane, including the albedo. The sensor elements are usually thermoelectric, thermomechanical or photovoltaic. However, there are studies that indicate that pyranometers are subject to numerous problems that impair the accuracy of measurements (MARTINAZZO, 2004; CRESESB, 2006).

Thus, when radiation is not available locally, it can be estimated more accurately by means of empirical methods (DORNELAS, SILVA and OLIVEIRA, 2006). Among the most widespread existing methods models based on sunshine hours (Angström, 1924; Prescott, 1940) and those based on air temperature can be cited (HARGREAVES, 1981; HARGREAVES and SAMANI, 1982; BRISTOW and CAMPBELL, 1984; RICHARDSON, 1985; ALLEN, 1997; DONATELLI and CAMPBELL, 1998; HUNT et al., 1998; CHEN et al., 2004).

The Angström-Prescott equation (Prescott, 1940) is widely used, and estimates the global solar radiation from the number of sunshine hours. Angström (1924) presented an equation in which the quotient between global solar radiation and extraterrestrial solar radiation was linearly correlated with the quotient of the number of hours of solar brightness by the maximum possible sunshine. Prescott (1940) simplified the equation so that the linear and angular coefficients could be obtained from statistical adjustments, and the method was called Angström-Prescott.

This equation can be used to estimate global solar radiation and to obtain the number of hours of solar brightness in automatic wheather stations that do not normally measure this value. The Food and Agriculture Organization of the United Nations (FAO) presents the values of coefficients a (0.25) and b (0.50) considered standard, however, these coefficients can be estimated for each locality, reflecting in more reliable values of global solar radiation (ALLEN et al., 1997; JERSZURKI and SOUZA, 2013).

PHOTOVOLTAIC SOLAR ENERGY

Photovoltaic systems are responsible for converting sunlight into electricity. The photovoltaic effect, reported by Edmond Becquerel in 1839, is the appearance of a potential difference at the ends of a semiconductor material structure, produced by the absorption of light (CRESESB, 2006). As for semiconductor materials, silicon is

the most used. According to Campos et al. (2014), they are basically divided into autonomous photovoltaic systems, also called isolated systems (off-grid), or systems connected to the grid (on-grid).

Autonomous systems can be used in places that do not have a power grid. On the other hand, the connected systems, can generate electricity for own consumption, and also reduce or eliminate network consumption and even generate surplus energy, since they do not use energy storage, all the generation is delivered directly in the network (CAMPOS et al., 2014). This system represents a complementary source to the large electrical system to which it is connected. The entire arrangement is connected in inverters and then directly guided in the network (CRESESB, 2006).

According to Vera (2004), a photovoltaic system comprises grouping modules of photovoltaic panels and other pieces of equipment. The system is usually composed of three parts: the photovoltaic generator, the power conditioning and protection elements and the batteries, which store the electricity generated. The power conditioning subsystem consists of the load controller, inverter, maximum power point converter (MPPT) and inverter.

Photovoltaic cells are photosensitive semiconductor devices capable of converting incident solar energy into electrical energy. Photovoltaic cells are mostly fabricated using silicon and may consist of mono crystalline, polycrystalline or amorphous silicon crystals (CRESESB, 2006). Nogueira (2014) explains that the cells are grouped to form a photovoltaic module. In turn, the grouping of several modules is called the photovoltaic panel.

The modules can be grouped by series, parallel or mixed connections, obtaining different values of voltage and current specific to the applications. The modules differ from each other due to the relevant technical characteristics, such as their electrical and physical specifications.

Physical characteristics are dimensions, weight, cover material, encapsulation, assembly aspects and grounding methods. Regarding the electrical specifications, the main ones are: open circuit voltage (Voc), short circuit current (Isc), maximum power (Pm), maximum power voltage (Vmp), maximum power current (Imp), filling, temperature coefficients and efficiency (NOGUEIRA, 2014).

For powering alternating current (AC) equipment an inverter is required. This device generally incorporates a maximum power point follower required to optimize

the final output power (CRESESB, 2006). There are basically two types of inverters, those connected to the low voltage distribution network and those isolated from the distribution network. The first uses the network itself as an external source to perform switching (natural switching), while the second type performs forced switching (auto switching) (NOGUEIRA, 2014).

For the batteries, this function is to store the energy produced by the photovoltaic generator and deliver it to the load when the generation is zero or insufficient, such as during night or low-radiation periods (VERA, 2004). In systems that require energy storage in batteries, a device is used to control charge and discharge to the battery. The main function of the charge controller is not to allow battery damage due to overload or deep discharge (CRESESB, 2006).

Photovoltaic generation of electric power has great potential in Brazil, but only from 2012 the regulatory agency ANEEL (National Electric Power Agency) established the rules and regulations for the so-called micro and mini generation. By means of the Normative Resolution nº 482/2012, the country adopted the energy compensation mechanism, in which a solar roof can be connected in the public electricity grid through the Consumer Unit (UC) and inject the surplus in the electric grid as if it were a battery of infinite capacity, accumulating credits to be compensated in kWh (PEREIRA et al., 2017; EPE, 2017).

The photovoltaic modules installed over the roofs of the buildings, next to the point of consumption, inject into the public electricity grid the generated surplus energy and, they can use the electricity network as a backup battery at night, or when the amount of energy generated is not sufficient to meet the consumer's installation.

PHOTOTHERMAL SOLAR ENERGY

Photothermal solar energy is directly associated with the amount of energy that a given body is able to absorb, in the form of heat, from the incident solar radiation. The use of this form of energy implies knowing how to capture it and store it. For this, solar collectors are the pieces of equipment commonly used to capture photothermal solar energy (PEREIRA, 2010). The solar collector is a device that promotes the heating of a fluid, such as water, by converting the electromagnetic radiation from the Sun to thermal energy. For solar water heating systems, it is

necessary to know the area available to receive the solar incidence (SANTOS, 2015).

The most popular solar technology equipment is the flat solar collector that converts solar energy into thermal energy. The system supplies hot water at varying temperatures between 40 ºC and 60 ºC, which meets the needs of residential use in kitchens and bathrooms. In Brazil, in most cases, the solar thermal system is used to replace the electric shower (FRAIDENRAICH, 2014). However, if there is cloudy weather and there is not sufficient water heating, the electric shower can be used to compensate for the lack of solar heating. Electricity is an excellent complement to water heating, so it should not be used as the main source (SANTOS, 2015).

A flat plate solar collecting system consists of three basic units: the fluid transfer circuit, a storage system and the solar collector. For the flat plate models two systems are adopted: the thermosyphon system and the pumping system. In the thermosyphon system the storage tank is placed above the manifold and as the fluid in the manifold is heated, it naturally flows up through the circuit. In the pumping system the fluid is moved by the circuit by means of a pump and an electronic control allows a stable temperature (SANTOS, 2007).

According to Pereira (2010), the flat collectors are constituted by a container wrapping that has as a function to shelter and mechanically protect the other components. The casing has a cover that can be of tempered glass. The main part of the equipment is the heat exchanger, which is a flat plate designed to absorb the greatest amount of energy and effectively transfer it to the circulating fluid. Plates can be made of copper or aluminum painted with special dark-colored paints because they influence the maximum absorption of solar radiation.

The operation takes place through the following processes: the cold water from the water tank follows the pipeline, passes through the boiler, flows through the pipeline, is heated in the solar collector and goes to the top of the tank, through the pipeline, and then used. The water contained in the boiler circulates through the solar collectors continuously, that is, it does not remain stored. The heated water does not mix with the cold water because the hot fluid is less dense than the cold fluid, which causes the heated fluid to rise, taking the place of what is cold. For this principle to work, it is necessary that the boiler be positioned at the top of the solar collector (SANTOS, 2015).

The use of solar energy for heating water at temperatures below 100 °C is currently the most widespread application in Brazil, because the technology for converting solar energy into thermal energy is simple and available in the Brazilian market, with several suppliers and economic feasibility easily achieved in good projects. In addition, they collaborate in increasing the use of the system in homes, government incentives such as tax exemption, social housing programs *(Minha Casa Minha Vida)* and opportunities to purchase equipment through ANEEL programs (BASSO et al., 2010; PEREIRA et al., 2017).

Brazil has the third largest installed capacity of solar heating systems, but in per capita terms it occupies only the 30th position, which indicates that there are opportunities for growth, considering that the availability of this resource in the country is higher than those that occupy positions.

According to Pereira et al. (2017), a higher annual production of thermal energy per installed collector area, is not necessarily in the regions with the highest incidence of solar radiation. This is attributed to the fact that the demand for thermal energy is higher in the colder regions, making the heating potential of the system better utilized. Therefore, it is necessary to size the equipment according to local climatic characteristics.

CLIMATE CHANGES

In 1988, the World Meteorological Organization (WMO) and the United Nations Environment Program (UNEP) established the Intergovernmental Panel on Climate Change (IPCC) (MARENGO, 2001). The IPCC is responsible for reviewing existing scientific studies to evaluate possible future scenarios of climate change and was created to provide technical and scientific information on climate change.

By definition of the report, climate change refers to a change in the state of the climate that can be identified (by means of statistical tests, for example) by changes in the mean and / or variation of its properties and which persist over a long period of time. The climatic changes that are attributed to human activities and that alter the atmospheric composition differ from the variability of the climate attributed to natural causes (IPCC, 2014).

Thus, the latest IPCC report (IPCC, 2014) has documented that human influence on the climate system is clear and the recent anthropogenic emissions of greenhouse gases (GHG) are the highest in history. These emissions have increased

since the pre-industrial era, driven largely by economic and population growth, and from 2000 to 2010, the highest recorded emissions occurred.

Impacts on human systems are often geographically heterogeneous because they depend not only on changes in climate variables but also on the magnitude of change, location, and social and economic factors. Extreme changes have been observed in many climatic events since 1950, and many have been related to human influences, including an increase in the frequency of heat waves, a decrease in the frequency of cold waves, an increase in the frequency of intense rainfall events, sea level rise, tropical cyclone increase (IPCC, 2014).

Climate scenarios are representations of the climate future, with descriptions of how changing atmospheric composition from human activities can change the planet's climate over time. These representations of future climate are based on a set of assumptions, which include future energy demand trends, greenhouse gas emissions, changes in land use, and approximations in the laws governing the behavior of the climate system over large periods of time (HAMADA et al., 2007).

Emission scenarios projected by the IPCC take into account factors such as population size, consumption patterns, use of fossil fuels and energy efficiency. According to Marengo (2001), it is estimated that, by the year 2100, the average global temperature increases between 1.3 ºC and 4.6 ºC, which represents heating rates of 0.1 ºC to 0.4 ºC per decade.

Throughout history, people and societies have adapted and dealt with the climate variability and with extremes events, presenting varying degrees of success. The impacts of climate change have direct implications on urban centers and their infrastructures. It is necessary to rethink the way of living in cities, in order to continue enjoying the benefits of community life that only the city allows, but minimizing the impacts of urban agglomerations (SIEBERT, 2012; IPCC, 2014).

To reduce the risks of socio-environmental disasters, mitigation and adaptation strategies must be adopted. Thus, populations will have to adapt to the new reality of a change that already appears as inevitable since, even with great mitigation efforts, climate change must be observed during the course of that century (MARTINS and FERREIRA, 2010).

For Siebert (2012), urban planning needs to incorporate knowledge of the vulnerabilities and risks to which the population is subjected in order to propose mitigation and adaptation measures that increase urban resilience, which is the

ability to absorb disturbances while maintaining their normal functioning. Mitigation is the reduction of the environmental impact, for example, the reduction of the emission of gases that cause the greenhouse effect. Adaptation is the adjustment of anthropic systems to coexist with natural systems (IPCC, 2014).

With mitigation actions, one can substantially reduce the environmental impact of urban areas and, consequently, transform infrastructure and consumption patterns, improving the environment in general. Adaptive measures, on the other hand, seek to increase the resilience of cities and their population in relation to the impacts and inherent risks caused by climatic events (MARTINS and FERREIRA, 2010).

CHAPTER 1

EVALUATION OF EMPIRICAL MODELS TO ESTIMATE GLOBAL SOLAR RADIATION FROM AIR TEMPERATURE IN THE STATE OF PARANA

ABSTRACT

Global solar radiation is the fundamental source of energy on Earth. Despite their importance, sunshine or solar radiation data are rarely available in weather stations. In the absence of available data, there are empirical methods that can be used to estimate solar radiation. The objective of this work was to calibrate the parameters and to evaluate the performance of four empirical models of solar radiation estimation (Chen, Hargreaves, Hunt and Richardson) from air temperature data for eight localities in the State of Paraná. Data were obtained from the Meteorological Database for Teaching and Research (BDMEP) and applied to the equations. For the comparison of means among the models, the Kruskal-Wallis non-parametric test was used, and Dunn's multiple comparison test was used to analyze which models presented different means among them. The performance of each model was assessed using statistical indices: Pearson correlation coefficient (r), Mean bias error (MBE), Square root mean square error (RMSE), Wilmott concordance index (d), Index (c) and Nash-Sutcliffe (NSE) efficiency coefficient. It was observed that the models proposed by Chen and Hunt presented the best performances in the estimation of the global solar radiation for the studied Paraná state localities, because they are closer to the observed historical data.

Keywords: Global solar radiation; Estimation models; Calibration.

RESUMO

A radiação solar global é a fonte fundamental de energia na Terra. Apesar da sua importância, os dados de insolação ou radiação solar raramente estão disponíveis em estações meteorológicas. Na ausência de dados disponíveis, há métodos empíricos que podem ser utilizados para estimar a radiação solar. O trabalho objetivou calibrar os parâmetros e avaliar os desempenhos de quatro modelos empíricos de estimativa de radiação solar (Chen, Hargreaves, Hunt e Richardson) a partir de dados de temperatura do ar para oito localidades do Estado do Paraná. Foram obtidos dados doBanco de Dados Meteorológicos para Ensino e Pesquisa (BDMEP) e aplicados nas equações. Para comparação de médias entre os modelos, foi utilizado o teste não-paramétrico de Kruskal-Wallis, e o teste de comparação múltipla de Dunnpara analisar quais modelos apresentaram médias distintas entre si. O desempenho de cada modelo foiavaliado por meio dos índices estatísticos: Coeficiente de correlação de Pearson (r), Erro médio de viés (MBE), Raiz quadrada do quadrado médio do erro (RMSE), Índice de concordância de Wilmott (d), Índice de desempenho (c) e Coeficiente de eficiência de Nash–Sutcliffe (NSE).Constatou-seque os modelos propostos por Chen e por Hunt apresentaram os melhores desempenhos na estimativa da radiação solar global para as localidades paranaenses estudadas, por se aproximarem mais dos dados históricos observados.

Palavras-chave: Radiação solar global; Modelos de estimativa; Calibração.

1.1 INTRODUCTION

Solar radiation is the main source of energy responsible for chemical, physical and biological processes. Since it is a conditioning factor of air temperature, it has a wide variety of applications in hydrology, meteorology, agrology, limnology, agriculture, ecology, oceanography, architecture, industry and the environment. In addition, global solar radiation (R_G) is a key element in the planning and use of efficient solar thermal and photovoltaic systems in buildings (DAUT et al., 2011; SILVA et al., 2012; MORADI, MUELLER and PEREZ, 2014).

Global solar radiation can be defined as the amount of solar energy that reaches the Earth's surface, being composed of direct solar radiation and diffuse solar radiation and can be measured by means of devices called pyranometers. On the other hand, it is called insolation the number of hours of solar brightness, which is the direct solar radiation that reaches the earth's surface without the presence of clouds and which is measured by heliographs (BRASIL, 2007; WREGE et al., 2012).

Despite their importance, sunshine or solar radiation data are rarely available in meteorological weather stations, probably due to the cost of instrumentation and their difficulty in maintenance and calibration (HUNT et al., 1998). Thus, the existing data series are relatively short for climate studies, and often present discontinuities or failures, which may be associated with changes in sensors or processing algorithms (PODESTÁ et al., 2004; DAUT et al., 2011).

In the absence of available data, several alternatives have been proposed to obtain daily estimates of global solar radiation. Three large groups of methods include satellite derived estimates, stochastic generation and empirical methods (PODESTÁ et al., 2004). There are many empirical methods that can be used to estimate solar radiation and require the development of a set of empirical equations to estimate global solar radiation from variables normally available in most meteorological stations (ALMOROX, HONTORIA and BENITO, 2011).

These models can be classified into three categories delimited by Yang, Koike and Ye (2006): models based on hours of sunshine (ANGSTROM, 1924; PRESCOTT, 1940); in the air temperature (HARGREAVES, 1981; BRISTOW and CAMPBELL, 1984; RICHARDSON, 1985; ALLEN, 1997; DONATELLI and CAMPBELL, 1998; HUNT et al., 1998; CHEN et al., 2004) and in cloudiness (NIELSEN et al., 1981; SUPIT and VAN KAPPEL, 1998; EHNBERG and BOLLEN, 2004). Estimation models based on solar brightness and cloudiness tend to be more

accurate, however, application is limited due to the scarcity of these data because satellites and cloud observations are not readily available to most Brazilian locations.

In the opposite, the air temperature is the most registered climatological variable, due to the great availability of sensors for its measurement. Thus, a temperature-based model to estimate global solar radiation can be a viable for estimating this element in different geographic and climatic characteristics (PRIETO, MARTÍNEZ-GARCÍA and GARCÍA, 2009). The models based on the air temperature estimate the values of global solar radiation as a function of extraterrestrial solar radiation, which is based on the concept of atmospheric transmittance, which in turn is defined as a linear function related to the duration of solar brightness, or, from the daily temperature range (difference between maximum and minimum daily air temperatures) (ALMOROX, HONTORIA and BENITO, 2011; SILVA et al., 2012).

However, the importance of the calibration of these models for each site is emphasized, since the empirical relations vary spatially. Some authors (Meza and Varas, 2000; Podestá et al., 2004; Weiss and Hays, 2004; Mavromatis and Jagtap, 2005; Liu et al., 2009; Almorox, Hontoria and Benito, 2011; Daut et al., 2011; Silva et al., 2012; Zirebwa et al., 2015) have evaluated these models in different locations (Chile, Argentina, Nebraska-USA, Florida-USA, China, Spain, Malaysia, Minas Gerais-Brazil and Zimbabwe respectively) and calibration coefficients varied considerably.

Thus, the determination of an empirical model estimating the amount of global solar radiation incident locally, through series of air temperature data, should make available many possibilities of techniques and methods for conducting research, that have as scope the use of the solar source as an option for the energy matrix.

In this context, the objective of this work was to calibrate the parameters and to evaluate the performance of four empirical models of estimation of global solar radiation from air temperature data in eight localities of the State of Paraná, Brazil.

1.2 MATERIALS AND METHODS

This research was developed in the Laboratory of Applied Computational Statistics - LECA, of the State University of Ponta Grossa. Eight localities of the State of Paraná (Figure 1.1) were selected from climatological data of conventional meteorological stations (Table 1.1), which are available in the Meteorological

Database for Teaching and Research (BDMEP) by the National Institute of Meteorology (INMET).

Figure 1.1 - Selected locations in the State of Paraná

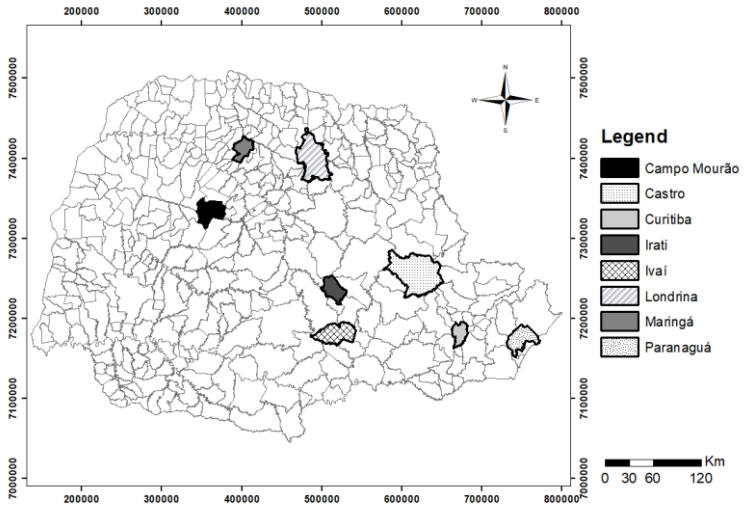

Table 1.1 - Geographical coordinates of selected locations

ID	Locality	Latitude (S)	Longitude (W)	Elevation (m)
L1	Campo Mourão	-24º05’	-52º36’	616
L2	Curitiba	-24º78’	-50º00’	1009
L3	Castro	-25º43’	-49º26’	924
L4	Irati	-25º46’	-50º63’	837
L5	Ivaí	-25º00’	-50º85’	808
L6	Londrina	-23º31’	-51º13’	566
L7	Maringá	-23º40’	-51º91’	542
L8	Paranaguá	-25º53’	-48º51’	5

The State of Paraná belongs to the region of southern Brazil and is located between the parallels 22º30'58 "and 26º43'00" south latitude and between the meridians 48º05'37 "and 54º37'08" west longitude. According to Köppen's climate classification, the State has two types: Cfa - Subtropical climate with average temperature in the coldest month below 18 ºC (mesothermic) and average temperature in the hottest month above 22 ºC, with hot summers, infrequent frosts and trend of rainfall concentration in the summer months, however without a defined dry season; Cfb - Temperate climate with average temperature in the coldest month below 18 ºC (mesothermic), with fresh summers, average temperature in the hottest month below 22 ºC and no dry season defined (IAPAR, 2018).

The daily historical series of pluviometric precipitation, insolation (or hours of solar brightness), minimum and maximum temperatures of the evaluated localities comprised a period of 31 years (1987-2017). The data consistency for the correction of possible faults, as well as the calculation of the global solar radiation from the sunshine data in the unit langley per day (ly/dia), were carried out through the software PGECLIMA_R (VIRGENS FILHO et al., 2013). The software calculates the global solar radiation using the equation of Angström-Prescott (Equation 1), and it is necessary to inform the value of the radiation at the top of the atmosphere (R_A) for each day of the year, determined by Equation 2, and the values of parameters "a" and "b", which can be 0.25 and 0.50 respectively, in the absence of the adjusted values for each locality.

$$R_G = R_A \times (a + b \times \frac{n}{N}) \quad (1.1)$$

where,
R_G is the global solar radiation in ly/dia;
R_A is the solar radiation at the top of the atmosphere, in ly/dia, given by Equation 2;
n is the daily sunshine;
N is the maximum daily value of hours of solar brightness.

$$R_A = \frac{916{,}7}{R^2}(\text{sen}\phi\text{sen}\delta\text{H} + \cos\phi\cos\delta\text{senH}) \quad (1.2)$$

where,
R is the medium vector radius Earth-Sun = 0,9915;
ϕ is the location latitude;
δ it is the solar declination;
H it is the arccos(-tgϕtgδ)

Four models of global solar radiation estimation were used from the air temperature data. Table 1.2 presents the empirical equations used.

Table 1.2 - Summary of models for radiation estimation

ID	Model	Equation	Reference
Hg	Hargreaves	$R_G = R_A \times (a + b\sqrt{\Delta T})$	Hargreaves (1985)
R	Richardson	$R_G = R_A \times (a + \Delta T^b)$	Richardson (1985)
Hu	Hunt	$R_G = \left(b \times \sqrt{\Delta T} \times R_A\right) + a$	Hunt et al. (1998)
Ch	Chen	$R_G = R_A \times (b \ln \Delta T + a)$	Chen et al. (2004)

R_G – surface incidente solar radiation incidente (MJ/m².day); R_A – solar radiation at the top of the atmosphere (MJ/m².day); ΔT – thermal amplitude (difference between the maximum and minimum temperatures) (°C); a e b coefficients of the empirical models (dimensionless).

To compare the performance among the models, the Kruskal-Wallis non-parametric test was used with Dunn's test for averages, at a significance level of 5%. The analysis of the bias of the data estimated by the models in relation to the historical data was evaluated through the statistical indices of Table 1.3, namely: Pearson correlation coefficient (r), Mean bias error (MBE), Root mean square errors (RMSE), Wilmott's Concordance Index (d), Performance Index (c), and Nash-Sutcliffe Efficiency Coefficient (NSE).

Table 1.3 – Statistical indices used

Sigla	Índice	Equação
r	Pearson correlation coefficient	$r = \frac{\sum_{i=1}^{n}(x \times y) - (\sum x) \times (\sum y)}{\sqrt{n\sum x^2 - (\sum x)^2} \times \sqrt{n\sum y^2 - (\sum y)^2}}$
MBE	Mean bias error	$MBE = \frac{1}{n}\sum_{i=1}^{n}(Pi - Oi)$
RMSE	Square root mean square	$RMSE = \sqrt{\frac{1}{n}\sum_{i=1}^{n}(Pi - Oi)^2}$
d	Wilmott's Concordance Index	$d = 1 - \left[\frac{\sum_{i=1}^{n}(Pi - Oi)^2}{\sum_{i=1}^{n}(\lvert Pi - \bar{O}\rvert + \lvert Oi - \bar{O}\rvert)^2}\right]$
c	Performance Index “c”	$c = r \times d$
NSE	Nash-Sutcliffe Efficiency Coefficient	$NSE = 1 - \left[\frac{\sum_{i=1}^{n}(Oi - Pi)^2}{\sum_{i=1}^{n}(Oi - \bar{O})^2}\right]$

Pi is the estimated radiation, Oi is the observed radiation, O is the a average of observed radiation and n is the number of data.

According to Camargo and Sentelhas (1997), Pearson's correlation coefficient indicates the degree of the data dispersion obtained in relation to the mean. The mean bias error (MBE) indicates the average "bias" of the model, ie, medium or lower precision. The root mean square errors (RMSE) can vary from 0 to infinity, being that the smaller the better the radiation estimate. The Wilmott concordance index (d) defines the accuracy of the estimated values in relation to those observed, varying from 0 to 1, and the closer to 1 the better the estimate.

The values of the index "c" can vary between -∞ and 1, and the value above 0.85 is considered optimal (CAMARGO and SENTELHAS, 1997). The Nash-Sutcliffe coefficient of efficiency is a normalized statistic that expresses the relative magnitude of the residual variance ("noise") in comparison with the variance of the measured data, the NSE values vary between -∞ and 1, where NSE = 1 is the ideal value. In

order to study the symmetry of the distributions and to detect the outliers, which consist of points sampled in the space whose values differ from the others, boxplot graphs and line graphs have been elaborated to evaluate the annual trends of global solar radiation values.

1.3 RESULTS AND DISCUSSION

Table 1.4 shows the calibrated coefficients of the models tested for the locations L1 and L2, for all months of the year. The coefficient α of the Ch model varied between -0.548 and 0.973, while the coefficient b ranged from -0.097 to 0.467 considering all the localities.

For the Hg model, the α coefficient ranged from -0.453 to 0.995 while the b coefficient varied from -0.172 to 0.311 for all the locations. The coefficient α of the Hu model varied between -17.505 and 43.048 and the coefficient b varied between -0.178 and 0.313 considering all the localities. The Hu model showed the greatest oscillation in the values of its coefficients. For the R model, α values varied between 0.039 and 1.404, while values of b varied between -0.530 and 0.995, for all locations.

Table 1.4 – Linear and angular coefficients obtained confronting the estimated and measured values of global solar radiation in Campo Mourão (L1) and Curitiba (L2) for the period between 1987 and 2017.

(to be continued)

	Ch		**Hg**		**Hu**		**R**	
L1	α	**b**	α	**b**	α	**b**	α	**b**
Jan	-0.409	0.393	-0.284	0.244	-12.37	0.244	0.070	0.832
Feb	-0.359	0.371	-0.221	0.224	-9.266	0.226	0.078	0.783
Mar	-0.072	0.254	0.051	0.145	1.960	0.144	0.143	0.533
Apr	-0.031	0.243	0.073	0.142	2.892	0.136	0.172	0.467
May	-0.075	0.264	-0.061	0.183	-1.452	0.182	0.141	0.553
Jun	-0.155	0.293	-0.002	0.162	-0.027	0.161	0.114	0.636
Jul	-0.243	0.329	-0.132	0.199	-3.875	0.209	0.083	0.762
Aug	0.031	0.208	0.067	0.135	1.904	0.135	0.178	0.431
Sep	-0.155	0.272	-0.087	0.171	-3.118	0.173	0.108	0.605
Oct	-0.241	0.307	-0.132	0.185	-5.018	0.185	0.101	0.637
Nov	0.136	0.166	0.182	0.104	7.599	0.105	0.172	0.450
Dec	-0.330	0.359	-0.210	0.221	-9.189	0.221	0.071	0.824
L2	α	b	α	b	α	b	α	b
Jan	-0.305	0.313	-0.331	0.234	-13.91	0.230	0.060	0.825
Feb	0.030	0.170	0.056	0.114	2.386	0.113	0.131	0.486
Mar	-0.153	0.254	-0.106	0.167	-3.444	0.164	0.083	0.693
Apr	0.107	0.152	0.061	0.122	2.486	0.116	0.183	0.375

Table 1.4 – Linear and angular coefficients obtained confronting the estimated and measured values of global solar radiation in Campo Mourão (L1) and Curitiba (L2) for the period between 1987 and 2017.

(conclusion)

	Ch		Hg		Hu		R	
L2	α	b	α	b	α	b	α	b
May	-0.548	0.417	-0.412	0.254	-8.662	0.236	0.039	0.995
Jun	-0.262	0.292	-0.212	0.191	-4.715	0.191	0.072	0.728
Jul	-0.008	0.192	0.204	0.074	3.876	0.084	0.149	0.436
Aug	-0.241	0.285	-0.147	0.172	-3.731	0.169	0.075	0.709
Sep	0.087	0.140	0.098	0.095	4.120	0.087	0.132	0.450
Oct	0.084	0.135	0.009	0.119	-0.664	0.127	0.124	0.471
Nov	0.973	-0.232	0.995	-0.172	43.05	-0.178	1.404	-0.530
Dec	-0.076	0.206	-0.282	0.209	-12.40	0.209	0.113	0.523

Table 1.5 shows the calibrated coefficients of the models tested for the locations L3 and L4, for all months of the year.

Table 1.5 – Linear and angular coefficients obtained confronting the estimated and measured values of global solar radiation in Castro (L3) and Irati (L4) for the period between 1987 and 2017.

(to be continued)

	Ch		Hg		Hu		R	
L3	α	**b**	α	**b**	α	**b**	α	**b**
Jan	-0.252	0.315	-0.219	0.217	-9.347	0.216	0.086	0.723
Feb	-0.359	0.372	-0.309	0.253	-12.72	0.254	0.068	0.848
Mar	-0.077	0.249	-0.058	0.173	-2.157	0.174	0.119	0.601
Apr	-0.138	0.283	-0.112	0.195	-3.486	0.197	0.127	0.581
May	0.049	0.196	0.066	0.135	1.710	0.134	0.172	0.439
Jun	0.162	0.141	0.162	0.100	3.589	0.099	0.194	0.374
Jul	-0.068	0.248	-0.050	0.171	-1.155	0.171	0.133	0.549
Aug	0.047	0.194	0.076	0.128	2.188	0.127	0.170	0.432
Sep	-0.267	0.316	-0.232	0.213	-7.338	0.210	0.086	0.696
Oct	-0.011	0.198	-0.001	0.139	-0.113	0.139	0.146	0.456
Nov	-0.224	0.304	-0.193	0.208	-8.226	0.209	0.084	0.728
Dec	-0.268	0.319	-0.197	0.207	-8.619	0.207	0.073	0.787
L4								
Jan	-0.181	0.278	-0.139	0.186	-5.951	0.186	0.098	0.651
Feb	-0.528	0.432	-0.431	0.280	-17.51	0.280	0.046	0.990
Mar	-0.139	0.265	-0.108	0.180	-3.558	0.177	0.099	0.658
Apr	-0.031	0.219	-0.009	0.149	-0.002	0.146	0.148	0.483
May	0.172	0.131	0.131	0.105	3.141	0.106	0.222	0.301
Jun	0.050	0.185	0.011	0.142	0.260	0.142	0.148	0.483
Jul	-0.242	0.311	-0.192	0.204	-4.439	0.205	0.095	0.672
Aug	0.151	0.144	0.197	0.087	5.681	0.084	0.237	0.283

Table 1.5 – Linear and angular coefficients obtained confronting the estimated and measured values of global solar radiation in Castro (L3) and Irati (L4) for the period between 1987 and 2017.

(conclusion)

	Ch		Hg		Hu		R	
L4	α	**b**	α	**b**	α	**b**	α	**b**
Sep	0.111	0.146	0.112	0.102	3.329	0.105	0.179	0.369
Oct	-0.097	0.235	-0.089	0.164	-3.475	0.164	0.114	0.566
Nov	0.018	0.191	-0.097	0.171	-4.246	0.172	0.136	0.506
Dec	0.012	0.192	0.025	0.133	1.132	0.133	0.159	0.436

Table 1.6 shows the calibrated coefficients of the models tested for the locations L5 and L6, for all months of the year.

Table 1.6 – Linear and angular coefficients obtained confronting the estimated and measured values of global solar radiation in Ivaí (L5) and Londrina (L6) for the period between 1987 and 2017.

	Ch		Hg		Hu		R	
L5	α	**b**	α	**b**	α	**b**	α	**b**
Jan	0.114	0.152	0.077	0.120	3.393	0.120	0.226	0.290
Feb	-0.117	0.255	-0.058	0.165	-2.100	0.163	0.114	0.595
Mar	-0.298	0.338	-0.252	0.227	-8.376	0.222	0.070	0.812
Apr	-0.014	0.222	-0.005	0.155	0.321	0.151	0.139	0.527
May	0.594	-0.037	0.540	-0.010	12.184	0.004	0.537	-0.051
Jun	-0.058	0.222	-0.152	0.186	-3.264	0.185	0.092	0.659
Jul	-0.226	0.302	-0.149	0.190	-3.318	0.188	0.109	0.604
Aug	0.029	0.205	0.037	0.141	1.377	0.137	0.162	0.461
Sep	0.114	0.156	0.071	0.122	2.389	0.121	0.152	0.452
Oct	0.282	0.078	0.248	0.065	9.580	0.065	0.391	0.042
Nov	0.593	-0.041	0.500	-0.001	21.152	-0.001	0.611	-0.109
Dec	0.368	0.046	0.384	0.028	16.869	0.028	0.394	0.060
L6								
Jan	-0.143	0.277	-0.081	0.180	-3.461	0.179	0.109	0.635
Feb	0.234	0.120	0.249	0.082	10.137	0.082	0.268	0.261
Mar	0.527	0.011	0.543	0.003	20.537	-0.004	0.454	0.066
Apr	0.360	0.088	0.335	0.070	11.215	0.061	0.372	0.161
May	-0.109	0.275	-0.047	0.177	-1.091	0.176	0.114	0.632
Jun	0.304	0.106	0.326	0.069	7.449	0.069	0.301	0.238
Jul	0.494	0.031	0.905	-0.096	20.168	-0.078	0.612	-0.046
Aug	0.353	0.094	0.427	0.046	12.732	0.038	0.359	0.181
Sep	0.587	-0.015	0.602	-0.015	21.244	-0.024	0.548	-0.023
Oct	0.631	-0.047	0.582	-0.019	22.639	-0.019	0.658	-0.122
Nov	0.232	0.120	0.254	0.079	10.509	0.080	0.254	0.277
Dec	0.239	0.111	0.259	0.073	11.224	0.074	0.228	0.312

Table 1.7 shows the calibrated coefficients of the models tested for the locations L7 and L8, for all months of the year.

Table 1.7 – Linear and angular coefficients obtained confronting the estimated and measured values of global solar radiation in Maringá (L7) and Paranaguá (L8) for the period between 1987 and 2017.

	Ch		Hg		Hu		R	
L7	α	**b**	α	**b**	α	**b**	α	**b**
Jan	-0.202	0.319	-0.150	0.214	-6.466	0.214	0.110	0.668
Feb	0.074	0.201	0.146	0.123	6.006	0.122	0.183	0.452
Mar	-0.519	0.467	-0.336	0.279	-10.99	0.269	0.060	0.945
Apr	0.685	-0.055	0.914	-0.112	27.303	-0.104	0.906	-0.233
May	0.144	0.181	0.082	0.150	2.071	0.150	0.223	0.371
Jun	-0.136	0.311	-0.023	0.187	-0.481	0.186	0.121	0.658
Jul	0.293	0.126	0.277	0.095	6.495	0.097	0.273	0.307
Aug	-0.436	0.428	-0.453	0.311	-12.95	0.313	0.077	0.834
Sep	-0.357	0.378	-0.298	0.252	-9.604	0.248	0.066	0.858
Oct	-0.257	0.336	-0.220	0.229	-8.232	0.227	0.114	0.632
Nov	0.067	0.203	0.106	0.134	4.389	0.134	0.170	0.476
Dec	-0.084	0.264	-0.008	0.167	-0.359	0.167	0.144	0.546
L8								
Jan	0.611	-0.097	0.623	-0.075	27.742	-0.080	0.721	-0.304
Feb	0.397	0.019	0.392	0.015	15.901	0.016	0.329	0.108
Mar	0.246	0.093	0.238	0.070	8.716	0.068	0.237	0.269
Apr	0.460	-0.005	0.445	0.002	13.378	0.000	0.388	0.041
May	0.481	-0.017	0.525	-0.028	12.800	-0.029	0.276	0.210
Jun	0.227	0.105	0.194	0.086	4.144	0.087	0.190	0.382
Jul	0.372	0.027	0.388	0.013	9.028	0.010	0.300	0.136
Aug	0.044	0.178	0.054	0.124	1.719	0.120	0.162	0.404
Sep	-0.022	0.204	0.167	0.072	1.654	0.117	0.118	0.544
Oct	0.337	0.004	0.419	-0.029	16.187	-0.029	0.187	0.284
Nov	0.326	0.031	0.291	0.035	12.499	0.034	0.249	0.186
Dec	0.596	-0.091	0.574	-0.058	25.378	-0.058	0.506	-0.131

The distribution of the observed historical monthly averages (Obs) and of the models tested in the analyzed period of global solar radiation for all evaluated locations were summarized in boxplot graphs (Figure 2). For L1, the data of the Hg model presented high variability, with mean and median with discrepant differences in relation to the observed values. The other models had mean and median values close to each other and similar to the observed values. Similarly, the performance of the models in L2, L3 and L4 is similar to that presented in L1, with high variability in

Hg and similarity between Ch, Hu and Obs, except in L4, where the R model also presented similarity when compared to Obs.

While for L1 to L4 and L7, the mean values of Hg were above the averages of the other models, this situation is reversed in L5, L6 and L8, that is, the mean values were shown below in the other models. For L5 and L7, the Hg values presented a very high variability, for L6 and L8, the Hg values were found to be well below the values of the other models. For the locations L5 to L8, the models that approached the Obs were Ch and Hu.

Figure 1.2 –The estimated and measured values of global solar radiation in all localities for the period between 1987 and 2017.

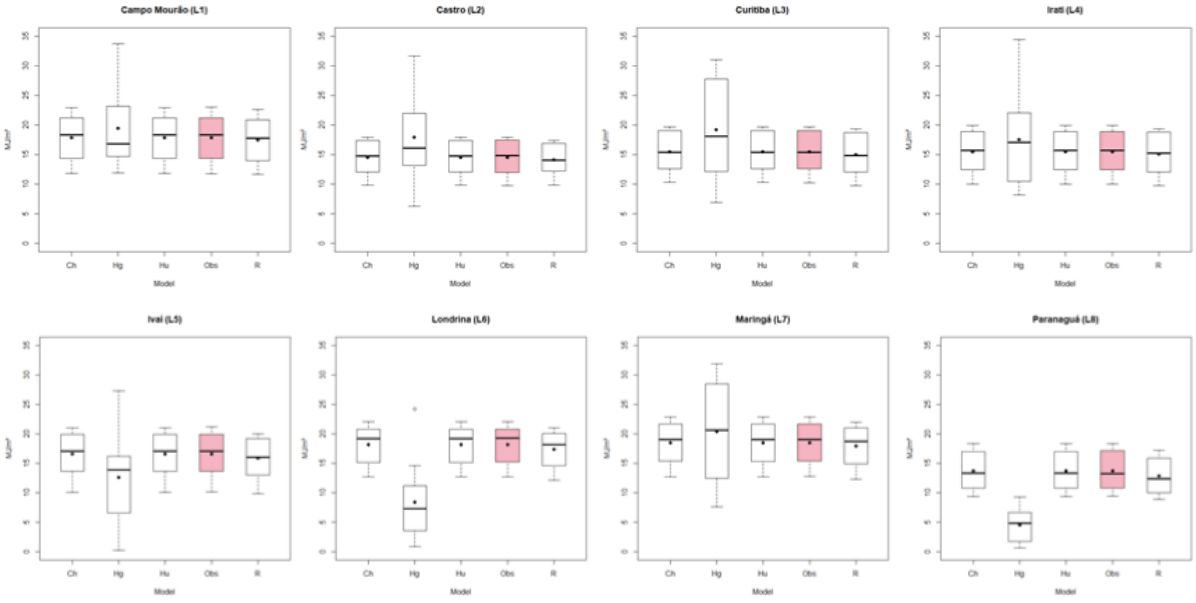

In the comparison of the means of global solar radiation between the models and values observed, the Kruskal-Wallis test was used with the Dunn method. Table 1.8 presents the results of the comparison test by the Dunn method for all months in the evaluated locations.

It was observed that for L1, the values of the Ch, Hu, R, and Obs models do not differ statistically from each other, but have a significant difference in relation to the Hg model. This behavior was verified in all the months, except for the month of June, in which, all the models did not present statistical significance among themselves. The same behavior was observed for L2, except for the month of October, in which the R model differs statistically from the others, less than Hg.

For L3, Ch, Hu, Obs and R models did not present statistical differences, except for the months of June and August, whose behavior observed for the Ch and Hu models did not present statistical difference in relation to the observed values (Obs), however, all the three statistically differed from R and Hg, which in turn also presented statistical significance among themselves.

Table 1.8 - Dunn Test Result for comparison among models

(to be continued)

	Jan	Feb	Mar	Apr	May	Jun	Jul	Aug	Sep	Oct	Nov	Dec
L1												
Ch	b	b	a	a	b	a	b	a	b	b	a	b
Hg	a	a	b	b	a	a	a	b	a	a	c	a
Hu	b	b	a	a	b	a	b	a	b	b	a	b
Obs	b	b	a	a	b	a	b	a	b	b	a	b
R	b	b	a	a	b	a	b	a	b	b	b	b
L2												
Ch	b	a	b	a	b	b	a	b	a	a	b	b
Hg	a	b	a	b	a	a	b	a	b	ab	a	a
Hu	b	a	b	a	b	b	a	b	a	a	b	b
Obs	b	a	b	a	b	b	a	b	a	a	b	b
R	b	a	b	a	b	b	a	b	a	b	b	b
L3												
Ch	b	b	b	b	a	a	b	a	b	a	b	b
Hg	a	a	a	a	b	c	a	c	a	b	a	a
Hu	b	b	b	b	a	a	b	a	b	a	b	b
Obs	b	b	b	b	a	a	b	a	b	a	b	b
R	b	b	b	b	a	b	b	b	b	a	b	b
L4												
Ch	b	b	b	a	a	a	b	a	a	b	b	a
Hg	a	a	a	a	b	a	a	c	b	a	a	b
Hu	b	b	b	a	a	a	b	a	a	b	b	a
Obs	b	b	b	a	a	a	b	a	a	b	b	a
R	b	b	b	a	a	a	b	b	a	b	b	ab
L5												
Ch	a	b	b	ab	a	b	b	a	ab	a	a	a
Hg	c	a	a	a	c	a	a	b	c	c	c	c
Hu	a	b	b	ab	a	b	b	a	ab	a	a	a
Obs	a	b	b	ab	a	b	b	a	a	a	a	A
R	b	b	b	b	b	b	b	ab	b	b	b	b
L6												
Ch	b	a	a	a	b	a	a	a	a	a	a	a
Hg	a	c	c	c	a	c	c	c	c	c	c	c
Hu	b	a	a	a	b	a	a	a	a	a	a	a
Obs	b	a	a	a	b	a	a	a	a	a	a	a
R	b	b	b	b	b	b	b	b	b	b	b	b
L7												
Ch	b	a	b	a	a	ab	a	b	b	b	a	a
Hg	a	b	a	c	c	a	c	a	a	a	c	b
Hu	b	a	b	a	a	ab	a	b	b	b	a	a
Obs	b	a	b	a	a	ab	a	b	b	b	a	a
R	b	a	b	b	b	b	b	b	b	b	b	a

Table 1.8 - Dunn Test Result for comparison among models

(conclusion)

L8	Jan	Feb	Mar	Apr	May	Jun	Jul	Aug	Sep	Oct	Nov	Dec
Ch	a	a	a	a	a	a	a	a	a	a	a	a
Hg	c	c	c	c	c	c	c	c	b	c	c	c
Hu	a	a	a	a	a	a	a	a	a	a	a	a
Obs	a	a	a	a	a	a	a	a	a	a	a	a
R	b	b	b	b	b	b	b	b	a	b	b	b

Note: Equal lowercase letters in the column for all months and locations do not differ statistically from each other at the significance level of 5% by the Dunn Test.

For L4, in the months of April and June, there was no statistical significance among the models. In the month of August, the Ch and Hu models did not present statistical difference in relation to the observed values (Obs), but the three statistically differed from R and Hg, which, in turn, also presented statistical significance among themselves. In the month of December, the Hg model differs statistically from the others, less than R, which is not different from any other. In the other months, the models Ch, Hu, R and Obs do not differ statistically among themselves, however, they have a significant difference in relation to the Hg model.

In L5, in the months of February, March, June and July, the Ch, Hu, R and Obs models do not differ statistically from one another, but differ from the Hg model. In the months of January, May, October, November and December, the R and Hg models differ from each other. In April, only the Hg and R models differ from each other. In August, the Hg model differs statistically from the others, less than R, which differs from none of the others. And in the month of September, the observed values do not differ from Ch and Hu, which, in turn, do not differ from R, but the Hg model differs statistically from all of them.

For L6, in the months of January and May, the Hg model differs statistically from the others, whereas for the other months the observed values do not differ from Ch and Hu, but the Hg and R models differ from each other and from the others. In L7, only the Hg model differs statistically from the others in the months of January, February, March, August, September, October and December. In April, May, July and November the observed values do not differ from Ch and Hu, however, the Hg and R models differ from each other. In June, the statistical significance was found only between Hg and R. For L8, only in September, the statistical significance was only found in the Hg model. In the other months, it was verified that the observed values

did not differ from Ch and Hu, however, the Hg and R models differed from each other.

Tables 1.9 to 15 present the results of the statistical indexes of the models for all the locations, from L1 to L8. The highlighted values indicate the best result of each index, for each analyzed month and model. It was noticed that for L1 (Table 8), the model of Ch presented a higher number of highlitghted ones, with values of r between 0.429 and 0.858; of MBE between -0.052 and 0.054; RMSE between 0.617 and 1.808; d between 0.695 and 0.824; c between 0.298 and 0.738 and NSE between -0.162 and 0.734.

Table 1.9 - Results of the statistical indexes of the models for L1.

	Jan	**Feb**	**Mar**	**Apr**	**May**	**Jun**	**Jul**	**Aug**	**Sep**	**Oct**	**Nov**	**Dec**
Ch												
r	**0.785**	0.774	**0.640**	**0.751**	0.858	**0.732**	**0.682**	0.636	**0.790**	**0.688**	**0.721**	0.429
MBE	**0.036**	-0.034	**0.024**	**0.025**	**0.005**	**0.054**	-0.039	-0.052	**0.049**	-0.027	**-0.001**	**-0.033**
RMSE	**1.390**	1.318	**1.037**	**0.732**	0.644	**0.617**	**0.828**	**0.856**	**1.050**	**1.056**	**1.114**	1.808
d	0.827	0.818	0.779	0.823	0.861	0.818	**0.774**	**0.790**	**0.824**	0.786	**0.820**	0.695
c	**0.649**	0.633	**0.499**	**0.619**	0.738	**0.599**	**0.528**	0.502	**0.651**	**0.541**	**0.591**	0.298
NSE	**0.581**	0.568	**0.387**	**0.563**	0.734	**0.516**	**0.394**	0.394	**0.581**	**0.437**	**0.486**	-0.162
Hg												
r	0.777	**0.775**	0.625	0.746	**0.866**	0.706	0.648	**0.648**	0.776	0.677	0.718	0.446
MBE	12.070	8.782	-1.764	-2.118	1.476	0.101	2.932	-1.832	2.861	4.945	-7.499	8.990
RMSE	12.150	8.878	2.053	2.243	1.603	0.636	3.051	2.019	3.057	5.057	7.583	9.168
d	0.236	0.290	0.575	0.493	0.648	0.817	0.405	0.528	0.525	0.343	0.259	0.238
c	0.183	0.225	0.360	0.368	0.562	0.577	0.263	0.342	0.407	0.232	0.186	0.106
NSE	-31.01	-18.61	-1.401	-3.099	-0.648	0.485	-7.237	-2.372	-2.549	-11.90	-22.80	-28.90
Hu												
r	0.777	**0.775**	0.625	0.746	**0.866**	0.706	0.648	**0.648**	0.776	0.677	0.718	0.446
MBE	0.039	**-0.013**	0.028	0.044	0.020	0.056	**-0.033**	**-0.048**	0.062	**-0.019**	0.008	-0.020
RMSE	1.399	**1.308**	1.049	0.744	**0.625**	0.631	0.860	0.848	1.084	1.059	1.123	**1.795**
Hu												
d	**0.828**	**0.822**	**0.782**	**0.824**	**0.868**	**0.819**	0.764	0.787	0.816	**0.787**	0.818	**0.703**
c	0.643	**0.636**	0.489	0.615	**0.752**	0.578	0.495	**0.510**	0.633	0.533	0.588	**0.313**
NSE	0.576	**0.574**	0.374	0.549	**0.749**	0.494	0.346	**0.405**	0.554	0.435	0.478	**-0.146**
R												
r	0.770	0.773	0.624	0.747	**0.866**	0.694	0.621	0.647	0.771	0.673	0.719	**0.455**
MBE	-0.313	-0.433	-0.530	-0.480	-0.339	-0.142	-0.053	-0.551	-0.440	-0.682	-0.874	-0.359
RMSE	1.465	1.413	1.207	0.879	0.710	0.671	0.942	1.008	1.167	1.256	1.391	1.972
d	0.818	0.799	0.730	0.777	0.839	0.801	0.732	0.743	0.797	0.742	0.746	0.699
c	0.630	0.617	0.455	0.580	0.727	0.556	0.455	0.481	0.614	0.500	0.536	0.318
NSE	0.534	0.503	0.170	0.370	0.677	0.426	0.214	0.159	0.483	0.204	0.199	-0.383

According to Table 1.10, for L2, the Hu model was the most expressive, followed by the Ch model. It was observed that the Hu model showed values of r between -0.145 and 0.627; of MBE between -0.157 and 0.108; RMSE between 0.971 and 2.460; d between 0.580 and 0.796; c between -0.101 and 0.495 and NSE between -0.580 and 0.364. It should be noted that, although the Hu model has the highest number of indexes, the applied statistical indices did not present such good results for the models in this locality.

Table 1.10 - Results of the statistical indexes of the models for L2.

	Jan	**Feb**	**Mar**	**Apr**	**May**	**Jun**	**Jul**	**Aug**	**Sep**	**Oct**	**Nov**	**Dec**
Ch												
r	0.481	0.468	**0.522**	0.606	**0.680**	0.554	**0.401**	**0.205**	0.483	0.364	-0.133	0.286
MBE	**-0.155**	-0.039	-0.137	**0.011**	**0.020**	**0.100**	0.084	0.026	-0.109	-0.111	**-0.101**	**-0.031**
RMSE	1.476	1.242	**1.350**	1.034	**1.053**	0.998	1.134	**1.355**	1.295	1.490	**2.369**	**1.726**
d	0.721	0.766	**0.761**	0.790	0.762	0.756	0.750	**0.646**	0.766	**0.761**	**0.709**	0.466
c	0.347	0.358	**0.397**	0.479	**0.518**	0.419	**0.301**	0.133	0.370	0.277	-0.094	0.133
NSE	0.015	0.217	**0.250**	0.328	**0.313**	0.246	0.112	**-0.577**	0.227	**0.127**	**-0.313**	**0.034**
Hg												
r	0.529	**0.476**	0.497	**0.622**	0.627	0.581	0.371	0.199	**0.502**	**0.395**	**0.145**	0.350
MBE	13.897	-2.275	3.574	-1.772	9.798	4.574	-4.439	3.909	-3.256	-0.425	5.432	12.064
RMSE	13.975	2.589	3.829	2.035	9.860	4.675	4.578	4.141	3.497	1.529	5.849	12.195
d	0.144	0.533	0.443	0.546	0.186	0.312	0.309	0.317	0.459	0.752	0.408	0.185
c	0.076	0.254	0.220	0.340	0.117	0.181	0.115	0.063	0.230	0.297	**0.059**	0.065
NSE	-87.29	-2.402	-5.040	-1.603	-59.29	-15.53	-13.46	-13.73	-4.639	0.080	-7.001	-47.21
Hu												
r	0.529	**0.476**	0.497	**0.622**	0.627	0.581	0.371	0.199	**0.502**	**0.395**	-0.145	0.350
MBE	-0.157	**-0.019**	**-0.126**	0.018	0.044	0.108	**0.079**	**0.024**	**-0.108**	**-0.095**	-0.105	-0.051
RMSE	1.467	**1.235**	1.376	**1.006**	1.067	**0.971**	**1.123**	1.356	**1.279**	**1.477**	2.460	1.783
d	0.721	**0.767**	0.756	**0.796**	**0.763**	**0.762**	**0.757**	0.645	**0.769**	0.760	0.696	**0.580**
Hu												
c	0.381	**0.366**	0.375	**0.495**	0.478	**0.442**	0.281	**0.128**	**0.386**	**0.300**	-0.101	**0.203**
NSE	0.028	**0.225**	0.220	**0.364**	0.294	**0.287**	**0.130**	-0.580	**0.246**	0.143	-0.415	-0.031
R												
r	**0.552**	**0.476**	0.485	0.621	0.572	**0.588**	0.375	0.195	0.500	0.394	-0.116	**0.352**
MBE	-0.341	-0.649	-0.468	-0.519	0.426	0.131	-0.335	-0.090	-0.870	-0.854	-0.658	-0.620
RMSE	**1.389**	1.399	1.478	1.145	1.257	0.955	1.188	1.403	1.552	1.698	2.495	1.764
d	**0.737**	0.726	0.734	0.754	0.716	0.769	0.740	0.629	0.711	0.722	0.686	0.491
c	**0.406**	0.346	0.356	0.468	0.410	0.452	0.277	0.123	0.356	0.284	-0.080	0.173
NSE	**0.128**	0.007	0.100	0.176	0.021	0.310	0.027	-0.690	-0.111	-0.133	-0.456	-0.009

According to Table 1.11, for L3, the Hu model showed greater prominence, followed by the Ch model. It was observed that the Hu model showed values of r

between 0.406 and 0.893; of MBE between -0.071 and 0.056; RMSE between 0.656 and 1.237; d between 0.758 and 0.882; c between 0.308 and 0.787 and NSE between 0.156 and 0.757. The model of Ch also presented good results of the indices for L3, with performance similar to the Hu model.

Table 1.11 - Results of the statistical indexes of the models for L3

	Jan	Feb	Mar	Apr	May	Jun	Jul	Aug	Sep	Oct	Nov	Dec
Ch												
r	0.827	0.848	0.884	0.807	0.778	**0.426**	0.842	0.768	**0.774**	**0.684**	**0.769**	0.704
MBE	**-0.019**	**-0.022**	-0.010	**0.022**	-0.010	**0.053**	**-0.001**	**0.000**	**-0.067**	0.002	-0.019	**0.036**
RMSE	0.980	0.934	0.906	0.918	**0.625**	**0.833**	0.665	0.753	**1.068**	**1.030**	**1.215**	1.000
d	0.855	0.869	0.877	0.843	**0.833**	**0.761**	0.861	0.828	**0.820**	**0.806**	**0.832**	0.790
C	0.707	0.737	0.775	0.680	**0.648**	**0.325**	0.725	0.636	**0.635**	**0.552**	**0.641**	0.556
NSE	0.684	0.718	0.744	0.616	**0.592**	**0.177**	0.691	0.564	**0.586**	**0.450**	**0.570**	0.449
Hg												
r	**0.835**	0.869	**0.893**	**0.821**	0.778	0.406	**0.845**	**0.772**	0.745	0.674	0.753	0.717
MBE	9.296	12.248	2.000	3.227	-1.556	-3.307	1.079	-1.996	7.314	0.055	7.976	8.544
RMSE	9.345	12.280	2.187	3.353	1.678	3.412	1.263	2.132	7.402	1.040	8.072	8.599
d	0.256	0.208	0.646	0.469	0.553	0.302	0.702	0.518	0.280	0.804	0.294	0.219
c	0.213	0.181	0.577	0.385	0.430	0.123	0.594	0.399	0.209	0.542	0.221	0.157
NSE	-27.78	-47.79	-0.489	-4.128	-1.935	-12.82	-0.116	-2.489	-18.87	0.439	-17.97	-39.74
Hu												
r	**0.835**	0.869	**0.893**	**0.821**	0.778	0.406	**0.845**	**0.772**	0.745	0.674	0.753	0.717
MBE	-0.025	-0.024	**-0.002**	**0.020**	**0.001**	0.056	-0.007	-0.012	-0.071	**-0.001**	**-0.013**	0.047
RMSE	**0.962**	**0.878**	**0.883**	**0.906**	0.629	0.843	**0.656**	**0.751**	1.137	1.038	1.237	**0.966**
d	**0.860**	**0.879**	**0.882**	**0.845**	0.832	0.758	**0.863**	**0.829**	0.805	0.804	0.828	**0.799**
c	**0.718**	**0.764**	**0.787**	**0.693**	0.647	0.308	**0.729**	**0.639**	0.600	0.542	0.624	**0.573**
NSE	**0.695**	**0.751**	**0.757**	**0.626**	0.587	0.156	**0.698**	**0.567**	0.531	0.441	0.554	**0.486**
R												
r	**0.835**	**0.877**	**0.893**	0.820	**0.779**	0.412	**0.845**	0.771	0.731	0.676	0.744	**0.719**
MBE	-0.405	-0.276	-0.559	-0.450	-0.505	-0.474	-0.445	-0.650	-0.375	-0.740	-0.419	-0.288
RMSE	1.055	0.902	1.036	1.046	0.806	0.967	0.802	0.995	1.198	1.291	1.324	1.020
d	0.843	0.874	0.844	0.813	0.769	0.713	0.822	0.754	0.799	0.741	0.810	0.781
c	0.704	0.766	0.754	0.667	0.600	0.294	0.694	0.581	0.584	0.500	0.603	0.562
NSE	0.633	0.737	0.666	0.501	0.322	-0.109	0.550	0.241	0.479	0.136	0.490	0.426

According to Table 1.12, for L4, the Hu model showed greater prominence, followed by the Ch model, with equivalence in the performance of the two models. It was observed that the Hu model showed values of r between 0.529 and 0.876; of MBE between -0.068 and 0.035; RMSE between 0.357 and 1.616; d between 0.760 and 0.875; c between 0.411 and 0.766 and NSE between 0.274 and 0.751.

Table 1.12 - Results of the statistical indexes of the models for L4.

	Jan	Feb	Mar	Apr	May	Jun	Jul	Aug	Sep	Oct	Nov	Dec
Ch												
r	**0.591**	**0.639**	0.842	**0.887**	0.702	0.840	**0.697**	**0.559**	0.728	0.706	0.624	0.764
MBE	**-0.021**	**0.017**	**0.013**	0.036	0.033	**0.000**	**0.001**	-0.050	**-0.030**	**-0.015**	-0.076	0.036
RMSE	**1.308**	**1.608**	0.770	**0.580**	0.851	0.383	0.807	**0.765**	0.978	0.980	1.240	0.883
d	**0.780**	0.759	0.850	**0.880**	0.807	0.848	0.780	**0.780**	0.811	0.800	**0.786**	0.827
c	**0.461**	**0.486**	0.716	**0.780**	0.566	0.712	0.544	**0.436**	0.591	0.565	0.491	0.632
NSE	**0.348**	**0.295**	0.709	**0.761**	0.437	0.698	0.349	**0.307**	0.527	0.493	0.387	0.553
Hg												
r	0.570	0.635	0.849	0.876	**0.718**	**0.865**	**0.697**	0.529	**0.751**	0.720	0.658	**0.771**
MBE	5.871	17.170	3.774	0.292	-3.031	-0.239	4.157	-5.183	-3.612	3.322	3.949	-1.027
RMSE	6.021	17.246	3.848	0.656	3.139	0.430	4.231	5.241	3.734	3.459	4.131	1.338
d	0.340	0.163	0.421	0.850	0.423	0.822	0.315	0.236	0.421	0.430	0.408	0.705
c	0.193	0.104	0.358	0.745	0.304	0.712	0.220	0.125	0.316	0.309	0.268	0.544
NSE	-12.80	-80.10	-6.260	0.694	-6.649	0.620	-16.87	-31.50	-5.895	-5.312	-5.799	-0.026
Hu												
r	0.570	0.635	0.849	0.876	**0.718**	**0.865**	**0.697**	0.529	**0.751**	0.720	0.658	**0.771**
MBE	-0.024	0.019	0.014	**0.035**	**0.016**	-0.003	-0.015	**-0.042**	-0.049	-0.024	**-0.068**	**0.034**
RMSE	1.335	1.616	**0.755**	0.593	**0.816**	**0.357**	0.791	0.783	**0.944**	**0.965**	**1.215**	**0.858**
d	0.773	**0.760**	**0.853**	0.875	**0.813**	**0.855**	**0.787**	0.777	**0.818**	**0.801**	0.776	**0.831**
c	0.440	0.483	**0.724**	0.766	**0.584**	**0.740**	**0.549**	0.411	**0.614**	**0.576**	**0.511**	**0.641**
NSE	0.322	0.288	**0.720**	0.751	**0.483**	**0.737**	**0.376**	0.274	**0.559**	**0.509**	**0.411**	**0.578**
R												
r	0.562	0.627	**0.850**	0.876	**0.718**	**0.865**	0.695	0.544	0.747	**0.721**	**0.659**	**0.771**
MBE	-0.342	0.192	-0.324	-0.379	-0.527	-0.264	-0.044	-0.694	-0.656	-0.406	-0.615	-0.577
RMSE	1.386	1.650	0.821	0.715	0.998	0.442	**0.764**	1.041	1.158	1.037	1.342	1.052
d	0.767	0.756	0.831	0.847	0.757	0.817	0.793	0.688	0.765	0.787	0.756	0.777
c	0.431	0.474	0.706	0.742	0.544	0.706	0.551	0.374	0.572	0.568	0.498	0.600
NSE	0.269	0.258	0.670	0.637	0.226	0.599	0.417	-0.281	0.337	0.433	0.283	0.366

For L5, (Table 1.13), the Hu model showed greater prominence, followed by the Ch model. It was observed that the Hu model showed values of r between 0.334 and 0.727; of MBE between -0.174 and 0.047; RMSE between 0.076 and 1.681; d between 0.702 and 0.818; c between -0.432 and 0.594 and NSE between -0.018 and 1.585. It is noteworthy that, despite the presented values, the models did not obtain good results regarding the statistical indices.

Table 1.13 - Results of the statistical indexes of the models for L5.

	Jan	Feb	Mar	Apr	May	Jun	Jul	Aug	Sep	Oct	Nov	Dec
Ch												
r	0.671	**0.496**	0.593	0.624	-0.578	0.307	0.368	0.711	0.594	0.475	-0.518	0.464
MBE	-0.046	**0.009**	**0.013**	**0.011**	**0.029**	**0.019**	**0.031**	-0.006	0.003	**-0.006**	-0.175	**0.043**
RMSE	1.207	**1.677**	**1.298**	0.083	1.236	0.199	1.269	0.801	**0.076**	1.273	1.661	1.245
d	0.807	**0.772**	**0.710**	0.792	0.732	**0.747**	0.725	0.815	**0.781**	0.768	0.731	0.764
c	0.542	**0.383**	**0.421**	0.495	-0.423	0.229	0.267	0.580	0.464	0.365	-0.379	0.355
NSE	0.429	0.243	**0.116**	**1.184**	**-0.146**	1.578	-0.006	0.506	1.173	0.152	-0.149	**0.116**
Hg												
r	**0.703**	0.493	**0.594**	**0.631**	**-0.655**	0.334	0.389	**0.727**	**0.608**	**0.529**	**-0.578**	**0.503**
MBE	-3.327	2.301	8.848	0.021	-12.72	0.342	3.307	-0.979	-0.139	-9.308	-20.84	-16.47
RMSE	3.520	2.850	8.946	0.084	12.77	0.426	3.528	1.255	0.155	9.389	20.90	16.52
d	0.479	0.595	0.219	0.788	0.125	0.445	0.395	0.681	0.513	0.211	0.105	0.111
c	0.337	0.294	0.130	0.497	-0.082	0.149	0.154	0.495	0.312	0.112	-0.061	0.056
NSE	-3.852	-1.185	-41.01	1.186	-121.5	5.081	-6.774	-0.212	1.839	-45.11	-180.8	-154.6
Hu												
r	**0.703**	0.493	**0.594**	**0.631**	**0.655**	0.334	0.389	**0.727**	**0.608**	**0.529**	**-0.578**	**0.503**
MBE	**-0.042**	0.015	0.047	0.012	0.039	0.020	0.040	**0.005**	**0.002**	0.018	**-0.174**	0.044
RMSE	**1.151**	1.681	1.303	**0.082**	**1.141**	0.198	1.228	**0.784**	**0.076**	**1.229**	**1.564**	**1.241**
d	**0.814**	0.771	0.702	**0.793**	**0.753**	0.741	**0.736**	**0.818**	0.770	**0.775**	**0.747**	**0.765**
c	**0.572**	0.380	0.417	**0.501**	0.493	**0.248**	**0.286**	**0.594**	**0.468**	**0.410**	-0.432	**0.385**
NSE	**0.482**	**0.240**	0.108	1.181	0.022	**1.585**	**0.059**	**0.527**	**1.175**	**0.210**	-0.018	0.122
R												
r	0.691	0.492	0.587	**0.631**	-0.548	**0.339**	**0.392**	0.726	0.607	0.352	-0.499	0.467
MBE	-0.947	-0.602	-0.224	-0.023	-0.730	-0.009	-0.262	-0.455	-0.048	-1.275	-1.235	-0.985
RMSE	1.557	1.790	1.379	0.081	1.409	**0.190**	**1.226**	0.907	0.087	1.862	2.086	1.611
d	0.732	0.750	0.688	0.771	0.676	0.738	0.743	0.779	0.701	0.629	0.646	0.670
c	0.506	0.369	0.404	0.486	-0.370	0.251	0.291	0.565	0.426	0.222	-0.322	0.313
NSE	0.051	0.138	0.002	1.207	-0.490	1.599	0.061	0.367	1.264	-0.814	-0.812	-0.478

For L6, according to Table 1.14, the Ch model showed greater prominence, followed by the Hu model, with similar performance. It was observed that the Ch model presented values of r between -0.391 and 0.790; of MBE between -0.069 and 0.024; RMSE between 0.672 and 1.492; d between 0.736 and 0.822; c between -0.288 and 0.649 and NSE between -0.109 and 0.617.

Table 1.14 - Results of the statistical indexes of the models for L6.

(to be continued)

	Jan	Feb	Mar	Apr	May	Jun	Jul	Aug	Sep	Oct	Nov	Dec
Ch												
r	0.741	0.498	0.079	0.429	**0.790**	**0.767**	**0.625**	**0.419**	-0.212	**-0.391**	0.644	0.607
MBE	**-0.057**	**0.000**	-0.038	**0.002**	-0.041	**-0.038**	-0.069	-0.021	**-0.064**	**0.000**	**-0.037**	0.024
RMSE	1.199	1.450	**1.327**	1.037	**0.676**	**0.672**	**0.988**	**0.840**	**1.490**	1.450	1.151	1.492

Table 1.14 - Results of the statistical indexes of the models for L6.

(conclusion)

	Jan	Feb	Mar	Apr	May	Jun	Jul	Aug	Sep	Oct	Nov	Dec
d	0.820	0.774	**0.750**	0.767	**0.822**	**0.814**	**0.761**	**0.766**	**0.746**	0.736	0.793	0.781
c	0.608	0.386	0.059	0.329	**0.649**	**0.624**	**0.476**	**0.321**	-0.158	-0.288	0.511	0.474
NSE	0.548	0.229	**0.003**	0.162	**0.617**	**0.443**	**0.092**	**0.168**	**-0.028**	-0.109	0.344	0.244
Hg												
r	0.762	**0.518**	**0.418**	**0.468**	0.780	0.760	-0.607	0.390	-0.422	-0.436	**0.664**	**0.626**
MBE	3.373	-9.943	-19.24	-9.921	1.107	-7.167	-20.78	-11.54	-19.67	-21.94	-10.50	-11.03
RMSE	3.565	10.05	19.29	9.972	1.303	7.199	20.83	11.58	19.73	21.99	10.56	11.13
d	0.529	0.237	0.106	0.154	0.644	0.174	0.071	0.116	0.112	0.090	0.170	0.204
c	0.403	0.123	0.044	0.072	0.502	0.132	-0.043	0.045	**-0.047**	**-0.039**	0.113	0.128
NSE	-2.994	-36.01	-209.5	-76.48	-0.422	-62.93	-402.9	-157.0	-179.1	-254.0	-54.15	-41.03
Hu												
r	0.762	**0.518**	**-0.418**	**0.468**	0.780	0.760	-0.607	0.390	-0.422	-0.436	**0.664**	**0.626**
MBE	-0.062	0.006	**-0.029**	0.026	**-0.017**	-0.042	**-0.068**	**-0.019**	-0.078	0.008	-0.042	**0.023**
RMSE	**1.157**	**1.432**	1.338	**1.023**	0.686	0.683	1.254	0.861	1.551	**1.429**	**1.136**	**1.476**
d	**0.830**	**0.777**	0.748	**0.771**	0.821	0.810	0.697	0.764	0.736	**0.740**	**0.796**	**0.783**
c	**0.632**	**0.402**	-0.313	**0.361**	0.640	0.616	-0.423	0.298	-0.311	-0.323	**0.529**	**0.490**
NSE	**0.580**	**0.248**	-0.013	**0.185**	0.605	0.425	-0.464	0.125	-0.114	**-0.077**	**0.362**	**0.260**
R												
r	**0.765**	0.509	0.362	0.445	0.775	0.766	-0.559	0.412	**-0.177**	-0.408	0.658	0.620
MBE	-0.698	-0.811	-0.794	-0.693	-0.489	-0.579	-0.660	-0.639	-1.132	-1.112	-1.036	-1.041
RMSE	1.344	1.651	1.518	1.245	0.858	0.871	1.262	1.056	1.866	1.848	1.532	1.774
d	0.782	0.729	0.695	0.704	0.766	0.733	0.678	0.685	0.665	0.639	0.695	0.716
c	0.598	0.371	**0.251**	0.313	0.593	0.561	-0.379	0.282	-0.117	-0.261	0.457	0.444
NSE	0.432	0.000	-0.303	-0.207	0.383	0.064	-0.484	-0.315	-0.611	-0.801	-0.160	-0.068

According to Table 1.15, for L7, the Ch model showed greater prominence, followed by the Hu model, with similar performance. It was observed that the Ch model presented values of r between -0.164 and 0.851; of MBE between -0.097 and 0.058; RMSE between 0.992 and 2.114; d between 0.728 and 0.862; c between -0.1212 and 0.734 and NSE between -0.026 and 0.720.

Table 1.15 - Results of the statistical indexes of the models for L7.

(to be continued)

	Jan	Feb	Mar	Apr	May	Jun	Jul	Aug	Sep	Oct	Nov	Dec
Ch												
r	0.851	0.640	0.542	-0.164	0.496	**0.368**	0.669	0.523	0.761	0.510	**0.813**	**0.725**
MBE	**-0.034**	**0.058**	**-0.069**	-0.039	**-0.006**	**-0.071**	-0.097	0.020	**-0.053**	-0.018	**-0.042**	**0.020**
RMSE	**1.005**	**1.437**	1.442	**2.114**	1.618	1.538	0.992	1.096	1.133	1.235	**1.161**	**1.122**
d	0.862	**0.795**	0.766	**0.747**	0.775	0.754	0.788	0.728	0.808	**0.755**	**0.829**	**0.819**
c	**0.734**	**0.509**	0.415	-0.122	0.384	**0.277**	0.527	0.381	0.615	0.385	**0.674**	**0.594**
NSE	**0.720**	**0.360**	0.260	**-0.026**	0.220	**0.117**	0.300	0.110	0.547	0.234	**0.530**	**0.516**

Table 1.15 - Results of the statistical indexes of the models for L7.

(conclusion)

	Jan	Feb	Mar	Apr	May	Jun	Jul	Aug	Sep	Oct	Nov	Dec
Hg												
r	0.851	0.640	0.544	**-0.134**	**0.503**	0.352	0.674	0.549	**0.762**	0.596	0.793	0.718
MBE	6.292	-5.740	11.84	-27.18	-2.040	0.424	-6.487	12.30	9.659	8.276	-4.413	0.365
RMSE	6.373	5.922	11.92	27.27	2.594	1.593	6.561	12.35	9.724	8.354	4.569	1.199
d	0.359	0.367	0.195	0.082	0.617	0.743	0.246	0.137	0.240	0.231	0.382	0.801
c	0.306	0.235	0.106	-0.011	0.310	0.261	0.166	0.075	0.183	0.137	0.303	0.575
NSE	-10.24	-9.864	-49.58	-169.6	-1.006	0.052	-29.63	-112.1	-32.39	-34.03	-6.283	0.448
Hu												
r	0.851	0.640	0.544	**-0.134**	**0.503**	0.352	0.674	0.549	**0.762**	0.596	0.793	0.718
MBE	-0.035	0.065	-0.077	**-0.010**	-0.013	-0.076	**-0.094**	**0.005**	-0.054	**-0.010**	-0.044	0.025
RMSE	1.009	1.461	**1.418**	2.171	**1.602**	**1.537**	**0.981**	1.113	**1.115**	**1.140**	1.184	1.142
d	**0.863**	0.792	**0.772**	0.738	**0.777**	**0.757**	**0.791**	0.716	**0.809**	0.774	0.824	0.816
c	0.734	0.507	**0.420**	**-0.099**	**0.390**	0.266	**0.533**	0.393	**0.616**	**0.461**	0.654	0.586
NSE	0.718	0.339	**0.284**	-0.082	**0.235**	0.118	**0.316**	0.083	**0.561**	**0.347**	0.511	0.499
R												
r	0.851	**0.641**	**0.547**	-0.181	0.502	0.346	**0.676**	**0.550**	0.751	**0.613**	0.794	0.717
MBE	-0.625	-0.631	-0.340	-0.860	-0.777	-0.508	-0.694	-0.138	-0.375	-0.709	-0.880	-0.657
RMSE	1.190	1.551	1.487	2.329	1.797	1.635	1.177	**1.057**	1.206	1.321	1.434	1.313
d	0.829	0.773	0.759	0.711	0.743	0.738	0.724	**0.736**	0.791	0.733	0.762	0.775
c	0.705	0.495	0.415	-0.129	0.373	0.255	0.489	**0.405**	0.594	0.449	0.605	0.556
NSE	0.608	0.254	0.213	-0.244	0.038	0.002	0.014	**0.172**	0.487	0.124	0.282	0.338

According to Table 1.16, for L8, the Ch model showed greater prominence, followed by the Hu model, with similar performance. It was observed that the Ch model presented values of r between -0.206 and 0.399; of MBE between -0.156 and 0.050; RMSE between 0.771 and 1.826; d between 0.725 and 0.761; c between -0.150 and 0.294 and NSE between -0.182 and 0.114. It should be noted that, for this location, the indices did not present good results for the models.

Table 1.16 - Results of the statistical indexes of the models for L8.

(to be continued)

	Jan	Feb	Mar	Apr	May	Jun	Jul	Aug	Sep	Oct	Nov	Dec
Ch												
r	-0.206	**0.302**	0.383	0.062	-0.107	0.191	0.333	**0.367**	**0.399**	-0.055	0.139	0.028
MBE	0.032	**-0.055**	-0.153	**0.050**	**0.005**	-0.051	-0.028	**0.013**	**0.025**	**0.091**	-0.156	-0.024
RMSE	**1.544**	**1.633**	**1.481**	**1.266**	**0.976**	0.771	**0.882**	**0.857**	1.286	**1.403**	1.826	**1.626**
d	**0.725**	**0.753**	**0.761**	**0.750**	**0.748**	0.746	**0.757**	0.736	0.736	**0.749**	0.750	**0.745**
c	-0.150	**0.228**	0.292	0.046	-0.080	0.142	0.252	0.270	**0.294**	-0.041	0.104	0.021
NSE	**-0.182**	**0.030**	**0.114**	**0.002**	**-0.016**	0.017	**0.057**	0.045	0.084	**-0.007**	0.010	**-0.023**
Hg												
r	-0.234	0.301	**0.392**	0.238	-0.269	**0.339**	**0.382**	0.366	0.373	-0.171	**0.193**	-0.003
MBE	-26.48	-15.63	-8.443	-12.70	-12.23	-4.062	-8.439	-1.387	-5.295	-15.59	-12.21	-24.73

Table 1.16 - Results of the statistical indexes of the models for L8.

(conclusion)

	Jan	Feb	Mar	Apr	May	Jun	Jul	Aug	Sep	Oct	Nov	Dec
RMSE	26.52	15.71	8.570	12.76	12.27	4.127	8.486	1.623	5.441	15.66	12.34	24.79
d	0.077	0.145	0.230	0.148	0.118	0.251	0.160	0.519	0.298	0.132	0.206	0.092
c	**-0.018**	0.044	0.090	0.035	-0.032	0.085	0.061	0.190	0.111	**-0.023**	0.040	0.000
NSE	-347.9	-88.89	-28.68	-100.4	-159.6	-27.16	-86.25	-2.424	-15.41	-124.4	-44.21	-236.7
Hu												
r	-0.234	0.301	**0.392**	0.238	-0.269	**0.339**	**0.382**	0.366	0.373	-0.171	**0.193**	-0.003
MBE	**0.031**	-0.058	**-0.146**	0.072	0.019	**-0.048**	**-0.016**	0.035	0.037	0.105	**-0.140**	**-0.019**
RMSE	1.561	**1.633**	1.483	1.269	1.003	**0.733**	0.893	0.839	**1.254**	1.441	**1.810**	1.628
d	0.722	**0.753**	**0.761**	0.749	0.740	**0.759**	0.754	**0.745**	**0.755**	0.741	**0.752**	**0.745**
c	-0.169	0.227	**0.298**	0.178	-0.199	**0.257**	**0.288**	**0.273**	0.281	-0.127	**0.145**	**-0.002**
NSE	-0.208	**0.030**	0.111	-0.003	-0.073	**0.111**	0.034	**0.085**	**0.129**	-0.062	**0.027**	-0.026
R												
r	**-0.185**	0.288	0.388	**0.294**	**0.322**	0.305	0.357	**0.367**	0.371	**0.172**	0.168	**0.036**
MBE	-0.891	-1.102	-1.054	-0.866	-0.790	-0.522	-0.748	-0.773	-0.588	-0.861	-1.298	-1.113
RMSE	1.823	1.952	1.805	1.522	1.211	0.911	1.141	1.133	1.404	1.634	2.227	1.957
d	0.662	0.687	0.691	0.678	0.652	0.675	0.651	0.642	0.708	0.685	0.671	0.673
c	-0.122	0.198	0.268	**0.200**	**0.210**	0.206	0.233	0.235	0.262	0.118	0.113	0.024
NSE	-0.648	-0.387	-0.317	-0.441	-0.565	-0.372	-0.576	-0.669	-0.092	-0.366	-0.473	-0.483

Figure 1.3 shows the annual trends of observed and estimated R_G values through the studied models, for all the locations. It was observed that the Ch and Hu models showed a behavior similar to the observed values, for all localities, with values very close to each other. For these models, annual R_G values varied between 8 and 23 MJ/m².day^{-1} considering all the locations.

The model of R showed a seasonal behavior similar to the observed values, however, the data estimated by this model were approximately 3.6% lower than those observed for all the localities. On the other hand, the Hg model presented the worst annual trend for all the localities. The values oscillate every month, sometimes the model overestimates the data, sometimes underestimates them. The Hg model reached values of R_G between 0.26 and 33.7 MJ/m², very extreme values when compared with the values observed and obtained by the Ch and Hu models.

Figure 1.3 - Annual trends of observed and estimated R_G values

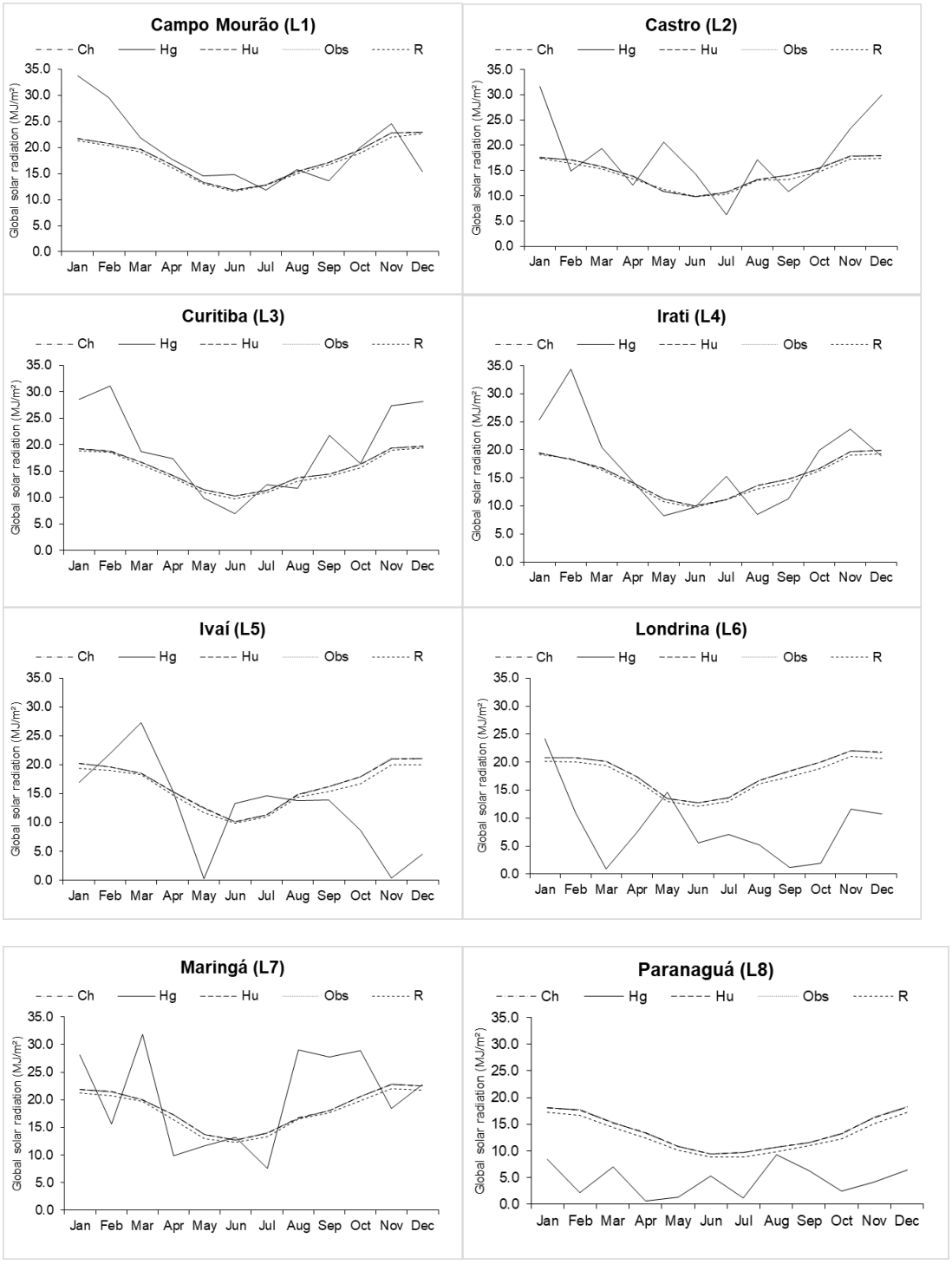

As for the calibrated coefficients of the models, considering all the localities, the coefficient α of the Ch model varied between -0.548 and 0.973, while the coefficient b varied between -0.232 and 0.467. For the Hg model, the coefficient α ranged from -0.453 to 0.995, while the coefficient b varied from -0.172 to 0.311. The coefficient α of the Hu model varied between -17.505 and 27.742and the coefficient b

varied between -0.178 and 0.313. For the R model, α values ranged from 0.046 to 0.906, while b values ranged from -0.304 to 0.995.

For the Ch model, Freitas, Simões and Martins (2015) found annual values of α coefficients of 0.236 and b of -0.186 for Belo Horizonte (MG), whereas for the same State, Silva et al. (2012) found values of α equal to 0.315 and of b equal to -0.458. Similarly, Chen et al. (2004), obtained α values between 0.16 and 0.42 and b values between -0.45 and 0.12 for China.

The differences in values are due to the differences in the characteristics of the sites studied and to the adjustment, which was performed annually in the cited works, while in this study, the data adjustment was performed on a monthly basis. Buriol et al. (2012) stresses the importance of adjusting the coefficients on a monthly basis. The significant differences between the lowest and highest values of each coefficient show that the local adjustment of the model can be fundamental in its performance, according to Meza and Varas (2000) on the importance of the models calibration for each locality.

By means of the boxplot graphs (Figure 2), it was possible to verify that, for all the localities, the Ch and Hu models were those that approached the observed values, being possible the use of these models in these localities. The R model only showed similarity to Obs in the locality of L4. It was also observed that the Hg model showed great variability, which makes the use of the model impractical, since it can estimate very extreme values.

Statistically analyzing all the localities (Table 7), the Ch and Hu models did not differ statistically from the values observed in any month, according to the Kruskal-Wallis test with the Dunn method. In general, it was observed that the Hg model presented statistical significance in relation to the other models and values observed for many months. It was also verified that the R model presented oscillation regarding the significance.

As for the studied statistical indices (Tables 8 to 15), the models that presented the highest efficiency were Hu and Ch, with equivalent performance among them. The results of the indexes showed an expressive oscillation, between very bad values and good values, according to each month and locality. Although the Hg model did not present a satisfactory performance for the studied localities of Paraná, Daut et al. (2011) found an excellent performance of this model for Malaysia, with NSE value above 0.8, whereas Chen et al. (2004) found an unsatisfactory NSE

value of 0.44 for China, which confirms that the model performance is influenced by the locality factor, which in turn is related to its local climatology.

The annual trends of observed and estimated RG values (Figure 3) showed that the Ch and Hu models showed a behavior similar to the values observed for all the locations, with values very close to each other. On the other hand, the Hg model presented the worst annual trend.

For the city of Belo Horizonte (MG), Freitas, Simões and Martins (2015) also found that Ch and Hu models were the most accurate to estimate solar radiation. The authors also point out that the Ch model was superior to estimate in the spring and fall months, while the Hu model was superior for the summer and winter months. For localities in China, Chen et al. (2004) showed that the presented model (Ch) obtained an NSE value of 0.85, considered good, and that this model was efficient for the region.

1.4 CONCLUSION

Based on the results found in this research, it was verified that the models proposed by Chen and Hunt showed the best performances in the estimation of the global solar radiation for the evaluated localities of Paraná, since they presented an annual trend and average values similar to the observed historical data.

Moreover, the methods used in this research for the estimation of global solar radiation have simplicity in their application, since they only require the value of the radiation at the top of the atmosphere, which is calculated by means of physical models and data of air temperature which are easily obtainable, which can certainly contribute to other environmental research, in places where there is no availability of solar radiation data or even where the historical series have failures in the chronological sequences.

CHAPTER 2

ESTIMATING PHOTOVOLTAIC SOLAR ENERGY PRODUCTION FOR BUILDINGS IN CLIMATE CHANGE SCENARIOS

ABSTRACT

Brazilian cities present a great potential for the use of photovoltaic solar energy. The use of this technology may be a strategy to mitigate the effects of regional climate change. This research aimed to determine the estimation of photovoltaic solar energy production for single family residences in scenarios of possible climatic changes projected until the end of the 21st century. For the simulation of the climatic scenarios the software PGECLIMA_R was used. To estimate the electrical power produced by the system, daily data of global solar radiation were used. In order to evaluate the data, the Analysis of Variance (ANOVA), with comparison of means (Tukey's test) were used. The simulated global solar radiation data showed a decreasing trend in relation to historical data. All localities indicated annual rates of 98% of system service, which proves that the State of Paraná has favorable climatic conditions for the installation of these systems.

Keywords: Global solar radiation; Photovoltaic solar energy; Climate changes.

RESUMO

As cidades brasileiras apresentam um grande potencial para a utilização da energia solar fotovoltaica. O uso desta tecnologia pode ser uma estratégia de mitigação dos efeitos da alteração do clima regional. Esta pesquisa objetivou determinar a estimativa de produção de energia solar fotovoltaica para residências do tipo unifamiliar, em cenários de possíveis mudanças climáticas projetadas para o final do século XXI. Para a simulação dos cenários climáticos foi utilizado o software PGECLIMA_R. Para estimar a energia elétrica produzida pelo sistema foram utilizados dados diários de radiação solar global. Para avaliar os dados obtidos foi utilizada a Análise de Variância (ANOVA), com comparação de médias (teste de Tukey). Os dados simulados de radiação solar global apresentaram tendência de decréscimo em relação aos dados históricos. Todas as localidades apontaram índices anuais de 98% de atendimento do sistema, o que comprova que o Estado do Paraná possui condições climáticas favoráveis para a instalação destes sistemas.

Palavras-chave: Radiação solar global; Energia solar fotovoltaica; Mudanças climáticas.

2.1 INTRODUCTION

The energy factor is an essential and a key principle that drives great part of human activity in modern society. The significant population growth observed since the 20th century has led to a considerable increase in demand for energy, especially electricity, and its planning is particularly relevant in the regional context. Therefore, environmental concerns have been raised in search of alternative energy sources, especially renewable sources, which promote the rational use of energy resources and reduction of environmental impacts.

The use of electric energy of hydraulic origin predominates in the Brazilian electrical matrix (68.1%), due to the hydrographic basins that exist in a major part of the territory. However, there are also other sources such as fossil fuels, nuclear and alternative sources such as biomass, wind and solar. Regarding the contribution of solar energy, one of its variants, photovoltaic, has not reached a very expressive interest yet, since it contributes less than 1% in the national electric matrix.

Despite of that, Brazilian cities exhibit great potential for the use of solar energy, due to the large area availability and the high incidence of global solar radiation, which is higher than some developed countries such as Germany, Spain, Japan and also China, which received incentives for their use in homes. In addition, coverage of less than 0.04% of the Brazilian territory with photovoltaic modules could generate more energy than the country's total annual electricity consumption, which is about 500 TWh/year (RÜTHER and SALAMONI, 2011; RÜTHER and ZILLES, 2011, TIEPOLO et al., 2014, TIEPOLO et al., 2016, PEREIRA et al., 2017).

It is estimated that Households represent approximately 21% of total electricity consumption in the country (BRAZIL, 2017), most part are used for the use of air conditioning, electric shower and refrigeration (ELETROBRÁS, 2007). According to Pereira et al. (2017), the maximum values of electric energy demand are recorded in the time between 12 and 15 hours, coinciding with the availability of solar radiation. Thus, the use of integrated systems connected to the grid can reduce demand peaks and eliminate transmission and distribution losses, since the system is installed at the consumption point (JARDIM et al, 2008; RÜTHER et al., 2008).

In Brazil, the regulation for photovoltaic systems connected to the distribution network was defined by the National Electric Energy Agency (ANEEL) in 2012 and the mechanism for compensation of electric energy was foreseen, that is, a system can inject the surplus in the electric grid, with the possibility of accumulating credits to

be compensated in kWh, when the amount of energy generated is lower than the one consumed (PINHO and GALDIINO, 2014, PEREIRA et al., 2017).

The solar energy radiated on the Earth surface is able to produce about 1,700 kWh/m².year of electrical power, enough to meet 10,000 times the world's energy consumption. However, Brazilian localities still have limitations on global solar radiation or sunshine data, either due to the scarcity of measurement equipment or to the flaws that cause data inconsistency. Therefore, in places with no data, it is possible to estimate them by means of empirical models (ALMOROX, HONTORIA and BENITO, 2011; SILVA et al., 2012).

The most widespread methods based on air temperature (HARGREAVES, 1981, BRISTOW and CAMPBELL, 1984, RICHARDSON, 1985, ALLEN, 1997, DONATELLI and CAMPBELL 1998, HUNT et al., 1998) estimated the values of global solar radiation in function of tthe solar extraterrestrial radiation, which is based on the concept of atmospheric transmittance, where it is defined as a linear function related to the duration of solar brightness, or even from the daily thermal amplitude (difference between maximum and minimum daily air temperatures), and these methods comes from a model proposed by Angström (ANGSTRÖM, 1924).

Climate change can affect the energy sector both in the exploration and transformation processes of energy resources, and in the aspects of transport and energy consumption (PBMC, 2013). It is estimated that, by the year 2100, the average global temperature will increase between 1.3 and 4.8ºC, which may lead to a tendency to decrease the demand for heating energy between 36 and 58%, and increase the demand for cooling between 223 and 1050% per year (MARENGO, 2001; FRANK, 2005; IPCC, 2014).

Silva et al. (2015) observed a significant increase in temperatures in most of the State of Paraná between 1976 and 2010. In addition, they found that the tendency of the elevation of minimum air temperatures was higher than the maximum temperatures and that the percentage of days and hot nights increased at a rate of 0.1 to 0.4% per year.

To reduce the risks of socio-environmental disasters, it is necessary to adopt strategies for mitigation and adaptation to climate change. Thus, the use of photovoltaic solar energy can be a strategy to mitigate the effects of regional climate change. This energy source is not very impacting to the environment, because it

does not emit greenhouse gases and avoids the downfalls of energy production during periods of water crisis (BRASIL, 2007; PINHO and GALDINO, 2014).

The State of Paraná holds 80.5% of its municipalities with annual average solar radiation above the Brazilian average (2 kWh/m²). From a comparative perspective, the municipality of Matinhos, which has the lowest annual mean of global solar radiation, is 35% higher than the annual average of Germany. In terms of estimated productivity, the total annual average of Paraná is 58.75% higher than Germany, 1.97% to Spain, and 31.28% to France, certifying the viability of the implantation of photovoltaic systems in the State (TIEPOLO et al., 2014, TIEPOLO et al., 2016).

In view of the foregoing and considering the mitigating and adaptive environmental context for the State of Paraná, this research aimed to determine the estimation of photovoltaic solar energy production for single family homes, in scenarios of possible climatic changes projected towards the end of the 21st century.

2.2 MATERIALS AND METHODS

This research was developed in the Laboratory of Applied Computational Statistics - LECA, of the State University of Ponta Grossa. Eight localities of the State of Paraná (Figure 2.1) were selected from climatological data of conventional meteorological stations (Table 2.1), which are available in the Meteorological Database for Teaching and Research (BDMEP) by the National Institute of Meteorology (INMET).

Figure 2.1 - Selected locations in the State of Paraná

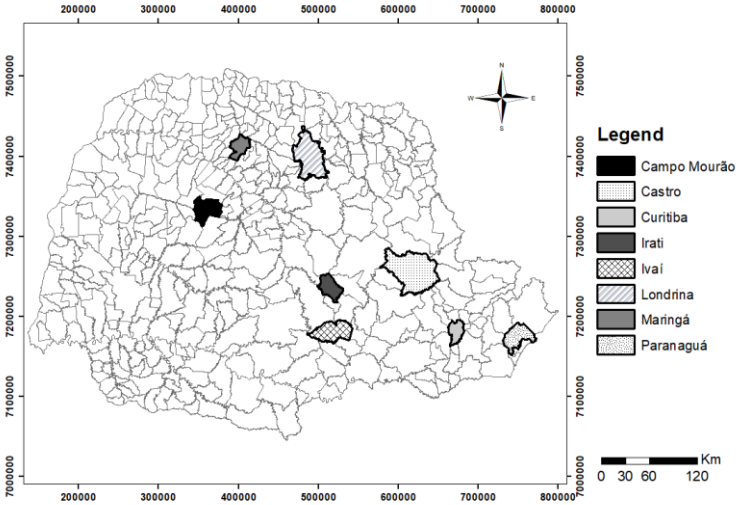

Table 2.1 - Geographical coordinates of selected locations

ID	Locality	Latitude (S)	Longitude (W)	Elevation (m)
L1	Campo Mourão	-24º05’	-52º36’	616
L2	Curitiba	-24º78’	-50º00’	1009
L3	Castro	-25º43’	-49º26’	924
L4	Irati	-25º46’	-50º63’	837
L5	Ivaí	-25º00’	-50º85’	808
L6	Londrina	-23º31’	-51º13’	566
L7	Maringá	-23º40’	-51º91’	542
L8	Paranaguá	-25º53’	-48º51’	5

The State of Paraná belongs to the region of southern Brazil and is located between the parallels 22º30'58 "and 26º43'00" south latitude and between the meridians 48º05'37 "and 54º37'08" west longitude. According to Köppen's climate classification, the State has two types: Cfa - Subtropical climate with average temperature in the coldest month below 18 ºC (mesothermic) and average temperature in the hottest month above 22 ºC, with hot summers, frosts infrequent and trend of rainfall concentration in the summer months, however without a defined dry season; Cfb - Temperate climate with average temperature in the coldest month below 18 ºC (mesothermic), with fresh summers, average temperature in the hottest month below 22 ºC and no dry season defined (IAPAR, 2018).

The daily historical series of pluviometric precipitation, insolation (or hours of solar brightness), minimum and maximum temperatures of the evaluated localities comprised a period of 31 years (1987-2017). The data consistency for the correction of possible faults, as well as the calculation of the global solar radiation from the sunshine data in the unit langley per day (ly/dia), were carried out through the software PGECLIMA_R (VIRGENS FILHO et al., 2013). The software calculates the global solar radiation using the equation of Angström-Prescott (Equation 2.1), and it is necessary to inform the value of the radiation at the top of the atmosphere (R_A) for each day of the year, determined by Equation 2.2, and the values of parameters "a" and "b", which can be 0.25 and 0.50 respectively, in the absence of the adjusted values for each locality.

$$R_G = R_A \times (a + b \times \frac{n}{N}) \quad (2.1)$$

where,
R_G is the global solar radiation in ly/dia;
R_A is the solar radiation at the top of the atmosphere, in ly/dia, given by Equation 2;
n is the daily sunshine;
N is the maximum daily value of hours of solar brightness.

$$R_A = \frac{916,7}{R^2}(\text{sen}\phi\text{sen}\ \delta\ \text{H} + \cos\phi\cos\ \delta\ \text{senH}) \quad (2.2)$$

where,
R is the medium vector radius Earth-Sun = 0,9915;
ϕ is the location latitude;
δ it is the solar declination;
H it is the arccos(-tgϕtgδ)

For the simulation of climatic scenarios in the eight evaluated locations, the PGECLIMA_R software was used, whose daily climatic data were simulated based on the temperature increase predicted by the fifth IPCC report (IPCC, 2014) for two scenarios. The least pessimistic scenario (C1) predicts an overall increase of up to 1.7 °C in the mean maximum and minimum temperatures, while the most pessimistic scenario (C2) predicts an increase of up to 4.8 °C. However, Marengo and Camargo (2008), Minuzzi, Caramori and Borrozino (2010) and Silva et al. (2015) found that the trend of increasing the minimum temperature tends to be higher in relation to the increase of the maximum temperature, that is, with a tendency of decrease of the thermal amplitude, for the South region of Brazil, until the end of the 21st century.

Thus, the simulations projected were: increases of 2.1ºC in the minimum temperature and 1.3ºC in the maximum temperature, for the least pessimistic scenario (C1); and increases of 5.9 ºC in the minimum temperature and 3.7 ºC in the maximum temperature, for the most pessimistic scenario (C2), which results in the average temperatures stipulated by the IPCC for the two scenarios. From these preestablished conditions, three simulations of each scenario were performed for each locality and at the end, the means of the three simulations were obtained, for purposes of reliability of the simulated data, since the simulation is stochastic, that is, based on distributions of probability.

Considering that the fifth IPCC report does not explicitly predict projections for global solar radiation, in the simulation of this climatic variable an estimation method was adopted based on the daily temperature range (which is based on temperature) and on the solar radiation at the top of the atmosphere. Among the existing methods for this, Chen et al. (2004) was chosen for being one of the most recent models and has shown good results in relation to others (BRISTOW and CAMPBELL 1984, HARGREAVES 1981, ALLEN 1997). In Equation 2.3, this method that is based on the technique of linear regression is detailed.

$$R_G = R_A \times a \times \ln(\Delta T) + b \quad (2.3)$$

where,
R_G is global solar radiation;
R_A radiation at the top of the atmosphere;
“a” and “b” are coefficients of the regression equation;
“ΔT” is the thermal amplitude (difference between the maximum and minimum temperatures).

For the determination of coefficients "a" and "b" in Equation 3, the data of the daily historical series of temperature for each locality and month of the year were summarized by the moving averages of 5 years, which were applied to the linear regression model given by Equation 2.4:

$$Y = aX + b \quad (2.4)$$

where,
Y is the atmospheric transmissivity (R_G/R_A), that is, the fraction of R_A that reaches the earth's surface;
X is the natural logarithm of ΔT.

For the survey of the potential residential photovoltaic a single family dwelling was considered in this research, an isolated housing destined to serve as a single family dwelling, consisting of at least a kitchen, a bathroom, a bedroom and a living room. This type of housing was chosen because a large part of the country's housing (around 80%) follows that pattern of house type, and has approximately an area built between 51m² and 75m². In this research, for the evaluation of the hypothetical residence, the value of 75 m² of constructed area was adopted.

Although in the South region, the average number of dwellers per residence is 3 people, in this investigation, it was defined that the residence in question would have 4 dwellers (ELETROBRÁS, 2007; FEDRIGO, GHISI and LAMBERTS, 2009) for this residence would be 10 kWh/day, making an average monthly consumption of 300 kWh/month. Figure 2.2 shows a representation of a standard single-family dwelling with solar panels.

Figure 2.2 - Graphic representation of a standard single family dwelling using solar panels

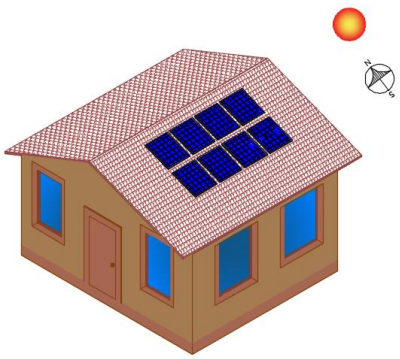

For the estimation of the electric power produced by a photovoltaic system in a residence, the methodology proposed by Marques et al. (2012) was used. The nominal power of installation (P_t) in the unit of kWp is obtained by Equation 5, which is the ratio between the daily electrical consumption of the residence (kWh/day) and the worst case of global solar radiation recorded in the year. However, this methodology was used, first, in the State of Amapá, which has high values of incident solar radiation. That being said, for the application in the State of Paraná, the model was adapted and the average annual global solar radiation (R_{Gyear}) was used in the calculation, because it was verified that the average of the R_G of the State of Paraná approaches the worst R_G case of Amapá.

$$P_t = \frac{Daily\ consumption}{R_{G\ year}} \tag{2.5}$$

To determine the number of solar plates (N_p) required, the nominal power of the installation (P_t) and the nominal power of the plate (P_p), according to Equation 2.6 were used.

$$Np = \frac{P_t}{P_p} \tag{2.6}$$

For application purposes in this research, the chosen solar panel has a P_p of 240 W, an area of 1.65 m² and is available in the market. The calculation of the energy generated, in kWh/m².month by the system (E_g) is expressed in Equation 2.7.

$$E_g = P_t \times \eta \times n_d \times R_{G\ month} \tag{2.7}$$

where:
P_t is the nominal installation power, in kWp;
η is the efficiency of the inverter;
n_d is the number of days in the month;
$R_{G\ month}$ is the monthly average of global solar radiation, in kWh/m².

The efficiency of Equation 2.7 refers to that of the inverter, which converts from direct current to alternating current (DC-AC). The chosen inverter has a yield of 0.97, and for inverters connected to the grid, the minimum acceptable efficiency is 94%.

In order to verify the availability of global solar radiation in the system implementation, the comparison between the observed monthly averages (historical

series) and the simulated monthly averages (2018-2099) were performed by means of statistical analysis. The R_G data were segmented into three periods, P39 (2018-2039), P69 (2040-2069), and P99 (2070-2099).

In the sequence, the data normality was tested by means of the Shapiro-Wilk test, for each locality and month. For data with normal distribution, the one-way ANOVA technique was used, with a significance level of 5%. For non-normal data sets, the Kruskal-Wallis test was used, which is a non-parametric one-way ANOVA for one factor. For the evaluation of trends, graphs were elaborated regarding the global solar radiation and the electric energy generated by the system, as well as determining a monthly percentage of service by the system for the residence.

2.3 RESULTS AND DISCUSSION

Table 2.2 shows the average monthly values of R_G for the historical period (Hist) and simulated periods P39, P69 and P99, in the scenarios C1 and C2 for the locality of Campo Mourão. It was observed that for C1, the months that presented significant differences during the year were February, April and December, whereas for C2, only the month of November did not present statistical significance in the comparison between the historical and simulated periods. It was found that, although impacted by climate change scenarios, the significant differences found in R_G in P39, P69 and P99 were not very significant in magnitude, since the decrease in monthly energy availability was on average of 0, 3 kWh/m^2 in C1 and 0.7 kWh/m^2 in C2.

Table 2.2 - Statistical analysis (ANOVA or KRUSKAL-WALLIS) of the means of R_G (kWh/m²) for Campo Mourão-PR.

(to be continued)

Scenario/Month	p-Anova	p-K-W	Hist	P39	P69	P99
C1						
Jan	0.0863	-	5.97**a**	5.78**a**	5.69**a**	5.53**a**
Fev	0.0059	-	5.91**a**	5.65**ab**	5.59**ab**	5.29**b**
Mar	-	0.1482	5.48**a**	5.33**a**	5.27**a**	5.20**a**
Apr	0.0354	-	4.68**a**	4.53**ab**	4.43**ab**	4.35**b**
May	-	0.1604	3.69**a**	3.62**a**	3.49**a**	3.54**a**
Jun	0.2430	-	3.22**a**	3.07**a**	3.06**a**	3.19**a**
Jul	-	0.2720	3.59**a**	3.44**a**	3.35**a**	3.32**a**
Aug	0.5350	-	4.19**a**	4.15**a**	4.06**a**	4.19**a**
Sep	0.2980	-	4.85**a**	4.59**a**	4.59**a**	4.61**a**
Oct	0.8750	-	5.22**a**	5.24**a**	5.33**a**	5.23**a**
Nov	-	0.3613	6.15**a**	6.31**a**	6.19**a**	6.19**a**
Dec	0.0005	-	6.62**a**	6.26**ab**	6.17**b**	5.87**b**

Table 2.2 - Statistical analysis (ANOVA or KRUSKAL-WALLIS) of the means of R_G (kWh/m²) for Campo Mourão-PR.

(conclusion)

Scenario/Month	p-Anova	p-K-W	Hist	P39	P69	P99
C2						
Jan	0.0000	-	5.97**a**	5.74**a**	5.16**b**	4.93**b**
Fev	0.0000	-	5.91**a**	5.63**a**	5.03**b**	4.72**b**
Mar	0.0001	-	5.48**a**	5.26**ab**	5.08**bc**	4.74**c**
Apr	-	0.0003	4.68**a**	4.34**ab**	4.27**ab**	4.04**b**
May	0.0028		3.69**a**	3.63**ab**	3.28**bc**	3.25**c**
Jun	0.0000	-	3.22**a**	3.09**ab**	2.84**bc**	2.73**c**
Jul	-	0.0016	3.59**a**	3.32**ab**	3.40**a**	2.99**b**
Aug	0.0004	-	4.19**a**	4.20**a**	3.98**ab**	3.82**b**
Sep	0.0197	-	4.85**a**	4.55**ab**	4.33**b**	4.35**b**
Oct	0.0035	-	5.22**a**	5.20**a**	4.94**ab**	4.62**b**
Nov	0.0975	-	6.15**a**	6.21**a**	5.97**a**	5.84**a**
Dec	0.0000	-	6.62**a**	6.15**ab**	5.65**bc**	5.38**c**

Note: Values followed by lower case letters do not differ statistically from each other at the 5% level of significance by the Tukey test

In Figures 3A and 3C, it was observed that for this locality, both the historical and simulated R_G in C1 and C2, presented the same pattern of variation among the months of the year, although the simulated values show a tendency of decrease over of the reproduced periods of P39, P69 and P99, in relation to historical values.

Still looking at Figures 3A and 3B we observed the relationship between R_G, understood in this work as available solar energy, and the generated electric energy (E_g) from R_G. Those of R_G are presented with a more intense color hue, corresponding to the left axis in the graph, while the columns of less intense color refer to the data of E_g, related to the right axis. It was observed a tendency of decrease of E_g over the periods, as a consequence of the reduction of R_G. It was also observed that the values of R_G and E_g were a little higher in C1 when compared to C2, due to the higher temperature increase in C2. Mean values of R_G for Campo Mourão (Figures 3A and 3C) ranged from 2.7 to 6.6 kWh/m², with an annual average of 4.7 kWh/m², while E_g values were in the range between 184 and 389 kWh/month.

Figure 2.3 - Available solar radiation (R_G), Electric power generated from R_G (Eg) and Percentage serviced monthly for each residence in the historical period and up to 2099 in scenarios C1 and C2 for Campo Mourão-PR.

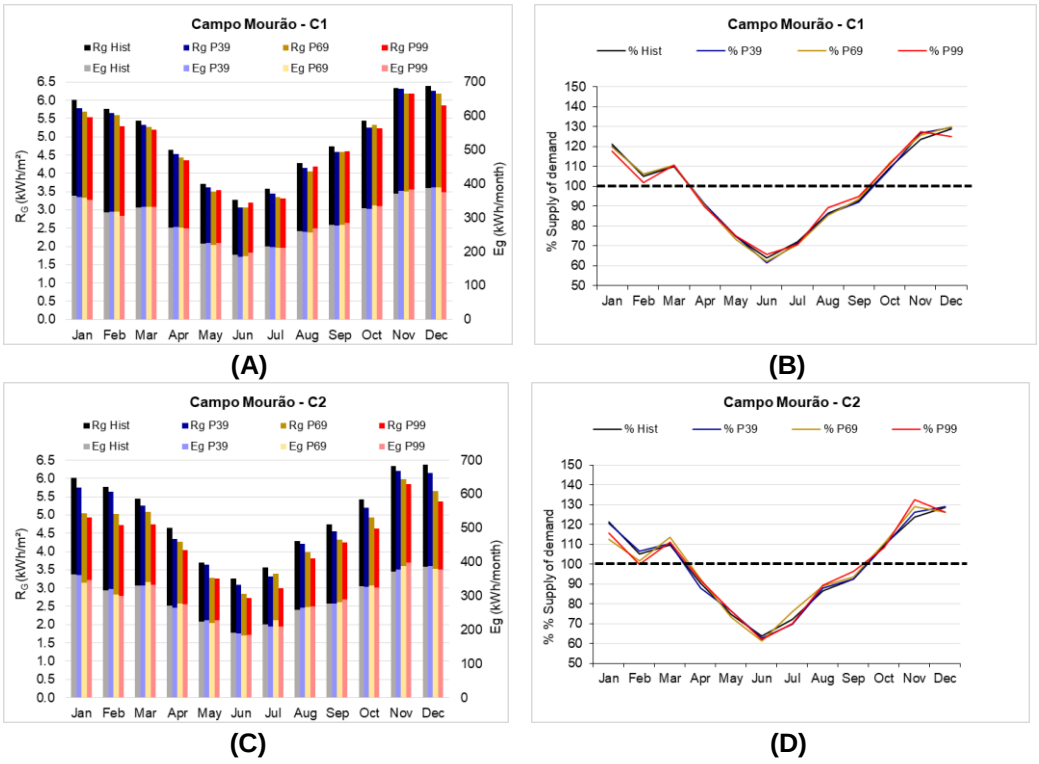

In Figures 3B and 3D the percentages of energy service are verified in the residence for the historical periods, P39, P69 and P99, in scenarios C1 and C2, in which it was considered the service of 100% of the month whose energy that was generated (E_g) was higher than the established consumption of 300 kWh/month. It was observed that the full attendance occurred in the months from October to March, due to the high R_G índices in the period. However, the system deficit period was verified between April and September, and the month that reached the worst energy generation was June, with attendance rates above 60%, while in the best situation, the month of December, provided close service to 130%.

It is possible to consider the percentage of attendance as an annual efficiency metric. When analyzing the annual service, the system presents efficiency of 98%, both for historical periods, P39, P69 and P99 in C1 and for the same periods in C2. That is, in an annual perspective, the residence in this case needs to pay to the concessionaire only 2% of the consumed electric energy. Regarding the number of plates required, the hypothetical residence of the locality of Campo Mourão would require 9 photovoltaic plates in the considered periods and scenarios.

Table 2.3 - Statistical analysis (ANOVA or KRUSKAL-WALLIS) of the means of R_G (kWh/m²) for Castro-PR.

Scenario/Month	p-Anova	p-KW	Hist	P39	P69	P99
C1						
Jan	0.0001	-	4.94**a**	4.74**a**	4.67**a**	4.38**b**
Fev	0.0482	-	4.90**a**	4.67**ab**	4.61**ab**	4.53**b**
Mar	-	0.4626	4.43**a**	4.28**a**	4.36**a**	4.23**a**
Apr	0.3300	-	3.68**a**	3.83**a**	3.77**a**	3.71**a**
May	0.0679	-	2.92**a**	2.87**a**	2.85**a**	2.57**a**
Jun	-	0.5668	2.69**a**	2.71**a**	2.59**a**	2.61**a**
Jul	0.8310	-	2.94**a**	2.98**a**	2.94**a**	2.87**a**
Aug	0.2100	-	3.60**a**	3.66**a**	3.52**a**	3.47**a**
Sep	-	0.8385	3.91**a**	3.88**a**	3.80**a**	3.81**a**
Oct	0.8590	-	4.22**a**	4.19**a**	4.26**a**	4.14**a**
Nov	-	0.2113	5.12**a**	5.13**a**	5.10**a**	5.30**a**
Dec	0.0008	-	5.25**a**	4.75**b**	4.89**ab**	4.58**b**
C2						
Jan	0.0000	-	4.94**a**	4.47**b**	4.10**bc**	3.82**c**
Fev	0.0006	-	4.90**a**	4.62**ab**	4.38**b**	4.25**b**
Mar	0.0023	-	4.43**a**	4.18**ab**	3.86**b**	3.68**b**
Apr	0.0532	-	3.68**a**	3.75**a**	3.57**a**	3.51**a**
May	0.0046	-	2.92**a**	2.71**ab**	2.45**b**	2.33**b**
Jun	-	0.0079	2.69**a**	2.70**ab**	2.41**ab**	2.34**b**
Jul	0.1220	-	2.94**a**	3.00**a**	2.87**a**	2.73**a**
Aug	0.0015	-	3.60**a**	3.58**a**	3.49**a**	3.16**b**
Sep	0.1110	-	3.91**a**	3.69**a**	3.71**a**	3.58**a**
Oct	0.1480	-	4.22**a**	4.20**a**	4.07**a**	3.92**a**
Nov	0.0590	-	5.12**a**	5.26**a**	5.53**a**	5.51**a**
Dec	0.0000	-	5.25**a**	4.80**b**	4.59**bc**	4.40**c**

Note: Values followed by lower case letters do not differ statistically from each other at the 5% level of significance by the Tukey test

For the locality of Castro (Table 2.3), it was verified that the estimated values of R_G n the periods P39, P69 and P99 exhibited significant differences in the C1 for the months of January, February and December, with a small trend of decreasing values, in a period considered of higher temperatures corresponding to the summer season. In the C2 scenario, the months that presented statistical significance were the majority, the months of April, July, September, October and November showing no significant differences in the available energy (R_G) among the periods P39, P69 and P99, demonstrating that the months related to summer tend to show decreases in R_G values throughout the century. However, in absolute terms, these differences with a mean decrease of 0.2 and 0.4 kWh / m² in C1 and C2, respectively, do not have a significant impact on energy availability.

Figure 2.4 - Available solar radiation (R_G), Electric power generated from R_G (Eg) and Percentage serviced monthly for each residence in the historical period and up to 2099 in scenarios C1 and C2 for Castro-PR.

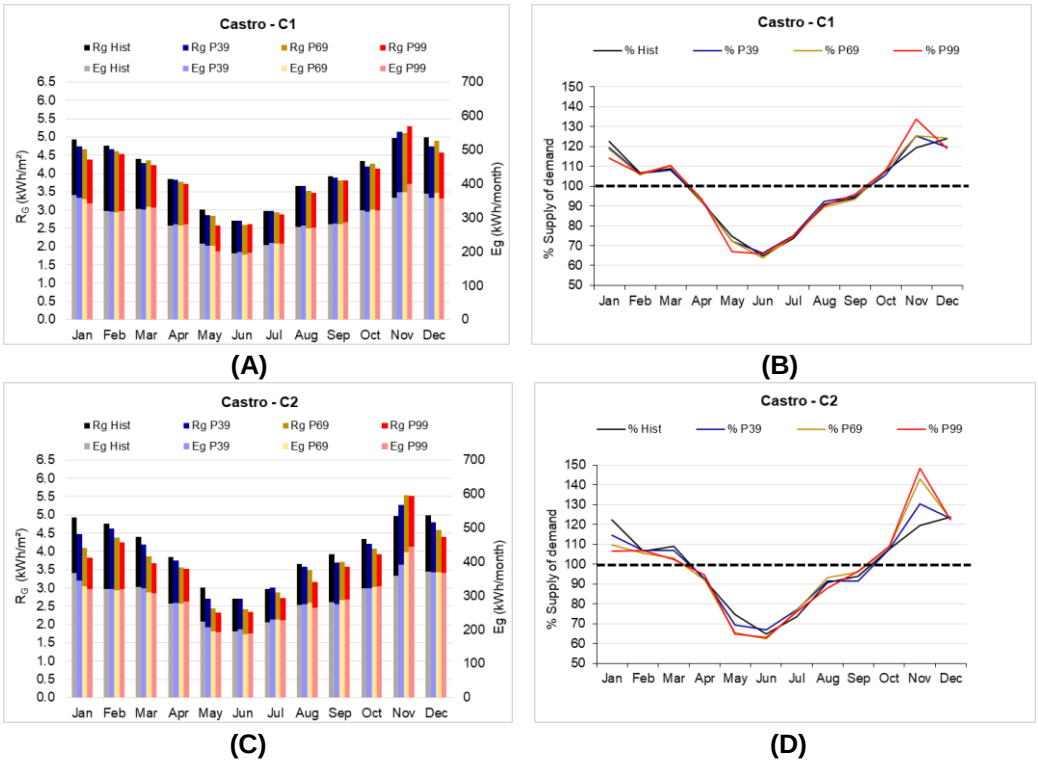

Figures 4A and 4C show that the highest R_G values were between October and March, which comprises approximately the spring and summer seasons, with an average annual value of 3.8 kWh/m² in both scenarios. November has a tendency to increase, with values above 5 kWh/m² in all the evaluated periods. In relation to E_g, values fluctuated between 191 and 445 kWh/month, with the highest generation peak in November, coinciding with the high R_G values for the same month. In general, a trend was found in which values from E_g to C1 (Figure 4A) are higher than for C2 (Figure 4B) in the months between October and March, excluding November, whereas between April and September the values tend to be higher in C2.

In relation to the percentage of monthly attendance (Figures 4B and 4D), the values varied between 62 and 148%, considering the two scenarios (C1 and C2), with the lowest percentages obtained in June and the highest in November. It was observed that the fullness of consumption is supplied by the system in the period from October to March. In the annual scope, the system presented a percentage of attendance of 98% considering all periods and scenarios. As for the number of plates required, the hypothetical residence for the locality of Castro would require 11 plates considering the periods of C1 and 12 plates for C2.

Table 2.4 - Statistical analysis (ANOVA or KRUSKAL-WALLIS) of the means of R_G (kWh/m²) for Curitiba-PR.

Scenario/Month	p-Anova	p-KW	Hist	P39	P69	P99
C1						
Jan	0.0544	-	5.35**a**	5.09**a**	4.94**a**	4.86**a**
Fev	-	0.0031	5.39**a**	4.67**b**	4.74**ab**	4.58**b**
Mar	-	0.2630	4.67**a**	4.55**a**	4.37**a**	4.35**a**
Apr	-	0.0675	3.69**a**	3.62**a**	3.74**a**	3.38**a**
May	0.9640	-	3.10**a**	3.11**a**	3.07**a**	3.10**a**
Jun	-	0.2458	2.76**a**	2.76**a**	2.82**a**	2.73**a**
Jul	0.0323	-	3.20**a**	3.12**ab**	3.01**ab**	2.89**b**
Aug	0.7350	-	3.75**a**	3.76**a**	3.72**a**	3.66**a**
Sep	0.0128	-	4.11**a**	3.76**ab**	3.89**ab**	3.37**b**
Oct	0.7240	-	4.39**a**	4.27**a**	4.30**a**	4.22**a**
Nov	0.0548	-	5.26**a**	5.23**a**	5.26**a**	4.79**a**
Dec	0.2030	-	5.50**a**	5.33**a**	5.13**a**	5.10**a**
C2						
Jan	-	0.0000	5.35**a**	4.94**a**	4.59**ab**	3.96**b**
Fev	0.0000	-	5.39**a**	4.75**b**	4.46**b**	3.76**c**
Mar	0.0003	-	4.67**a**	4.40**ab**	4.10**bc**	3.76**c**
Apr	0.0027	-	3.69**a**	3.64**a**	3.34**ab**	3.18**b**
May	-	0.0018	3.10**a**	3.02**a**	2.90**ab**	2.74**b**
Jun	-	0.0512	2.76**a**	2.81**a**	2.71**a**	2.63**a**
Jul	0.0036	-	3.20**a**	2.99**ab**	2.77**b**	2.73**b**
Aug	-	0.0167	3.75**a**	3.71**a**	3.55**ab**	3.39**b**
Sep	0.0000	-	4.11**a**	3.83**a**	3.29**b**	3.12**b**
Oct	0.0034	-	4.39**a**	4.47**a**	4.16**ab**	3.94**b**
Nov	0.0000	-	5.26**a**	5.13**ab**	4.75**bc**	4.37**c**
Dec	0.0001	-	5.50**a**	5.03**ab**	4.64**b**	4.51**b**

Note: Values followed by lower case letters do not differ statistically from each other at the 5% level of significance by the Tukey test

Table 2.4 presents the values for the Curitiba locality, where there is a trend of decreasing the energy available until the end of the century. In C1, only the months February, July and September have statistical significance, with na average decrease of 0.3 kWh/m² between the historical period and P99. Conversely, for C2, only the month of June did not show a significant decrease in R_G, and the mean reduction was 0.8 kWh/m² in absolute values between the historical period and P99.

The 61nual61 R_G values for Curitiba (Figures 5ª and 5C) varied between 2.7 and 5.5 kWh/m², with na 61nual average of 3.9 kWh/m², and in C1 the values (darker hue) are higher compared to C2. The variation of the energy availability between the historical period and P99 was more accentuated in C.

The values of E_g, considering the two scenarios, were in the range between 192 and 391 kWh/month and are slightly higher in C2, however, comparing the

monthly values, in the month of December in all periods of scenario C1, there was a higher power generation.

The attendance of the system in the two scenarios varied between 64 and 130% for this locality, and it was verified that this percentage increased about 5% in the worst month considered (June), in C2, when compared to C1. For the periods evaluated in scenario C1, 11 plates will be needed, while for C2, 12.

Figure 2.5 - Available solar radiation (R_G), Electric power generated from R_G (E_g) and Percentage serviced monthly for each residence in the historical period and up to 2099 in scenarios C1 and C2 for Curitiba-PR.

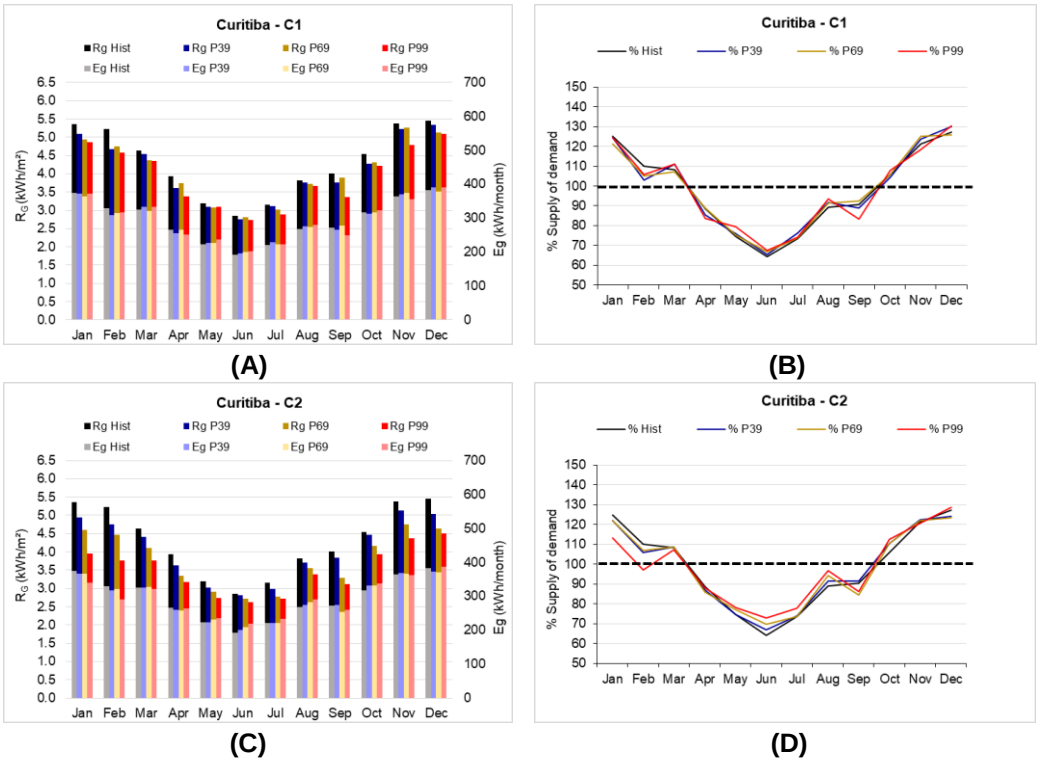

About the monthly average values of R_G or the historical period (Hist) and simulated periods P39, P69 and P99, in the scenarios C1 and C2, for the Irati locality (Table 2.5), it was observed that for C1, the months which presented significant differences during the year were February, June and December, whereas for C2, only the months of April and May did not present statistical significance in the comparison between the historical and simulated periods. It was found that the decline in monthly energy availability over the year in C1 and C2 was on average 0.2 and 0.6 kWh/m^2, respectively, and these differences in energy terms are not considered expressive.

Table 2.5 - Statistical analysis (ANOVA or KRUSKAL-WALLIS) of the means of R_G (kWh/m²) for Irati-PR.

Scenario/Mont	p-Anova	p-KW	Hist	P39	P69	P99
C1						
Jan	-	0.3272	5.48**a**	5.26**a**	5.10**a**	5.18**a**
Fev	0.0087	-	5.29**a**	4.89**ab**	4.71**b**	4.63**b**
Mar	-	0.1282	4.64**a**	4.68**a**	4.38**a**	4.42**a**
Apr	0.0704	-	3.78**a**	3.80**a**	3.60**a**	3.54**a**
May	-	0.8994	3.07**a**	3.12**a**	3.09**a**	3.09**a**
Jun	0.0079	-	2.76**ab**	2.85**a**	2.66**b**	2.74**ab**
Jul	-	0.8351	3.12**a**	3.11**a**	3.08**a**	3.06**a**
Aug	0.6670	-	3.74**a**	3.77**a**	3.69**a**	3.68**a**
Sep	-	0.1511	4.09**a**	4.01**a**	4.16**a**	4.01**a**
Oct	0.7410	-	4.49**a**	4.56**a**	4.47**a**	4.38**a**
Nov	-	0.2651	5.37**a**	5.42**a**	5.28**a**	5.20**a**
Dec	0.0237	-	5.67**a**	5.52**ab**	5.35**ab**	5.31**b**
C2						
Jan	0.0001	-	5.48**a**	5.16**ab**	4.92**bc**	4.60**c**
Fev	0.0000	-	5.29**a**	4.52**b**	4.02**bc**	3.57**c**
Mar	-	0.0034	4.64**a**	4.52**a**	4.31**ab**	3.95**b**
Apr	0.0569	-	3.78**a**	3.79**a**	3.58**a**	3.49**a**
May	0.2730	-	3.07**a**	3.09**a**	3.00**a**	2.95**a**
Jun	0.0004	-	2.76**a**	2.67**a**	2.62**ab**	2.46**b**
Jul	0.0037	-	3.12**a**	2.82**ab**	2.71**b**	2.57**b**
Aug	-	0.0117	3.74**a**	3.67**ab**	3.70**a**	3.50**b**
Sep	0.010	-	4.09**a**	4.11**a**	3.89**ab**	3.74**b**
Oct	-	0.0115	4.49**ab**	4.54**a**	4.09**ab**	3.99**b**
Nov	-	0.0056	5.37**a**	5.24**ab**	5.12**ab**	4.88**b**
Dec	0.0000	-	5.67**a**	5.25**b**	5.14**bc**	4.84**c**

Note: Values followed by lower case letters do not differ statistically from each other at the 5% level of significance by the Tukey test

In Figures 6A and 6C, a downward trend over the reproduced periods of P39, P69 and P99 was observed for this locality, in relation to historical values. The average monthly R_G for Irati ranged from 2.4 to 5.6 kWh/m², with the annual average being about 4.0 kWh/m².

It was found that the values of E_g were in the range between 187 and 394 kWh/month, with the peak of generation in the month of December. It was also observed that the values of R_G and E_g are shown to be slightly higher in C1 when compared to C2 due to the higher temperature increase in C2.

Figure 2.6 - Available solar radiation (R_G), Electric power generated from R_G (E_g) and Percentage serviced monthly for each residence in the historical period and up to 2099 in scenarios C1 and C2 for Irati-PR.

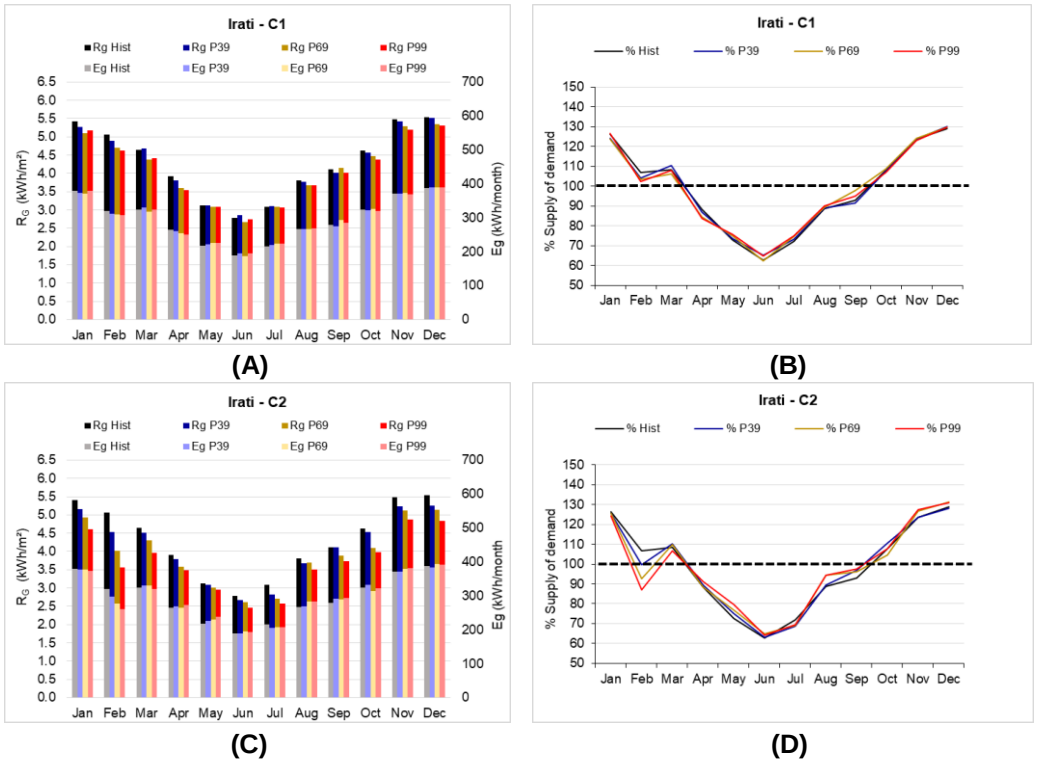

Moreover, according to Figures 6B and 6D, it was observed that, for C1, the fullness of care occurred in the months of October to March, while the deficit period of the system was verified between April and September, being the month that reached the worst power generation was June, with average attendance percentages of 64%. However, in C2, the month of February did not reach this totality, with average E_g values of 279 kWh/month, equivalent to 93%. When analyzing the annual service, the system presents efficiency of 98%, for all periods and scenarios. Regarding the number of plates required, the hypothetical residence of Irati locality requires 10 photovoltaic plates in the periods evaluated for scenario C1 and 11 plates for C2.

Table 2.6 shows the results for the locality of Ivaí, where the average monthly values of R_G for the historical period (Hist) and simulated periods P39, P69 and P99, in scenarios C1 and C2 tend to decrease over the period. It was observed that for C1, the months that presented significant 64resente64s were March and June, whereas for C2, the months of May, October and November did not 64resente statistical significance in the comparison between the historical and simulated

periods. It was found that this reduction in R_G values, in absolute terms, averaged 0.1 kWh/m² for C1, and 0.3 kWh/m² for C2.

Table 2.6 - Statistical analysis (ANOVA or KRUSKAL-WALLIS) of the means of R_G (kWh/m²) for Ivaí-PR.

Scenario/Month	p-Anova	p-KW	Hist	P39	P69	P99
C1						
Jan	-	0.5585	5.62**a**	5.63**a**	5.56**a**	5.49**a**
Fev	0.8150	-	5.35**a**	5.43**a**	5.27**a**	5.31**a**
Mar	0.0098	-	5.26**a**	5.14**ab**	4.80**b**	4.82**b**
Apr	-	0.2014	4.21**a**	4.14**a**	4.05**a**	3.99**a**
May	0.9970	-	3.49**a**	3.48**a**	3.49**a**	3.49**a**
Jun	-	0.0191	2.79**a**	2.68**ab**	2.68**ab**	2.57**b**
Jul	0.0823	-	3.23**a**	3.03**a**	3.09**a**	2.91**a**
Aug	0.3560	-	4.04**a**	4.08**a**	3.90**a**	4.00**a**
Sep	0.9070	-	4.50**a**	4.48**a**	4.49**a**	4.43**a**
Oct	0.2410	-	4.74**a**	4.95**a**	4.94**a**	4.94**a**
Nov	0.9600	-	5.82**a**	5.86**a**	5.88**a**	5.89**a**
Dec	0.0500	-	6.02**a**	5.84**a**	5.78**a**	5.80**a**
C2						
Jan	-	0.0099	5.62**a**	5.45**a**	5.34**ab**	5.17**b**
Fev	0.0084	-	5.35**a**	5.28**a**	5.02**ab**	4.77**b**
Mar	0.0000	-	5.26**a**	4.85**b**	4.66**b**	4.18**c**
Apr	0.0361	-	4.21**a**	4.04**ab**	3.94**ab**	3.80**b**
May	0.8030	-	3.49**a**	3.49**a**	3.52**a**	3.54**a**
Jun	0.0101	-	2.79**a**	2.62**ab**	2.63**ab**	2.39**b**
Jul	-	0.0003	3.23**a**	2.98**ab**	2.66**b**	2.60**b**
Aug	0.0314	-	4.04**a**	3.98**ab**	3.94**ab**	3.79**b**
Sep	0.0392	-	4.50**a**	4.41**ab**	4.29**ab**	4.19**b**
Oct	0.3220	-	4.74**a**	4.95**a**	4.88**a**	4.80**a**
Nov	0.8780	-	5.82**a**	5.86**a**	5.90**a**	5.93**a**
Dec	0.0124	-	6.02**a**	5.79**ab**	5.78**ab**	5.72**b**

Note: Values followed by lower case letters do not differ statistically from each other at the 5% level of significance by the Tukey test

By means of Figures 7A and 7C, it was noted that monthly average values of R_G for Ivai varied between 2.3 and 6.0 kWh/m², and that the annual average is about 4.4 kWh/m². It was found that the values of E_g were delimited between 164 and 408 kWh/month. It is important to note that it was during this period and scenario that both the worst (June of P99) and the best (November of P99) value of generation of E_g of the locality were recorded. Therefore, the monthly peak of energy generation was recorded in December when considering all periods and scenarios.

According to Figures 7B and 7D, the fullness of care was observed between the months of October to March, and the period of system deficit between the months

of April and September. However, it was noted that, for C2, the month of March did not reach the total of service in P99, with E_g of 297 kWh/month, equivalent to a percentage of 98%. The month of June was the one that reached the worst generation of energy, with average attendance percentages of 57%. It is important to note that, for Ivaí in C2, the month of February did not present an expressive surplus generation, which occurred in the other localities, and this surplus was on average 5%

For all periods and scenarios, the annual efficiency of the system is 98%. In relation to the number of plates required, the hypothetical residence of the locality of Ivaí requires 9 photovoltaic plates in the periods of C1 and 10 plates in the scenario C2.

Figure 2.7 - Available solar radiation (R_G), Electric power generated from R_G (E_g) and Percentage serviced monthly for each residence in the historical period and up to 2099 in scenarios C1 and C2 for Ivaí-PR.

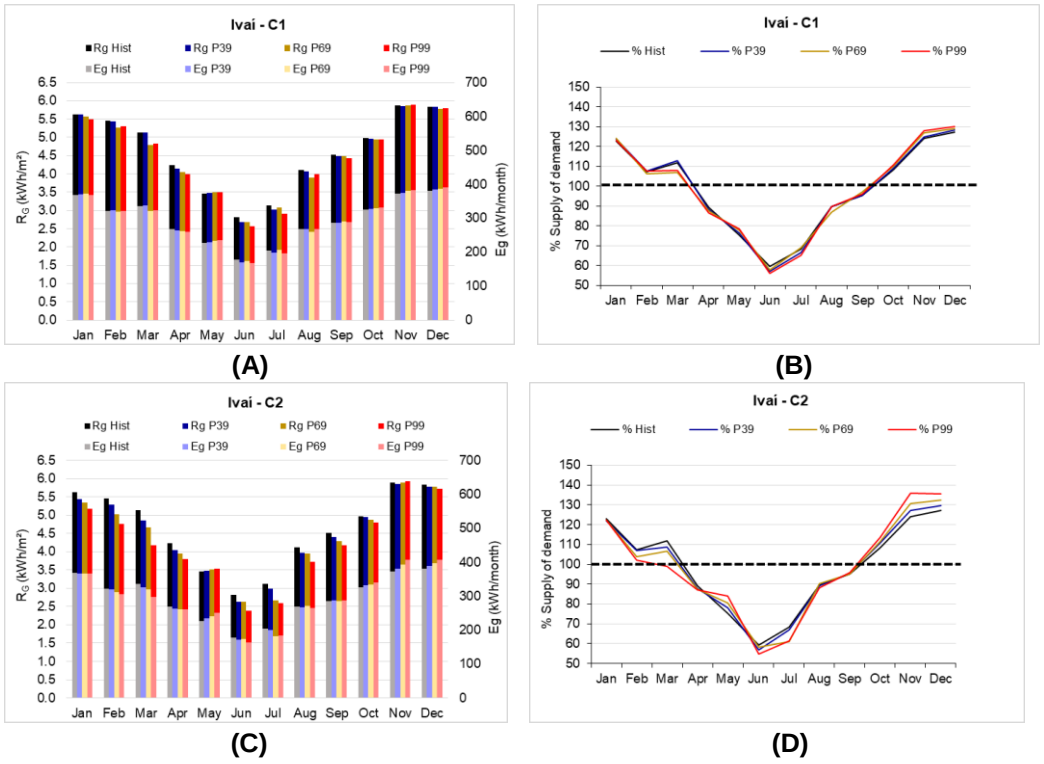

Table 2.7 shows the R_G values for the Londrina locality, where there is a downward trend towards the end of the century. In the C1, only the month of December has statistical significance, with an average decrease of 0.1 kWh/m² between the historical period and P99. For C2, January, February, May, June, November and December showed a significant decrease in R_G with a mean reduction

of 0.3 kWh/m² in absolute values between the historical period and P99. For this scenario and locality, winter was the only season of the year in which no month obtained a significant decrease of R_G.

It was observed that, despite being impacted by climate change scenarios, the average reduction values of R_G in both C1 and C2 do not energetically represent a restriction to be considered.

Table 2.7 - Statistical analysis (ANOVA or KRUSKAL-WALLIS) of the means of R_G (kWh/m²) for Londrina-PR.

Scenario/Month	p-Anova	p-KW	Hist	P39	P69	P99
C1						
Jan	-	0.1306	5.75**a**	5.70**a**	5.59**a**	5.40**a**
Fev	0.9640	-	5.98**a**	5.74**a**	5.71**a**	5.68**a**
Mar	0.8320	-	5.67**a**	5.59**a**	5.58**a**	5.58**a**
Apr	-	0.3658	4.76**a**	4.80**a**	4.76**a**	4.74**a**
May	0.1070	-	3.80**a**	3.57**a**	3.62**a**	3.51**a**
Jun	0.9680	-	3.54**a**	3.47**a**	3.49**a**	3.39**a**
Jul	-	0.2240	3.79**a**	3.78**a**	3.77**a**	3.76**a**
Aug	0.4400	-	4.54**a**	4.59**a**	4.58**a**	4.49**a**
Sep	-	0.9220	5.22**a**	5.12**a**	5.12**a**	5.12**a**
Oct	0.7490	-	5.48**a**	5.58**a**	5.61**a**	5.61**a**
Nov	0.5210	-	6.15**a**	6.11**a**	6.06**a**	6.01**a**
Dec	0.0019	-	6.30**a**	5.96**b**	5.89**b**	5.88**b**
C2						
Jan	0.0002	-	5.75**a**	5.71**ab**	5.22**bc**	4.93**c**
Fev	0.0003	-	5.98**a**	5.69**ab**	5.50**b**	5.38**b**
Mar	-	0.0500	5.67**a**	5.58**a**	5.57**a**	5.57**a**
Apr	-	0.0825	4.76**a**	4.74**a**	4.69**a**	4.65**a**
May	0.0017	-	3.80**a**	3.63**ab**	3.40**bc**	3.27**c**
Jun	-	0.0141	3.54**a**	3.46**a**	3.45**ab**	3.33**b**
Jul	-	0.3343	3.79**a**	3.75**a**	3.75**a**	3.73**a**
Aug	0.3170	-	4.54**a**	4.58**a**	4.48**a**	4.47**a**
Sep	0.8240	-	5.22**a**	5.12**a**	5.13**a**	5.14**a**
Oct	0.5030	-	5.48**a**	5.59**a**	5.66**a**	5.67**a**
Nov	0.0048	-	6.15**a**	6.05**a**	5.91**ab**	5.75**b**
Dec	-	0.0003	6.30**a**	5.98**ab**	5.78**bc**	5.67**c**

Note: Values followed by lower case letters do not differ statistically from each other at the 5% level of significance by the Tukey test

The average R_G values for Londrina (Figures 8A and 8C) varied between 3.2 and 6.3 kWh/m², with an annual average of 5.0 kWh/m², and in C1 the values are higher in comparison to C2. It was observed that the values of E_g were between 200 and 360 kWh/month, for the months of June and December, respectively. Therefore,

the peak energy generation was registered in December for all the periods and scenarios, although the highest R_G values were in the month of November .

The system attendance (Figures 8B and 8D) varied between 67 and 120% for this location. The month of June was the one that reached the worst level of energy generation, with average attendance rates of 68% considering all the three periods and scenarios. It was observed that the integrality of the system is reached in the months between October to March. Despite the fact that February showed sufficient performance (above 100%), it was noticed that there was a decrease in generation of E_g and, consequently, a drop in attendance of around 9% in relation to January and March. It is important to note that this behavior was not verified in relation to R_G data.

For all periods and scenarios, the annual efficiency of the system was 98%. Likewise, considering the hypothetical defined residence, in the locality of Londrina the need for photovoltaic panels would be 8 considering all the analyzed periods and scenarios.

Figure 2.8 - Available solar radiation (R_G), Electric power generated from R_G (E_g) and Percentage serviced monthly for each residence in the historical period and up to 2099 in scenarios C1 and C2 for Londrina-PR.

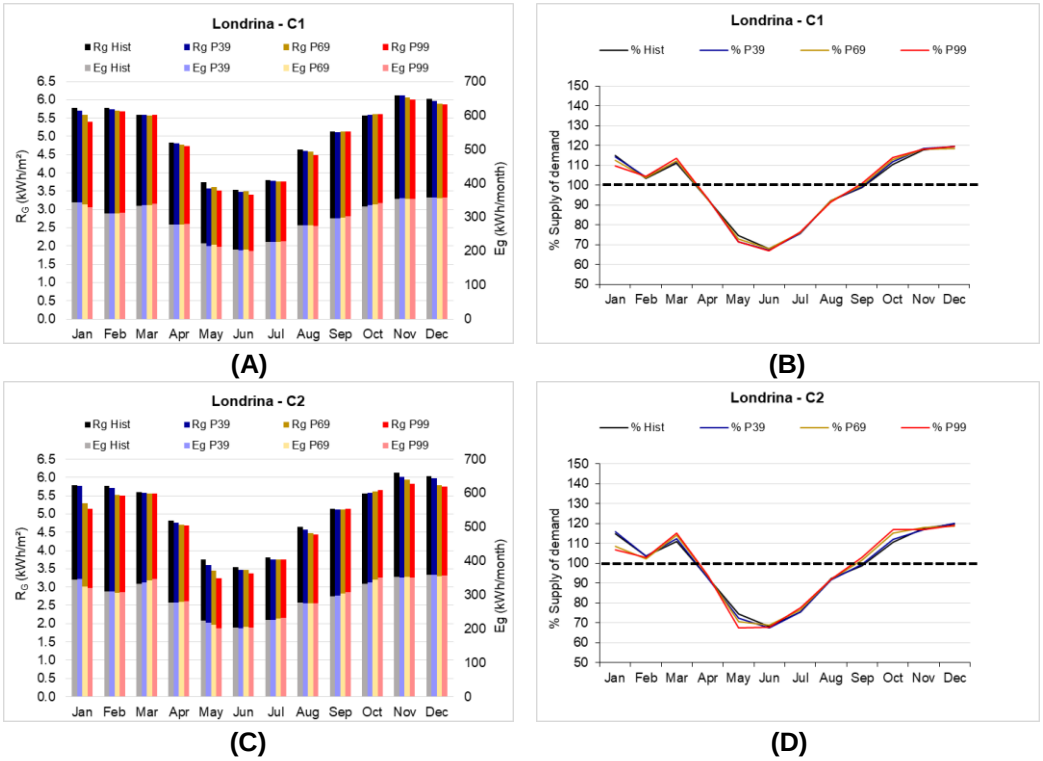

In the locality of Maringá, according to the results shown in Table 2.8, it was generally perceived that the average monthly values of R_G for the historical period (Hist) and simulated periods P39, P69 and P99, in scenarios C1 and C2 tend to decrease throughout the century. A safeguard should be made only for the month of April, which, for both scenarios, showed a slight increase of an average of 0.06 kWh/m².

It was observed that for C1, the months that presented significant differences were in March, June and December, whereas in C2, every month presented statistical significance in the comparison between the historical and simulated periods. It was found that this reduction of R_G values, in absolute terms, averaged 0.4 kWh/m² for C1 and 0.8 kWh/m² for C2.

Table 2.8 - Statistical analysis (ANOVA or KRUSKAL-WALLIS) of the means of R_G (kWh/m²) for Maringá-PR.

Scenario/Month	p-Anova	p-KW	Hist	P39	P69	P99
C1						
Jan	0.3090	-	5.99**a**	5.80**a**	5.82**a**	5.65**a**
Fev	-	0.1125	6.15**a**	5.89**a**	5.85**a**	5.76**a**
Mar	-	0.0247	5.63**a**	5.37**ab**	5.13**ab**	4.91**b**
Apr	-	0.1751	4.85**a**	4.84**a**	4.82**a**	4.88**a**
May	0.9150	-	3.86**a**	3.72**a**	3.65**a**	3.58**a**
Jun	-	0.00061	3.62**a**	3.32**ab**	3.28**ab**	3.00**b**
Jul	0.0701	-	3.96**a**	3.82**a**	3.77**a**	3.76**a**
Aug	0.1100	**-**	4.55**a**	4.35**a**	4.32**a**	4.19**a**
Sep	-	0.2892	5.09**a**	4.82**a**	4.53**a**	4.55**a**
Oct	0.5490	-	5.51**a**	5.40**a**	5.36**a**	5.23**a**
Nov	0.5750	-	6.30**a**	6.16**a**	6.21**a**	6.11**a**
Dec	0.0015	-	6.53**a**	6.07**b**	6.04**b**	6.03**b**
C2						
Jan	0.0002	-	5.99**a**	5.79**ab**	5.32**bc**	5.10**c**
Fev	0.0000	-	6.15**a**	5.86**ab**	5.54**bc**	5.38**c**
Mar	0.0000	-	5.63**a**	4.99**b**	4.68**b**	4.05**c**
Apr	-	0.0020	4.85**b**	4.85**b**	4.91**ab**	4.94**a**
May	0.0076	-	3.86**a**	3.60**ab**	3.51**b**	3.51**b**
Jun	0.0000	-	3.62**a**	3.29**ab**	3.15**bc**	2.93**c**
Jul	0.0002	-	3.96**a**	3.84**ab**	3.64**bc**	3.60**c**
Aug	0.0000	-	4.55**a**	4.28**ab**	4.10**b**	3.50**c**
Sep	-	0.0002	5.09**a**	4.38**ab**	4.34**ab**	3.74**b**
Oct	-	0.0001	5.51**a**	5.52**a**	4.89**b**	4.47**b**
Nov	0.0008	-	6.30**a**	6.12**ab**	5.82**bc**	5.66**c**
Dec	0.0000	-	6.53**a**	6.02**b**	5.72**b**	5.31**c**

Note: Values followed by lower case letters do not differ statistically from each other at the 5% level of significance by the Tukey test

From Figures 9A and 9C, it was verified that mean monthly R_G values for Maringá ranged from 2.9 to 6.5 kWh/m², with the annual average being around 4.8 kWh/m², whose extreme values of interval refer to the months of June and December, respectively. It was observed that E_g values were between 182 and 379 kWh/month, which refer to the months of June and November, respectively. Generally speaking, peak power generation was recorded in December for all periods and scenarios, although the highlight month for this location for R_G was November.

According to Figures 9B and 9D, it was observed that the percentage of attendance varied between 60 and 126%, and the fullness occurred between October and March, with the system deficit period between April and September. However, it was found that for C2, the month of March did not reach the total service, in P99, with E_g of 280 kWh/month, equivalent to a percentage of 93%. On the other hand, the month of April, which in all localities was insufficient to generate energy, for this period and scenario (P99/C2), had full and surplus service, with E_g of 331 kWh/month, corresponding to 110% of service. The month of June was the one that reached the worst generation of energy, with average attendance percentages of 65%. For all periods and scenarios, the annual efficiency of the system was 98%. The number of plates required, for the hypothetical residence in the locality of Maringá is 10 photovoltaic plates in all the evaluated periods and scenarios.

Figure 2.9 - Available solar radiation (R_G), Electric power generated from R_G (E_g) and Percentage serviced monthly for each residence in the historical period and up to 2099 in scenarios C1 and C2 for Maringá-PR.

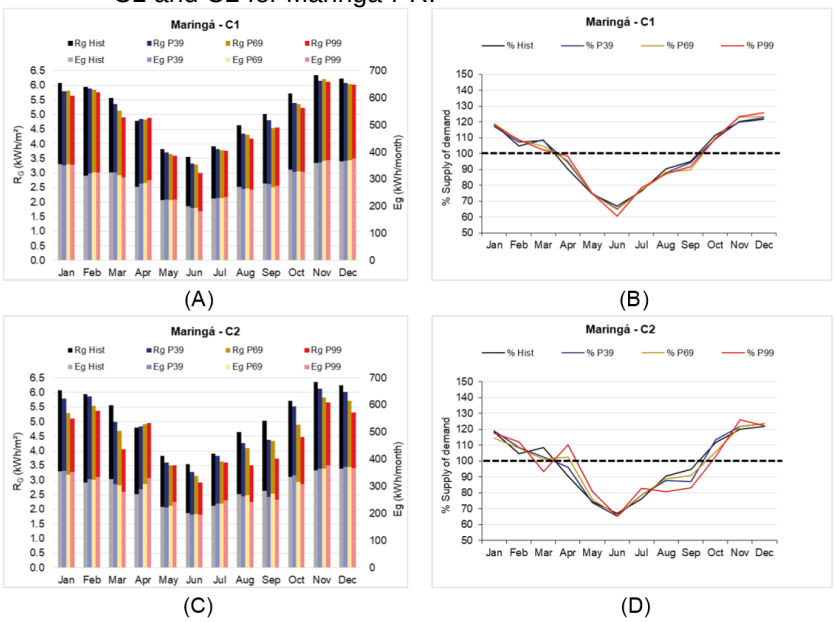

It was verified that the R_G values for the Paranaguá locality (Table 9) show a decreasing tendency until the end of the century, except for the months of January, April, May and December, that do not have or have a slight tendency of increase. For these months, the mean increase was 0.1 kWh/m² in C1 and 0.2 kWh/m² in C2, while for other months, the average reduction in R_G was 0.2 in C1 and of 0.3 kWh/m² in C2, between the historical period and P99. In C1, only the month of September presented statistical significance with decrease, in the monthly average of 0.33 kWh/m² between the historical period and P99. However, for C2, the months of January, March, May, August, September and December showed statistical significance of GR. It was noticed that the mean values of both reduction and RG increase were not expressive.

Table 2.9 - Statistical analysis (ANOVA or KRUSKAL-WALLIS) of the means of R_G (kWh/m²) for Paranaguá-PR.

Scenario/Month	p-Anova	p-KW	Hist	P39	P69	P99
C1						
Jan	0.2290	-	4.92**a**	5.05**a**	5.10**a**	5.18**a**
Fev	0.3290	-	5.10**a**	4.91**a**	4.90**a**	4.89**a**
Mar	0.0571	-	4.48**a**	4.23**a**	4.16**a**	4.16**a**
Apr	-	0.3334	3.72**a**	3.72**a**	3.71**a**	3.72**a**
May	-	0.9623	2.94**a**	3.04**a**	3.04**a**	3.04**a**
Jun	-	0.4157	2.60**a**	2.58**a**	2.56**a**	2.52**a**
Jul	0.9850	-	2.69**a**	2.67**a**	2.67**a**	2.67**a**
Aug	0.2520	-	3.04**a**	2.88**ab**	2.92**ab**	2.79**b**
Sep	0.0385	-	3.35**a**	3.12**ab**	3.09**ab**	3.02**b**
Oct	-	0.1224	3.75**a**	3.67**a**	3.68**a**	3.67**a**
Nov	0.9380	-	4.49**a**	4.50**a**	4.51**a**	4.45**a**
Dec	0.4940	-	5.18**a**	5.08**a**	5.18**a**	5.20**a**
C2						
Jan	-	0.0007	4.92**c**	5.15**bc**	5.36**ab**	5.42**a**
Fev	0.1910	-	5.10**a**	4.88**a**	4.86**a**	4.84**a**
Mar	0.0013	-	4.48**a**	4.12**b**	4.03**b**	3.99**b**
Apr	-	0.1136	3.72**a**	3.72**a**	3.72**a**	3.74**a**
May	-	0.0156	2.94**a**	3.04**b**	3.06**ab**	3.08**a**
Jun	0.2130	-	2.60**a**	2.54**a**	2.50**a**	2.44**a**
Jul	0.8590	-	2.69**a**	2.67**a**	2.65**a**	2.63**a**
Aug	0.0001	-	3.04**a**	2.90**ab**	2.71**bc**	2.57**c**
Sep	0.0000	-	3.35**a**	3.08**ab**	2.84**bc**	2.65**c**
Oct	-	0.1742	3.75**a**	3.67**a**	3.67**a**	3.66**a**
Nov	0.8070	-	4.49**a**	4.48**a**	4.45**a**	4.40**a**
Dec	-	0.0133	5.18**a**	5.17**b**	5.30**a**	5.39**a**

In Figures 10A and 10C, it was observed that the mean monthly R_G values for Paranaguá varied between 2.4 and 5.4 kWh/m², and that the annual average was

around 3.8 kWh/m², whose lower limit of interval belongs to the month of June, while the upper limit refers to the months of January and December. It was verified that the values of Eg were between 190 and 436 kWh/month, referring to June and January, respectively. Therefore, peak power generation was recorded in the months of January and December for the periods and scenarios analyzed, with values very close in these two months.

According to Figures 10B and 10D, it was observed that the percentage of attendance varied between 63 and 145% in this locality, where it was found that the totality of attendance of the system occurred between the months between November and March, and the month of October falls within the deficit period, along with the months of April to September.The average efficiency of the month of October for all periods and scenarios is 97%. The month of June was the one that reached the worst generation of energy, with average attendance percentages of 65%.

It was noticed that for this locality, the autumn-winter months showed a tendency of decrease in Eg values and, consequently, in the percentage of attendance during the periods, within each scenario. On the other hand, the months belonging to the spring-summer period tended to increase these values, and the percentage of attendance for these months may exceed up to 40% of the consumption need. For all the periods and scenarios, the annual efficiency of the system was 98%. Regarding the number of plates required, the hypothetical residence for the locality of Paranaguá requires 11 photovoltaic plates in all the considered periods and scenarios.

Figure 2.10 - Available solar radiation (R_G), Electric power generated from R_G (E_g) and Percentage serviced monthly for each residence in the historical period and up to 2099 in scenarios C1 and C2 for Paranaguá-PR.

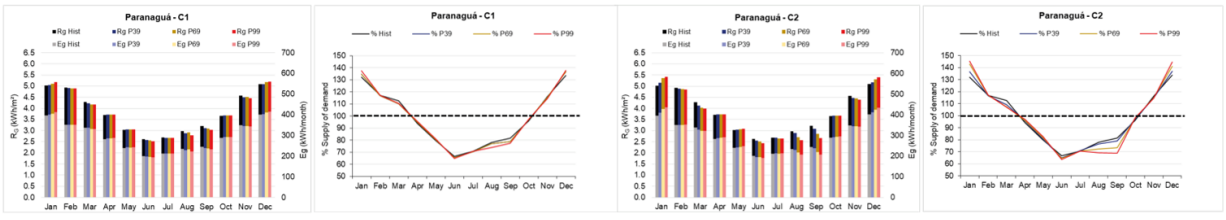

(A) (B) (C) (D)

In general, for all localities, it was observed that the simulated R_G values showed a decreasing trend over the simulated periods of P39, P69 and P99, in

relation to historical values. This pattern can be attributed to the model used for estimating R_G (CHEN et al., 2004), which is based on the daily thermal amplitude (ΔT), in which the climatic scenarios, with a minimum temperature increase of the maximum temperature, caused the decrease of this amplitude, which causes a reduction tendency of the R_G values.

Similarly, Bierhals et al. (2017) found that, for the State of Rio Grande do Sul, climate scenario models have shown that global solar radiation values tend to decline to 60% of the year through 2100. In addition, Huber et al. (2016) concluded that global solar radiation in the future (2035-2039) is likely to be reduced when compared to historical values (1995-1999), and that this decline is around 5% for regions in Africa. In contrast, the authors did not point to any change to North America. Similarly, Ohunakin et al. (2015) also observed a reduction of global solar radiation by the end of the century in Nigeria for the period from 2041 to 2070, whose range was in the range of 0.11 to 3.39%.

Tiepolo et al. (2014) found that even in winter periods of low solar intensity, the R_G values found in Paraná-Brazil (3.61 kWh/m²) were higher than those found in Germany (between 2.16 and 2, 98 kWh/m²) and in Belgium (between 2.33 and 2.74 kWh/m²), and close to the values found in France (between 2.26 and 4.11 kWh/m²), which shows that even in this period, the State of Paraná has significant potential for the installation of photovoltaic systems.

On the other hand, Kopp and Lean (2011) warn of the complexity of establishing the magnitude of long-term changes in global solar radiation, or of alleviating the conflicting claims of radiation variations that have driven significant climate change in recent decades, since the current database is too short and inaccurate for this purpose.

It is important to note that the highest values of R_G verified in this research refer to the months between October and March, coinciding with the spring and summer seasons, when the sun's rays illuminate the southern hemisphere brighter. With similar justification, the lowest values refer to the months from April to September, belonging to fall and winter, when the days are shorter and the solar rays have lower intensity, due to the apparent movement of the sun in relation to the Earth, due to the solar declination.

As a consequence of the decrease in the simulated R_G values, a decrease trend of the values of E_G over the periods was observed, which confirms that the

daily energy supplied by the panel is proportional to the solar radiation incident on the panel plane, also found by Gnoatto et al. (2008), to the city of Cascavel (PR). In all the localities, it was verified that there is a period of the year in which the attendance of the system does not reach the fullness, however, although in the period that includes the fall and the winter one has the impression to occur an energy debt, this does not mean that the system does not meet the annual energy demand.

Because the system is connected to the public electricity grid and there is the mechanism of energy compensation, the surplus in the spring and summer months is made available to the network, which can be reimbursed by means of credits, to be redeemed when the attendance of the system is not full. That is, the credit available at intervals in which Eg is greater than the demand for the residence can be reversed in the period in which the system does not meet the total need.

It was noted that, despite the impacts of climate change, the efficiency of the system did not change over time, reaching 98% of service for all locations, or a subtle increase of service was observed over the period with increasing temperature. This behavior was also perceived by Michels et al. (2010), who verified, for the city of Medianeira-PR, that the temperature increase in a photovoltaic system can negatively alter its power and efficiency. This situation was also found by Gnoatto et al. (2008), who, when analyzing the efficiency of a photovoltaic system, in the city of Cascavel-PR, pointed out that the lowest energy production occurred in May, and the highest in March. Analyzing the seasonal mean, the highest energy production occurred in the summer and the lowest in the winter, while in the spring and autumn production was equivalent.

It is important to highlight that in systems installed in Florianópolis-SC, studied by Urbanetz et al. (2011), showed an annual efficiency of 88%, and the service only supplied the demand and generated surplus energy in the months from November to February, a behavior attributed to this locality, characterized as the Brazilian capital with the lowest incidence of solar radiation. Likewise, Salamoni et al. (2014) obtained contributions from 19 to 70% in the supply of electric energy demand, through photovoltaic systems connected to the grid in hospitals of the cities of Pelotas-RS, Santa Maria-RS and Florianópolis-SC, and the absence of areas available on the roofs was the determining factor for not achieving higher efficiency values. On the other hand, Singh and Banerjee (2015) have found that a system

installed on the roof of a residence in Mumbai, India, can provide 12-20% of average daily demand and 31-60% of peak morning demand for many diferente months.

In relation to climate change, Hu et al. (2016) found in their experiments that solar energy has the potential to satisfy human demand now and in the future by 2100. In general, changes in solar radiation do not directly affect the regional and global climate but may affect changes in absorbed solar radiation, which directly influences energy production. However, contrary to Huber et al. (2016) argued that photovoltaic systems are unlikely to be affected by climate change.

From a Brazilian perspective, Monteiro et al. (2017) point out that since the South region of Brazil has a high energy consumption in the summer and imports energy from the southeast and center-west regions, where the solar energy supply is the highest among all Brazilian regions, the insertion of photovoltaic energy in the South region can result in great benefit to the national electricity system, as well as socioeconomic advantages, such as the generation of jobs in the area of renewable energy.

2.4 CONCLUSION

From the results found in this research, it was verified that the estimation of the production of solar energy in function of the regionality and possible scenarios of climate change are important aspects to evaluate the viability of installation of integrated systems of photovoltaic energy in the residences.

The method used to estimate the percentage of attendance of the system showed annual values of 98%, for all the studied localities, which proves that the State of Paraná has favorable climatic conditions for the installation of these systems. Although, for all the studied locations, about half of the year did not show the fullness of the service, the monthly values found in this period (above 60%) contribute to the reduction in the consumption of electric energy, besides, as these systems can be connected to the public power grid, there is the power compensation mechanism.

This research has shown that, if the system is installed in the residence nowadays, and if the maintenance instructions and maintenance issued by the manufacturer are followed, the same panels can be used until the end of the century, even in possible climate change scenarios. In some locations it would be necessary to add more panels over time.

The popularization of solar systems in Brazilian homes can bring benefits to users, the environment, and government. On the other hand, there is a lack of public incentive policies, such as the reduction of taxes, in order to promote the adoption of solar energy systems for residential use.

CHAPTER 3

ESTIMATING THE SOLAR FRACTION USED IN WATER HEATING SYSTEMS FOR SOUTH BRAZIL STATE LOCATIONS CONSIDERING CLIMATE CHANGE SCENARIOS

ABSTRACT

Solar photo thermal energy consists of water heating from the global solar radiation (R_G). When considering future climate change scenarios, increasing atmospheric concentrations of greenhouse gases tend to increase the earth's surface temperature. The main objective of this work was to estimate the solar fraction obtained by means of solar heating systems for residences of the single family type, for eight locations in the State of Paraná, in scenarios of possible climate changes projected until the end of the 21st century. F-Chart method was used to simulate the performance of solar heating systems based on the monthly average of solar radiation data, which determines the annual solar fraction or percentage of the energy demand that is covered by the solar installation. All localities present a characteristic seasonal behavior, with annual values of solar fraction between 82.4% and 129.8%, according to the studied localities, which proves that the State of Paraná has favorable climatic conditions for the installation of solar heating systems, even if it is installed for aggregation purposes, in order to reduce the electric power consumption.

Keywords: Solar water heating; Solar fraction; F-Chart.

RESUMO

A energia solar foto térmica consiste no aquecimento da água a partir da radiação solar global (R_G) por meio da conversão da radiação proveniente do Sol em energia térmica. Ao se considerar cenários futuros de mudanças climáticas, o aumento das concentrações atmosféricas de gases de efeito estufa tendem a aumentar a temperatura da superfície da terra. Esse trabalho teve como objetivo principal estimar a fração solar obtida por meio de sistemas de aquecimento solar para residências do tipo unifamiliar, para oito localidades do Estado do Paraná, em cenários de possíveis mudanças climáticas projetadas para o final do século XXI. Para simular o desempenho de sistemas de aquecimento solar com base na média mensal de dados de radiação solar foi utilizado o método F-Chart, que determinaa fração solar anual ou porcentagem dademanda energética que é coberta pela instalação solar. Todas as localidades apresentam um comportamento sazonal característico, com valores anuais de fração solar entre 82,4% e 129,8%, de acordo com as localidades estudadas, o que comprova que o Estado do Paraná possui condições climáticas favoráveis para a instalação dos sistemas de aquecimento solar, mesmo que seja instalado para fins de agregação, com a finalidade de reduzir o consumo de energia elétrica.

Palavras-chave: Aquecimento solar de água; Fração solar; F-Chart.

3.1 INTRODUCTION

Energy is considered a primordial agent in wealth generation and a significant factor in economic development. Over the last century, most of the energy demand was supplied by fossil fuels, due to the low cost and convenience of exploitation compared to energy from alternative sources, besides the environmental pollution was not considered relevant. Nowadays, it is observed a search for renewable energy sources, considering the energy efficiency of the system, due to policies of green development mechanism (KALOGIROU, 2004; CELUPPI et al., 2014). Among the available alternative sources, solar energy has become more accessible, especially the photothermal.

The Sun is a sphere of intense hot gases, however just a small fraction of emitted radiation is absorbed by the Earth. But, even with this small fraction, it is estimated that global energy demand could be supplied for one year by solar radiation emitted only for a period of 30 minutes (KALOGIROU, 2004). Photothermal solar energy consists of heating a liquid fluid, usually water, from the global solar radiation (R_G) which provides by mediation of the conversion of the radiant energy coming from the Sun into thermal energy. Therefore, solar collectors are used.

Brazilian cities have global solar radiation rates higher than the most developed countries such as Germany, Spain, Japan and also China. In addition, they present lower seasonal variability, since most of the country is located in the tropics. However, the use of solar thermal and photovoltaic energy in Brazil is lower than in countries that received government incentives for their use in homes (TIEPOLO et al., 2014; ALTOÉ et al., 2017).

According to Pereira et al. (2017), there are approximately 250,000 solar heaters installed in Brazil, totalizing more than 5 million m² of heaters, which represents only 0.6% of the total Brazilian residences. Although, the country has the third largest installed capacity of solar heating systems, but, in terms of per capita value it occupies only the 30th position, which indicates that there are opportunities for growth, considering that the availability of this resource in the country is greater than those that occupy better positions (MARTINS, ABREU and PEREIRA, 2012).

Martins, Abreu and Pereira (2012) argue that although the fraction of energy savings per dwelling is higher in places with a warmer climate, such as the North, Northeast and Central regions, the total energy savings per year is quite similar for all the Brazilian regions. According to Pereira et al. (2017), a higher annual production

of thermal energy, per area of installed collector, is not necessarily in the regions with the highest incidence of solar radiation. This is attributed to the fact that the demand for thermal energy is higher in the coldest regions, making the heating potential of the system well used.

Moreover, government incentives help to increase the use of the system in homes, such as tax exemption, social housing programs and opportunities to purchase equipment through programs of ANEEL (National Agency of Electricity) (BASSO et al., 2010; PEREIRA et al., 2017). On July 7th, 2011, the Ministry of Cities, through Resolution 325, determined that all residential construction projects consisting of single-family housing units should include solar water heating systems. This initiative is a direct incentive for the expansion of the solar heaters market.

Electric shower is present in more than 70% of the country's households, and water heating accounts for 25% of the total electric energy consumed in Brazilian homes, representing a consumption of around 20 billion kWh. Moreover, the power of this equipment exceeds the sum of all the other appliances together, and during its use, the demand for energy rises to more than 4.5 times the average consumption. Therefore, only the heating of bath water in Brazilian homes accounts for more than 6% of all the national electricity consumption (ELETROBRÁS, 2007; OLIVEIRA et al., 2008).

Thus, the replacement of the electric showerhead by a solar heater can imply savings in the electricity bill for the user, in addition to contributing to the reduction of electricity consumption peaks. The system supplies hot water with a temperature range of 40 ºC and 60 ºC, which meets the needs of residential use in kitchens and bathrooms. On the other hand, if there is cloudy weather and there is not enough water heating, the electric shower can be used to compensate the lack of solar heating or even support. Therefore, electricity is an excellent complement to water heating, and should not be used as the main source (MOGAWER e SOUZA, 2004).

Altoé, Oliveira and Carlo (2012) verified that the replacement of the electric shower by the solar heater with electric support reduced in average 70% the consumption of electric energy intended for water heating and 36% in the total consumption of electrical energy of the residence located in Minas Gerais. Dharuman, Arakeri and Srinivasan (2006) obtained efficiency between 40 and 60% in the heating system, with water temperature between 50 and 60 ºC, for localities of India. Similarly, Lenz et al. (2017) evaluated a thermosolar system and obtained from

33.7 to 53.54% of monthly efficiencies and Medeiros et al. (2014) found savings around 55% in a solar heating system compared to a conventional electrical system.

The most widely used method to simulate the performance of solar heating systems based on the monthly average solar radiation data is the F-Chart method (DUFFIE and BECKMAN, 1974; BECKMAN, KLEIN and DUFFIE, 1977). From the determination of the annual solar fraction or percentage of the energy demand that is covered by the solar installation, it is possible to trend the fraction of electricity saved by the adoption of these systems. Besides, considering future scenarios of climate change, increasing atmospheric concentrations of greenhouse gases tend to increase the amount of heat retained and consequently increasing the earth's surface temperature.

The emission scenarios projected until the end of the 21st century (IPCC, 2014), take into account factors such as population size, consumption patterns, use of fossil fuels and energy efficiency, and estimate rates of increase between 1.7 and 4.8 ºC in the average global temperature, which is stipulated for Brazil by Marengo (2001), who projects an increase in the air average temperature in 1.3 ºC and 4.6 ºC

Based on the above considerations and in view of future changes in the climate for Brazil, this research aimed to estimate the solar fraction obtained through solar heating systems for single family dwellings, considering scenarios of global climate change projected towards the end of the 21st century, in localities of the State of Paraná.

3.2 MATERIALS AND METHODS

This research was developed in the Laboratory of Applied Computational Statistics - LECA, of the State University of Ponta Grossa. Eight localities of the State of Paraná (Figure 1) were selected from climatological data of conventional meteorological stations (Table 1), which are available in the Meteorological Database for Teaching and Research (BDMEP) by the National Institute of Meteorology (INMET).

Figure 3.1 - Selected locations in the State of Paraná

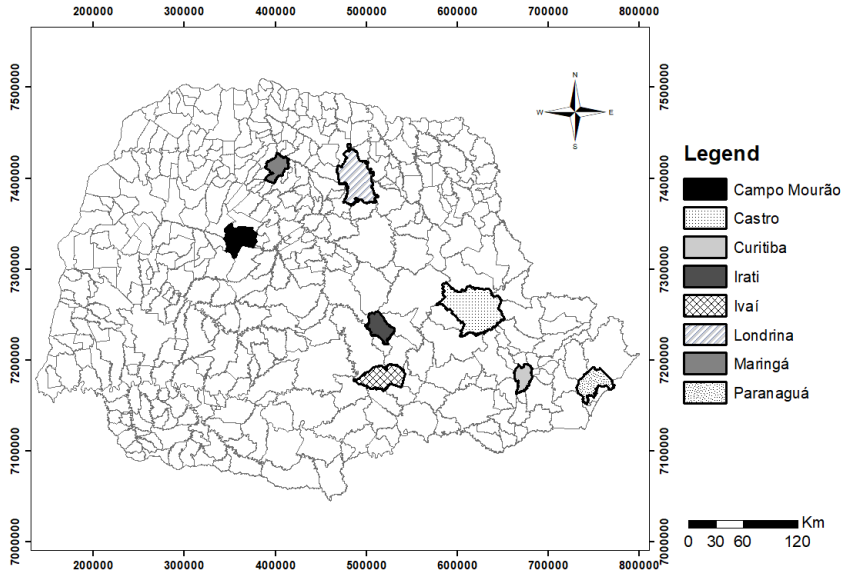

Table 3.1 - Geographical coordinates of selected locations

ID	Locality	Latitude (S)	Longitude (W)	Elevation (m)
L1	Campo Mourão	-24º05’	-52º36’	616
L2	Curitiba	-24º78’	-50º00’	1009
L3	Castro	-25º43’	-49º26’	924
L4	Irati	-25º46’	-50º63’	837
L5	Ivaí	-25º00’	-50º85’	808
L6	Londrina	-23º31’	-51º13’	566
L7	Maringá	-23º40’	-51º91’	542
L8	Paranaguá	-25º53’	-48º51’	5

The State of Paraná belongs to the region of southern Brazil and is located between the parallels 22º30'58 "and 26º43'00" south latitude and between the meridians 48º05'37 "and 54º37'08" west longitude. According to Köppen's climate classification, the State has two types: Cfa - Subtropical climate with average temperature in the coldest month below 18 ºC (mesothermic) and average temperature in the hottest month above 22 ºC, with hot summers, infrequente frosts and trend of rainfall concentration in the summer months, however without a defined dry season; Cfb - Temperate climate with average temperature in the coldest month below 18 ºC (mesothermic), with fresh summers, average temperature in the hottest month below 22 ºC and not defined dry season (IAPAR, 2018).

The daily historical series of pluviometric precipitation, insolation (or hours of solar brightness), minimum and maximum temperatures of the evaluated localities comprised a period of 31 years (1987-2017). The data consistency for the correction of possible faults, as well as the calculation of the global solar radiation from the

sunshine data in the unit langley per day (ly/dia), were carried out through the software PGECLIMA_R (VIRGENS FILHO et al., 2013). The software calculates the global solar radiation using the equation of Angström-Prescott (Equation 1), and it is necessary to inform the value of the radiation at the top of the atmosphere (R_A) for each day of the year, determined by Equation 2, and the values of parameters "a" and "b", which can be 0.25 and 0.50 respectively, in the absence of the adjusted values for each locality.

$$R_G = R_A \times (a + b \times \frac{n}{N}) \quad (3.1)$$

where,
R_G is the global solar radiation in ly/dia;
R_A is the solar radiation at the top of the atmosphere, in ly/dia, given by Equation 2;
n is the daily sunshine;
N is the maximum daily value of hours of solar brightness.

$$R_A = \frac{916{,}7}{R^2}(\text{sen}\phi\text{sen}\delta\text{H} + \cos\phi\cos\delta\text{senH}) \quad (3.2)$$

where,
R is the medium vector radius Earth-Sun = 0,9915;
ϕ is the location latitude;
δ it is the solar declination;
H it is the arccos(-tgϕtgδ)

For the simulation of climatic scenarios in the eight evaluated locations, the PGECLIMA_R software was also used, whose daily climatic data were simulated based on the temperature increase predicted by the fifth IPCC report (IPCC, 2014) for two scenarios. The less pessimistic scenario (C1) predicts an overall increase of up to 1.7 °C in the mean maximum and minimum temperatures, while the most pessimistic scenario (C2) predicts an increase of up to 4.8 °C. However, Marengo and Camargo (2008), Minuzzi, Caramori and Borrozino (2010) and Silva et al. (2015) found that the trend of increasing the minimum temperature tends to be higher in relation to the increase of the maximum temperature, that is, with a tendency of decrease of the thermal amplitude, for the South region of Brazil, until the end of the 21st century.

Thus, the simulations projected were: increases of 2.1 ºC in the minimum temperature and 1.3 ºC in the maximum temperature, for the less pessimistic scenario (C1); and increases of 5.9 ºC in the minimum temperature and 3.7 ºC in the maximum temperature, for the most pessimistic scenario (C2), which results in the

average temperatures stipulated by the IPCC for the two scenarios. From these preestablished conditions, three simulations of each scenario were performed for each locality and at the end, the means of the three simulations were obtained, for purposes of reliability of the simulated data, since the simulation is stochastic, that is, based on distributions of probability.

Considering that the fifth IPCC report does not explicitly predict projections for global solar radiation, in the simulation of this climatic variable an estimation method was adopted based on the daily temperature range (which is based on temperature) and on the solar radiation at the top of the atmosphere Among the existing methods for this, Chen et al. (2004) for being one of the most recent models and has shown good results in relation to others (BRISTOW and CAMPBELL 1984, HARGREAVES 1981, ALLEN 1997). In Equation 3.3 it is detailed this method that is based on the technique of linear regression.

$$R_G = R_A \times a \times \ln(\Delta T) + b \tag{3.3}$$

where,
R_G is global solar radiation;
R_A radiation at the top of the atmosphere;;
“a” and “b” are coefficients of the regression equation;
“ΔT” is the thermal amplitude (difference between the maximum and minimum temperatures).

For the determination of coefficients "a" and "b" in Equation 3, the data of the daily historical series of temperature for each locality and month of the year were summarized by the moving averages of 5 years, which were applied to the linear regression model given by Equation 3.4:

$$Y = aX + b \tag{3.4}$$

where,
Y is the atmospheric transmissivity (R_G/R_A), that is, the fraction of R_A that reaches the earth's surface;
X is the natural logarithm of ΔT.

For the survey of solar thermal potential residential it was considered a single-family residence, with 75 m² of built area, intended for four residents. This type of housing was chosen because 80% of the country's dwellings are houses with an approximate area from 51m² to 75m² (ELETROBRÁS, 2007; FEDRIGO, GHISI and LAMBERTS, 2009).

The design of the solar system was based on the methodology of the F-Chart, which consists of the determination of the annual solar fraction or percentage

of the energy demand that is covered by the solar installation (DUFFIE and BECKMAN, 1974; BECKMAN, KLEIN and DUFFIE 1977; COMGAS and ABRINSTAL, 2011). The chosen solar collector has a 2-m^2 area, range A in the INMETRO classification, with 60.7% efficiency, with a value of 0.739 of the optical efficiency factor of the collector (FR (τα)). Hot water consumption demand of 400 L/day was defined to be used in the bathroom and kitchen rooms, and 4 collectors were adopted, as shown in Figure 2.

Figure 3.2 - Graphic representation of a standard single family dwelling using solar collectors

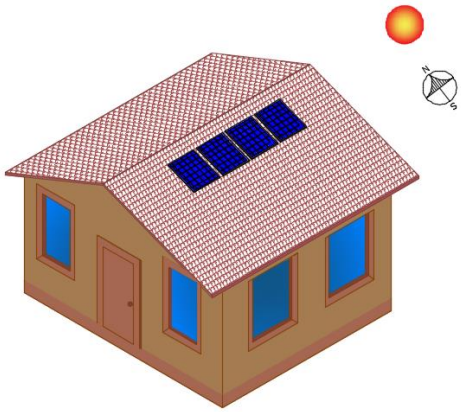

First of all, the useful energy demand must be obtained, according to Equation 3.5. The calculation of the solar thermal energy considers the monthly values of solar radiation, which allows an analysis of the solar thermal utilization throughout the year, allowing a schedule of oscillation according to the different climatic seasons.

$$DE_{month} = Q_{day} \times N \times (T_{HW} - T_{CW}) \times 1{,}16 \times 10^{-3} \quad (3.5)$$

where,
DE_{month} is the energy demand (kWh/month)
Q_{day} is the daily consumption of hot water at the reference temperature (L/day);
N is the number of days in the given month, days/month;
T_{HW} is the temperature used for the quantification of hot water consumption (°C);
T_{CW} is the cold water temperature in the network (°C).

In order to calculate the incident monthly solar radiation (EI_{month}) on the inclined surface of the collectors, Equation 3.6 was used.

$$EI_{month} = R_{G\,day} \times N \quad (3.6)$$

where,
EI_{month} is the energy incident on the collector, in kWh/m²;
$R_{G\,day}$ is the solar radiation incident on the inclined plan, in kWh/(m²xday);
N is the number of days in the month.

By means of Equation 3.7, it is needed calculate the parameter D1, which represents the energy gain of the system and is dependent on the collecting area.

$$D_1 = \frac{EA_{month}}{DE_{month}} \tag{3.7}$$

where,
EA_{month} is the energy absorbed by the collector plan
DE_{month} is the monthly energy demand of the building

Since that the energy absorbed by the collector (EA_{month}) is obtained by Equation 8:

$$EA_{month} = S_c \times F'_R\,(\tau\alpha) \times EI_{month} \tag{3.8}$$

where,
EA_{month} is the monthly solar energy absorbed by the collectors, in kWh/month;
S_c is the collector surface, in m²;
EI_{month} is the monthly solar energy incident on surface collectors, in kWh/(m².month);
$F'_R\,(\tau\alpha)$ is a dimensionless factor provided by the manufacturer, obtained by Equation 9.

$$F'_R\,(\tau\alpha) = F_R(\tau\alpha)_n \times \left[\frac{(\tau\alpha)}{(\tau\alpha)_n}\right] \times \frac{F'_R}{F_R} \tag{3.9}$$

where,
$F_R(\tau\alpha)_n$ is the optical efficiency factor of the collector, available in the INMETRO collector efficiency table;
$\left[\frac{(\tau\alpha)}{(\tau\alpha)_n}\right]$ is the modifier of the angle of incidence, in the lack of this information can adopt 0.96 to collectors with glass cover;
$\frac{F'_R}{F_R}$ is the correction factor of the collector-exchanger skid, in the lack of this information can adopt 0.95.

Through the Equation 10, it must calculate the parameter D2, which represents the thermal energy losses of the solar heating system.

$$D_2 = \frac{EP_{month}}{DE_{month}} \tag{3.10}$$

where,
EP_{month} is the monthly solar energy not used by the collectors, obtained by Equation 11.

$$EP_{month} = S_c \times F'_R U_L \times (100 - T_R) \times \Delta T \times K_1 \times K_2 \tag{3.11}$$

where,
EP_{month} is the monthly solar power not used by the collectors, in kWh/month;
S_c is the surface of the solar collector, in m²;
T_R is the average monthly room temperature in °C;
ΔT is the period of time considered in hours;
$F'_R U_L$ is a factor calculated by Equation 12, in kW/(m²xK);
K_1 is the correction factor for storage, obtained by Equation 13;

K_2 is the adjustment factor for the solar heating system that relates the different temperatures, obtained by Equation 14.

$$F'_R U_L = F_R U_L \times \frac{F'_R}{F_R} \times 10^{-3} \quad (3.12)$$

$$K_1 = \left[\frac{V}{75 \times S_c}\right]^{-0,25} \quad (3.13)$$

where,
V is the volume of solar accumulation (liters). It is recommended that the value be such that it obeys the condition 50 <$\frac{V}{S_c}$<100.

$$K_2 = \frac{(11,6 + 1,18\, T_{MHW} + 3,86\, T_{CW} - 2,32\, T_R)}{(100 - T_{R)}} \quad (3.14)$$

where,
T_{MHW} is the minimum permissible hot water temperature, usually 40 ° C.

The calculation of the power production of the solar installation that was carried out from the F-Chart model. With the values of D1 and D2 the value of f is calculated according to Equation 15.

$$f = 1,029\, D_1 - 0,065\, D_2 - 0,245\, D_1^2 + 0,0018\, D_2^2 + 0,0215\, D_1^3 \quad (3.15)$$

With the value of f calculated, the annual solar fraction F is determined by means of the monthly useful energy absorbed by the solar installation for the residence's hot water production, according to Equation 16. The useful power collected is the fraction of the power that is absorbed by the collector and converted into thermal energy, that is, the difference between the solar energy incident on the collector and the loss to the environment.

$$EU_{month} = f \times DE_{month} \quad (3.16)$$

where,
EU_{month} is the monthly useful power collected, in kWh/month;
f is the monthly solar fraction;
DE_{month} is the power demand, in kWh/month.

Thus, the annual solar fraction F that the surface of the collectors supplies to the residence is obtained by Equation 17.

$$F = \frac{\sum_1^{12} EU_{month}}{\sum_1^{12} DE_{month}} \quad (3.17)$$

In order to verify the availability of solar fraction in the system implementation, the balance between the observed monthly averages (historical series) and the simulated monthly averages (2018-2099) throughout the year was performed by means of statistical analysis. The monthly data of solar fraction were observed and simulated and after that segmented into four periods: Hist (1987-2017), P39 (2018-2039), P69 (2040-2069) and P99 (2070-2099). After checking the data normality for each location and month by the Shapiro-Wilk test, one-way blocked analysis of variance (ANOVA) was used, at a significance level of 1%, where the month was considered as the block and the period as the main factor. For the evaluation of trends, graphs were drawn, regarding the values of global solar radiation (R_G) with monthly solar fractions (f) and tables, with the annual values of solar fraction (f) obtained for all locations in the two scenarios of change climate (C1 and C2).

3.3 RESULTS AND DISCUSSION

From Table 2, it was observed that in the comparison of averages of the monthly values between the historical and simulated periods, all localities presented statistical significance among the values of solar fraction, for C1 and C2, for both blocks (month) and for the main factor (period). It was verified that the historical values presented significant positive differences in relation to all periods, in both scenarios, for all the localities, which implies a decrease of the solar fraction during the century.

It was found that with the impact of the climate change scenarios, the significant differences of f found in 2039, 2069 and 2099 were expressive in magnitude, once the decrease in the percentage of energy demand that is covered by the solar installation was on average 17.3% (14.8) in C1 and 11.3% (9.6) in C2, whereas for some localities (L3 and L4) this decrease was around 20%.

Table 3.2 – Comparison of averages of the monthly values between the historical and simulated periods

ID	ANOVA		Comparision of averages			
C1	**p-Block**	**p-Treat**	**Hist**	**P39**	**P69**	**P99**
L1	0.0000	0.0000	1.2521**a**	1.0462**c**	1.0584**bc**	1.0747**b**
L2	0.0000	0.0000	0.9692**a**	0.8510**b**	0.8653**b**	0.8673**b**
L3	0.0000	0.0000	1.1159**a**	0.8765**b**	0.8932**b**	0.8814**b**
L4	0.0000	0.0000	1.1120**a**	0.8933**c**	0.9801**b**	0.9084**c**
L5	0.0000	0.0000	1.1711**a**	0.9618**c**	0.9732**bc**	0.9879**b**
L6	0.0000	0.0000	1.3006**a**	1.1174**c**	1.1355**bc**	1.1517**b**
L7	0.0000	0.0000	1.3212**a**	1.1274**b**	1.1414**b**	1.1517**b**
L8	0.0000	0.0000	1.1444**a**	0.9398**c**	0.9600**bc**	0.9773**b**
C2						
L1	0.0000	0.0000	1.2521**a**	1.0669**c**	1.0899**c**	1.1268**b**
L2	0.0000	0.0000	0.9692**a**	0.8629**c**	0.8902**c**	0.9258**b**
L3	0.0000	0.0000	1.1159**a**	0.8918**c**	0.9050**bc**	0.9214**b**
L4	0.0000	0.0000	1.1120**a**	0.8974**d**	0.9236**c**	0.9502**b**
L5	0.0000	0.0000	1.1711**a**	0.9733**c**	1.0226**b**	1.0537**b**
L6	0.0000	0.0000	1.3006**a**	1.1346**d**	1.1701**c**	1.2147**b**
L7	0.0000	0.0000	1.3212**a**	1.1463**c**	1.1809**bc**	1.2160**b**
L8	0.0000	0.0000	1.1444**a**	0.9618**d**	1.0204**c**	1.0777**b**

Figure 3.3 – Available solar radiation (R_G) and solar fraction (f) of the system for the hypothetical residence in the historical period and until 2099 in scenarios C1 and C2 for Campo Mourão-PR (L1).

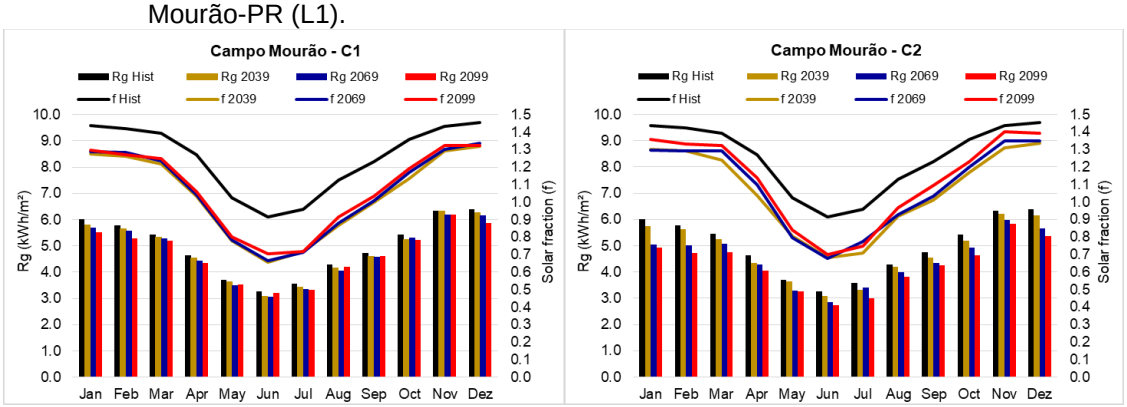

(A) **(B)**

It was observed that for this locality both R_G and a f (historical and simulated in C1 and C2) presented the same variation pattern among the months of the year, although the simulated values for the periods considered showed a slight decrease trend of R_G in relation to historical values. On the other hand, in the reproduced periods of 2039, 2069 and 2099 for f this tendency pointed to an increase of the solar fraction (Figure 3).

In Figure 3A, for L1, the average monthly values of f for C1 varied between 0.65 and 1.34, while in C2, available in Figure 3B, the values of f were in the range from 0.68 to 1.40.

In relation to the monthly solar fraction (Figures 3A and 3B), it was observed that the values between November and March presented a similar behavior, with averages of f in the order of 1.38. It was verified that from May to August, that are fall and winter months, the percentage of energy demand served by the solar installation does not reach the totality, although the average in this period is 0.77 and 0.80, for C1 and C2, respectively. Meanwhile, the monthly values ranged from 0.65 to 0.91 in C1 and from 0.68 to 0.97 in C2, with June being the worst month, with values between P39 and P99 from 0.65 to 0.70 for C1 and between 0.68 and 0.70 for C2.

Figure 3.4 – Available solar radiation (R_G) and solar fraction (f) of the system for the hypothetical residence in the historical period and until 2099 in scenarios C1 and C2 for Castro-PR (L2).

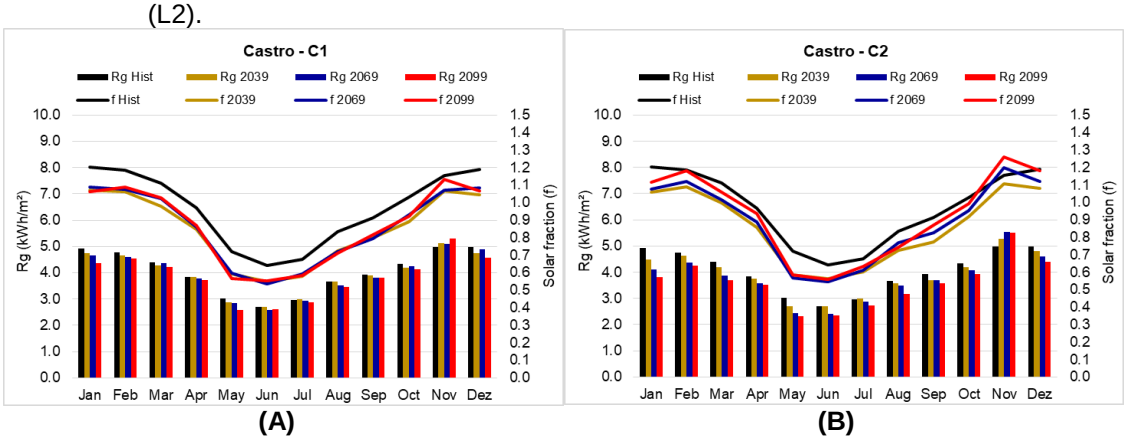

In Figure 4, referring to L2, there was a tendency of decreasing R_G and f (historical and simulated) in C1 and C2 over the periods, although there was a trend of increasing f among the periods between P39 and P99. It should be noted that the monthly values ranged from 0.54 to 1.09 and from 0.54 to 1.26, for C1 and C2, respectively.

Regarding to the monthly solar fraction (Figures 4A and 4B), it was verified that, from April to October, the power demand was not fully satisfied by the solar installation, although the average in this period was 0.75. In this interval, the monthly values ranged from 0.54 to 0.99, with June being the worst month, with an average of

0.55 for C1 and C2. It was observed that for both scenarios, the month of November presented the best performance of f, in the order of 1.11 and 1.18, on average.

Figure 3.5 – Available solar radiation (R_G) and solar fraction (f) of the system for the hypothetical residence in the historical period and until 2099 in scenarios C1 and C2 for Curitiba-PR (L3).

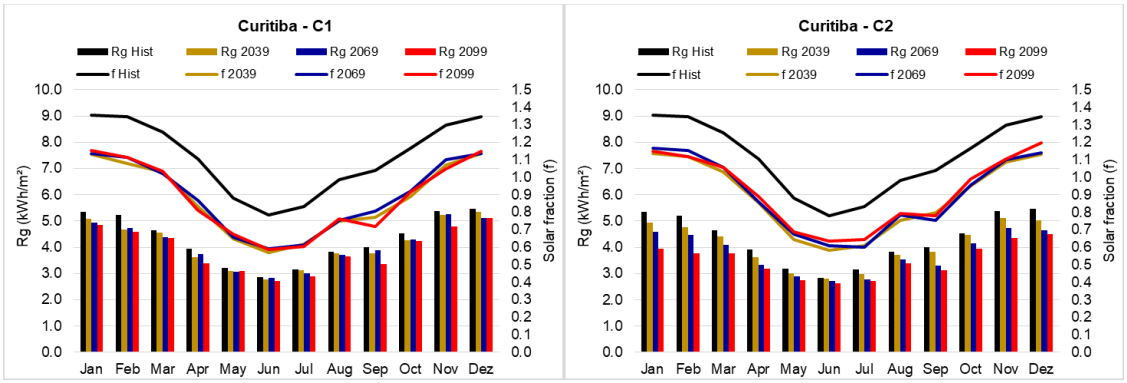

(A) **(B)**

For L3, it was observed that either R_G or f were decreasing trend over the simulated periods, relative to historical values. Based on Figure 5, it was found that the monthly values of f for C1 fluctuated between 0.57 and 1.15, while in C2, the values of f were in the range of 0.58 to 1.20.

In Figures 5A and 5B, in relation to the monthly solar fraction, it was observed that the values between December and February are similar, with averages of f in the order of 1.20. It was verified that the heating system does not supply the total demand during the period from April to October, although the average in this period was 0.74. In this interval, monthly values ranged from 0.57 to 0.99, considering the two scenarios, with June being the worst month, with values between P39 and P99 from 0.57 to 0.64.

Still according to Figures 5A and 5B, it was verified that for the historical data belonging to the months of April, September and October the values of f were above 1, that is, they met the total demand, but, from the simulation of the scenarios, these months presented attendance deficit. In addition, for P99 of C1 and P69 and P99 of C2, the month of September in the other periods of this increase was between the months of August and September.

Figure 6 also shows the downward trend of R_G data and f for L4. It was verified that the monthly values of oscillated between 0.55 and 1.26, considering the two scenarios.

Figure 3.6 – Available solar radiation (R_G) and solar fraction (f) of the system for the hypothetical residence in the historical period and until 2099 in scenarios C1 and C2 for Irati-PR (L4).

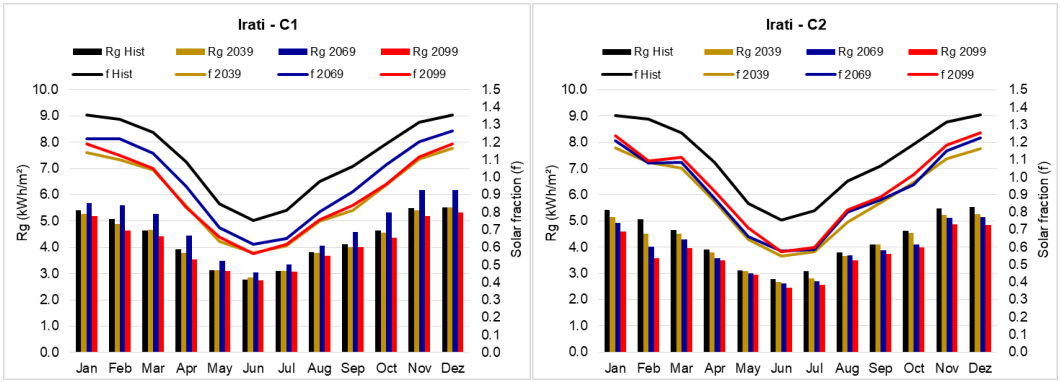

(A) **(B)**

In Figures 6A and 6B, in relation to the monthly solar fraction, it was verified that the demand was not fully supplied in the period from April to October, with the average in this period being 0.77. Meanwhile, the monthly values oscillated between 0.55 to 0.97, considering the two scenarios, which June being the worst month, with values between P39 and P99 of 0.55 to 0.62. Although the month of October does not reach full service, the averages of this month are close to 0.99, that is, very close to 1. It was also observed that the values from November to March have averages of f between 1.1 and 1.2.

Still according to Figures 6A and 6B, it was verified that for the historical data belonging to the months of April, September and October the values of f were above 1, that is, they met the total demand, but, from of the simulation of the scenarios, these months showed a service deficit. In addition, the month of August, despite not reaching the totality, showed a historical value of 0.98.

Figure 3.7 – Available solar radiation (R_G) and solar fraction (f) of the system for the hypothetical residence in the historical period and until 2099 in scenarios C1 and C2 for Ivaí-PR (L5).

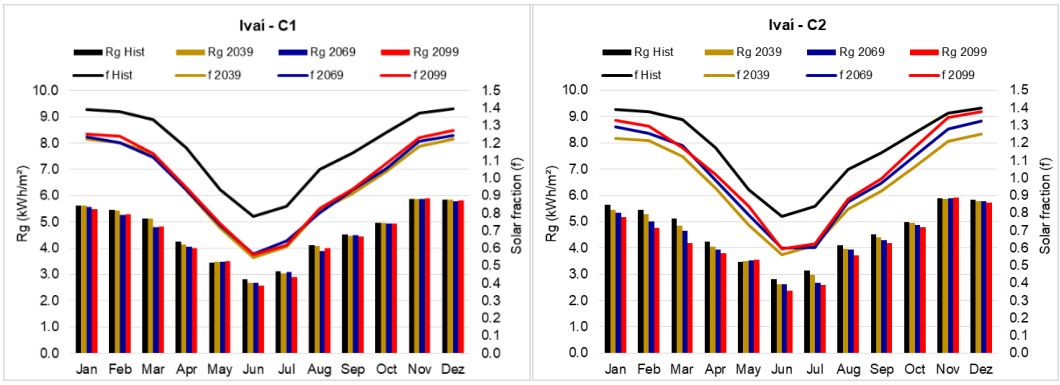

(A) **(B)**

The R_G and f data also showed a downward trend for L5, according to Figure 7, although November and December months of P99 of C2 approximate the historical values. It was found that the monthly values of f ranged between 0.55 and 1.40, considering the two scenarios.

Regarding the monthly solar fraction, in Figures 7A and 7B, it was verified that the demand was not fully supplied in the period from April to September, with the average in this period being 0.79. In this interval, the monthly values oscillated between 0.55 to 0.99, considering the two scenarios, with June being the worst month, with values of 0.55 to 0.60. Although the months of April and September did not reach full service, the averages of these months were respectively 0.96 and 0.95. In addition, in the period between October and March, the averages approximate 1.27 and 1.23, for C1 and C2 respectively.

As shown in Figures 7A and 7B, it can be seen that for historical data from April, August and September the values of f were above 1, that is, they met the total demand, however, from the simulation of the scenarios, these months presented attendance deficit. Besides, the month of May, despite not reaching the totality, presented historical value of f above 90%. It was observed that in C2, the differences between the values between the periods are more discrepants than the C1, which presents a lower variability between the months of the year.

Figure 3.8 – Available solar radiation (R_G) and solar fraction (f) of the system for the hypothetical residence in the historical period and until 2099 in scenarios C1 and C2 for Londrina-PR (L6).

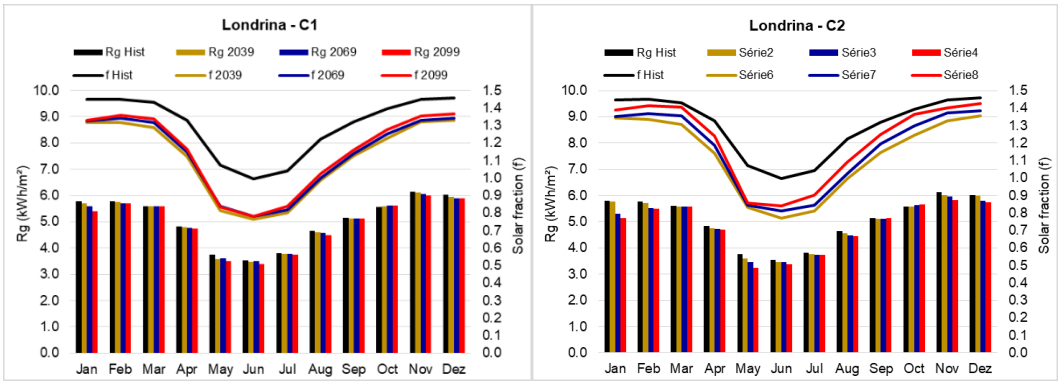

(A) **(B)**

According to Figure 8, for L6, the R_G and f data showed a downward trend in relation to the historical data, however, with a tendency to increase between P39 and

P99, being verified more expressively in C2. It was observed that the monthly values of f ranged from 0.76 to 1.46.

In relation to the monthly solar fraction, in Figures 8A and 8B, it was verified that the demand was not fully supplied in the period from May to July, and the average in this period was 0.83. However, for the historical data belonging to the same months, the values of f were above 1, that is, they met the total demand, but, from the simulation of the scenarios, these months suffered a service deficit. It was observed that, in C2, the differences of the values among the periods were more dissimilar in relation to the C1, which presents a better homogeneity among the months.

Figure 3.9 – Available solar radiation (R_G) and solar fraction (f) of the system for the hypothetical residence in the historical period and until 2099 in scenarios C1 and C2 for Maringá-PR (L7).

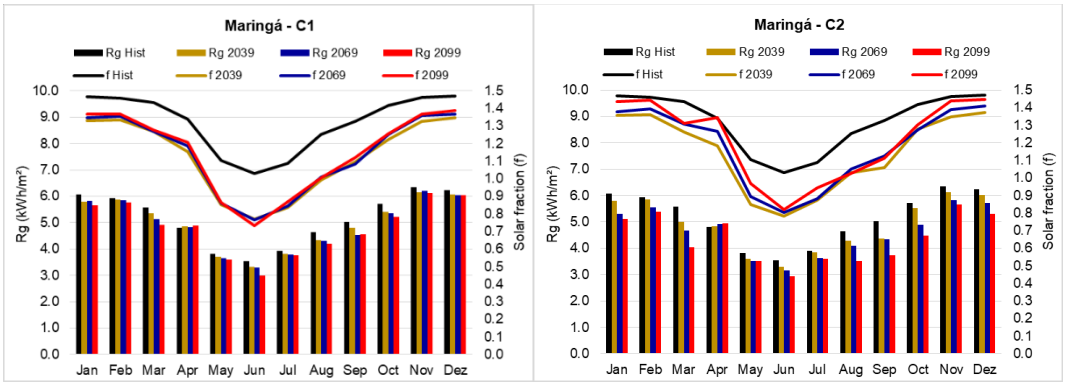

(A) **(B)**

According to Figure 9, for L7, the R_G and f data showed a reduction trend in relation to the historical data, however, with a tendency to increase between P39 and P99, being verified more expressively in C2. It was verified that the monthly values of f ranged from 0.73 to 1.47, considering the two scenarios.

Regarding the monthly solar fraction, in Figures 9A and 9B, it was observed that the demand was not fully supplied in the period from May to July, with the average in this period being 0.85. In this interval, the monthly values ranged from 0.73 to 0.97, considering the two scenarios, which June being the worst month, with mean values of 0.76 to 0.80, for C1 and C2, respectively. It was found that, for the historical data of these months, the values of f were above 1, that is, they met the total demand, but, from the simulation of the scenarios, these months showed insufficient attendance.

Figure 3.10 – Available solar radiation (R_G) and solar fraction (f) of the system for the hypothetical residence in the historical period and until 2099 in scenarios C1 and C2 for Paranaguá-PR (L8).

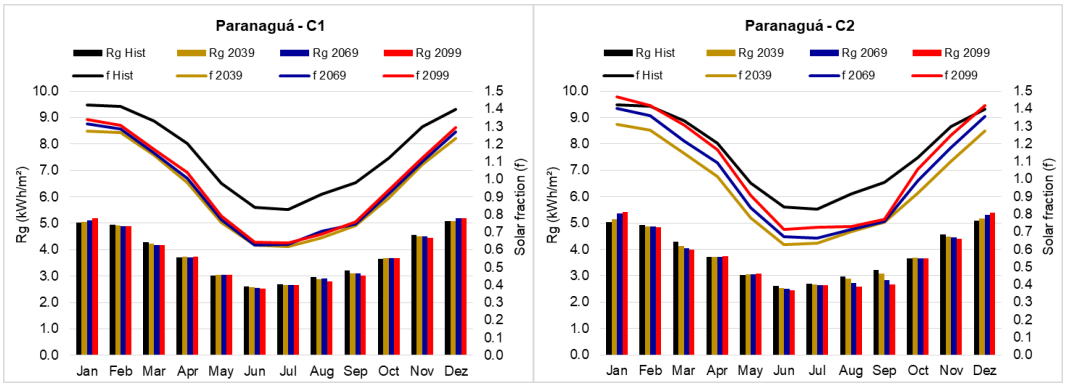

(A) **(B)**

As shown in Figure 10, for L8, the RG and f data presented a downward trend in relation to the historical data, however, with a tendency to increase between P39 and P99, and it was verified more expressively in C2. It was noticed that the monthly values of f ranged from 0.62 to 1.47, considering the two scenarios.

Regarding the monthly solar fraction, in Figures 10A and 10B, it was verified that the demand was not fully supplied in the period from May to October, with an average of 0.73 for C1, and in the period between May and September, for the period C2, with an average of 0.73 in the interval. The months of June and July exhibited the same behavior, with an average of 0.67 and were considered the worst months for the use of solar energy. Although the month of October does not reach full service, the average of this month is around 0.92, that is, very close to 1.

Table 3.3 – Annual solar fraction for all locations in all periods and scenarios

Scenario/Period		**C1**			**C2**		
ID	**Hist**	**P39**	**P69**	**P99**	**P39**	**P69**	**P99**
L1	1.223	1.010	1.019	1.036	1.029	1.048	1.076
L2	0.942	0.824	0.836	0.836	0.835	0.857	0.885
L3	1.089	0.850	0.865	0.853	0.863	0.873	0.889
L4	1.082	0.863	0.946	0.874	0.865	0.887	0.909
L5	1.140	0.926	0.938	0.949	0.937	0.979	1.004
L6	1.274	1.083	1.099	1.113	1.097	1.129	1.170
L7	1.298	1.096	1.107	1.114	1.113	1.141	1.171
L8	1.109	0.898	0.916	0.931	0.919	0.967	1.015

Table 3 presents the values of annual solar fraction (F) for all locations, in all periods and scenarios. It was observed that, for the historical series, all localities

except L2 presented values of F above 1, which represents the fullness of the annual demand for heated water, although the value of F of L2 was very satisfactory. It was observed that the simulated values showed a decreasing tendency in relation to historical values, although during the reproduced periods of 2039, 2069 and 2099 this tendency was shown to be increasing.

It was verified that, in spite of the decrease observed in relation to the historical period, the localities L1, L6 and L7 generally obtained values of F greater than 1 in C1 and C2. Although the other locations (L2, L3, L4, L5 and L8) did not reach full service, annual percentages were reached above 82%, values considered compatible with the climate of the localities and the expected seasonality of solar heating systems.

In general, for all the localities, it was observed that the simulated solar fraction values showed a decreasing tendency over the reproduced periods of 2039, 2069 and 2099, in relation to historical values. This fact can be explained by the method of calculation of the solar fraction that uses the global solar radiation data. Once it was verified that the estimated values of R_G from the simulated maximum and minimum temperatures also showed a tendency to decrease, this behavior could be attributed to the model used to estimate the R_G of Chen et al. (2004), which is based on the daily thermal amplitude (ΔT). Since the projections of the climatic scenarios caused the decrease of this amplitude, this tendency incorporated in the model caused the reduction of the values of solar radiation that, consequently, caused the decrease of the solar fraction.

Similarly, Bierhals et al. (2017) found that, for the State of Rio Grande do Sul, climate scenario models have shown that global solar radiation values tend to decline to 60% of the year through 2100. Furthermore, Huber et al. al. (2016) concluded that global solar radiation in the future (2035-2039) is likely to be reduced by comparing historical values (1995-1999).

It is important to note that the highest values of solar fraction verified, refer to the months between October and March, coinciding with the spring and summer seasons, when the sun's rays illuminate the southern hemisphere more. With similar justification, the lowest values refer to the months from April to September, belonging to fall and winter, when the days are shorter in the southern hemisphere and the solar rays have lower intensity, due to the apparent movement of the Sun in relation to the Earth and due to the solar declination.

In general, all the localities presented a characteristic seasonal behavior, with the total and surplus attendance of the system in the seasons corresponding to spring and summer, whereas in the months of fall and winter, the demand was not fully satisfied by the system, being that this behavior is compatible with the seasonality predicted in solar energy systems.

Similarly, Barbosa and Carvalho (2018) verified that the daily energy of the solar heating system, installed in the city of João Pessoa (PB), is not sufficient to meet the demand in five months of the year (from May to August). For this locality, this period is the one with the lowest incidence of solar radiation, which results in a smaller amount of collected useful energy and consequently of stored energy. In another research for this locality, Medeiros et al. (2014) found that the solar fraction calculated in most of the months was higher than 0.65, and only in June, July, August and November was less than 0.60, with an annual average of 0.65 and monthly fractions between 0.47 (July) and 0.87 (February).

In other places in Brazil, such as Florianópolis (SC), Colle et al. (2010) obtained solar fractions in the range from 0.5 to 0.9, with July being the worst recorded month, whereas the months of February and December were the only ones that reached values of f above 0.8. Sinigaglia et al. (2016) obtained annual solar fraction with an average value of 1,076, that is, 107.6% of the annual demand served in Tuparendi, in the northwest of the State of Rio Grande do Sul. In addition, the system presented values of monthly solar fraction in the interval between 0.40 (June) and 1.72 (January). In May, June, July, August and September, the collector would not be able to supply energy demand.

In general, the solar fraction can be understood as an efficiency metric of the solar water heating system. Therefore, all the studied localities had annual efficiency values above 80%. Basso et al. (2010), evaluated a prototype of a solar heating system in the city of Cascavel-PR and found average efficiency above 80% in the winter months, while Celuppi et al. (2014) obtained approximate efficiency of 65% in their experiments in the city of Chapecó-SC.

In other countries, such as India, for example, Dharuman, Arakeri and Srinivasan (2006) evaluated an integrated model of solar water heater and achieved about 60% efficiency during the day and 40% of total efficiency and classified the collector performance as satisfactory, even during cloudy days. Nevertheless, Delač,

Pavković and Lenić (2018) obtained a 68% efficiency rate in the heating system in Croatia.

Li et al. (2016) achieved about 78% energy savings in the hot period, in a rural residence in northwest China. Alajmi, Rodríguez and Sailor (2018) found a reduction in energy consumption of about 64%, or 3047 kWh/year, at a residence in Portland, USA. Parker (2003) presented a 61% reduction in energy demand in the solar system when compared to the electric heater in four residences in Florida, USA.

On the other hand, Hoffman and Ngo (2018) implemented heating systems in rural communities in the Dominican Republic and obtained efficiency indices between 406 and 827%, the lowest values being reached in the month of June and the highest in January, with temperatures of air recorded between 36 and 42 °C and performance results that exceeded the target temperature increase of at least 12 °C.

Altoé et al. (2017) found that the maximum economic viability of the solar water heater installation is in annual solar fractions between 80 and 90%. In addition, Naspolini, Militão and Rüther (2010) and Naspolini and Rüther (2017) found that the aggregation of solar thermal energy to the water heating for the bath in Florianópolis (SC), provides a significant annual reduction of 38 to 48% of the peak demand demanded from the utility to heat the water for the bath. While Cardemil, Starke and Colle (2018) found a 40% to 62% reduction in peak energy consumption for the same locality.

Altoé, Oliveira Filho and Carlo (2012) concluded that the replacement of the electric shower by the solar system with electric support caused a reduction of 70% in the electric energy consumption intended for domestic water heating and 36% in the total electric energy consumption of the residence. Medeiros et al. (2014) argued that the annual savings of the solar heating system is about 55% compared to a conventional system.

The solar heating system studied by Giglio, Santos and Lamberts (2018), in a residential condominium in Florianópolis (SC), presented a mean of 64% reduction of peak demand, compared to an electric system, which corresponds to 0.35 kW in average reduction of peak demand and an energy saving of approximately 48 kWh/month per residential unit.

Altoé et al. (2017) found in an economic feasibility analysis that the use of solar water heater in a typical Brazilian dwelling presented a payback period of about 4.5 years. Likewise, Li et al. (2016) had a return period of 4.4 years in China. Martins,

Abreu and Pereira (2012) stated that the time of return is lower mainly for regions with higher energy demand and located in the subtropical climate in the South and Southeast regions, and for the State of Paraná, this estimated period is every 3 years and 10 months, depending on the locality.

In addition, Naspolini and Rüther (2017) showed that the use of residential solar heating systems contributes to the economy between 38 and 42% in the annual cost of electric power, per consumer unit. Although the fraction of power savings per dwelling is higher in places with warmer climate, such as the North, Northeast and Central regions, the total energy savings per year is very similar for all the Brazilian regions (MARTINS, ABREU and PEREIRA, 2012).

It is important to highlight in this research that the solar collectors installed in the hypothetical residences would occupy an area of approximately 8m², that is, less than 10% of the available area of the considered roof. It should be noted that, in order to obtain higher efficiency values, more collectors could be installed. However, it was decided to keep the same number scaled for historical values. This is in contrast to that found in the United Kingdom by Ma, Bao and Roskilly (2018), who concluded that for eight cities the solar heating system that could be installed on the roofs of the houses would supply about 38.2 to 52.6% of the total heating demands, because the required solar collector area was larger than the average roof area available in the region's standard houses.

Since in Brazil the use of electric shower to heat water is the main cause of the "peak of demand" in the electricity consumption, between 6:00 p.m. and 09:00 p.m., the solar heating system presents itself as an important energy efficiency policy for Brazil, and should be considered as an effective measure to reduce energy demand at peak demand and improve the rational use of electricity, making it a relatively small subsidy that may reflect immeasurable benefits (NASPOLINI and RÜTHER, 2017; CARDEMIL, STARKE and COLLE, 2018; GIGLIO, SANTOS and LAMBERTS, 2018).

Moreover, according to Basso et al. (2010), there is technical feasibility in the installation of water heating equipment by solar energy in the State of Paraná, because it is possible to reach minimum temperatures of the bath water in sufficient number of days so that the electric heating is only complementary and used sporadically.

Regarding possible scenarios of climate change, it is believed that they can significantly impact the system efficiency, in this case, in a negative way, causing a small drop in the percentage of energy demand that is covered by the solar installation. Celuppi et al. (2014) found that small increases in air temperatures promote a significant decrease in the efficiency percentage. However, even in climate change scenarios for the 21st century, Hu et al. (2016) have found in their experiments that solar energy has the potential to supply human demand both now and in the future.

3.4 CONCLUSION

Considering the results found in this research, it can be inferred that the estimation of the solar fraction in function of the regionality and possible scenarios of climate change are important aspects in the evaluation of the viability of installation of integrated solar water heating systems in the residences.

The modeling applied to the analyzed localities for the estimation of the solar fraction showed annual values between 82.4% and 129.8%, which proves that the State of Paraná has favorable and satisfactory climatic conditions for the installation of solar heating systems. Even though in these localities, the winter months do not reach full service, through the solar heating system, the monthly solar fractions found (all above 50%) for the period evaluated, contribute to the reduction in the consumption of electric power in more than half, since these systems can function as aggregators in the residence and do not, necessarily, operate isolatedly.

The research showed that if the system is installed in the residence today, and by following the maintenance and conservation instructions issued by the manufacturer are followed, the same collectors can be used by the end of the century, even in possible scenarios of climate change, without a considerable loss of energy efficiency.

The popularization of solar water heaters in Brazilian homes should bring benefits to the users, due to the reduction of costs with energy consumption. However, the importance in relation to the environment is highlighted, due to the contribution to the reduction of emissions of greenhouse gases.

In addition, the installation of the systems can contribute to the reduction of the national demand for electric energy, benefiting the national electricity system and increasing the Brazilian energy matrix. On the other hand, it is important that there

are public incentive policies, either through laws, regulations, tax reductions, financing, awareness campaigns or research projects, that promote the adoption of solar heating systems in all types of residences.

FINAL CONSIDERATIONS

The first article, referring to Chapter 1, evaluated the performance of four empirical models of solar radiation estimation (Chen, Hargreaves, Hunt and Richardson) from air temperature data. It was verified that the models proposed by Chen and Hunt presented the best performances for the localities of Paraná, since they were closer to the estimates based on observed historical data.

The second article, referring to Chapter 2, determined the estimation of photovoltaic solar energy production for single-family dwellings, in scenarios of possible climatic changes projected towards the end of the 21st century, and in all the analyzed localities, annual average indices of 98% of system service.

The third article, referring to Chapter 3, estimated the solar fraction obtained by means of solar heating systems for single-family dwellings, in scenarios of climatic changes designed towards the end of the century. In all the localities annual values of solar fraction found were over 80%.

From the obtained results, it was verified that the State of Paraná has favorable climatic conditions for the installation of photovoltaic solar energy systems and solar water heating, even if they are installed for aggregation purposes, in order to reduce electricity consumption.

The relationships between climate change and sustainable development are more visible at the local level and can encourage cities and their governments to seek social and technological innovations that improve the urban environment and contribute to mitigating the energy problem by fostering the necessary adaptations in present and future situations.

REFERENCES

ALAJMIA, A.; RODRÍGUEZ, S.; SAILOR, D. Transforming a passive house into a net-zero energy house: a case study in the Pacific Northwest of the U.S. **Energy Conversionand Management**, v. 172, p. 39-49, 2018.

ALLEN, R.G. Self-calibrating method for estimating solar radiation from air temperature. **Journal of Hydrologic Engineering,** v. 2, n. 2, p. 56-67, 1997.

ALMOROX, J.; HONTORIA, C.; BENITO, M. Models for obtaining daily global solar radiation with measured air temperature data in Madrid (Spain). **Applied Energy**, v. 88, p. 1703–1709, 2011.

ALTOÉ, L.; OLIVEIRA FILHO, D.; CARLO, J. C. Análise energética de sistemas solares térmicos para diferentes demandas de água em uma residência unifamiliar. **Ambiente Construído**, Porto Alegre, v. 12, n. 3, p. 75-87, jul./set. 2012.

ALTOÉ, L.; OLIVEIRA FILHO, D.; CARLO, J. C.; MONTEIRO, P. M. B.; MARTINS, I. T. A. Analysis of the economic viability and greenhouse gas emissions reductions resulting from the use of solar water heaters in a typical Brazilian dwelling. **Latin American Journalof Energy Research**, v. 4, n. 2, p. 1-10, 2017.

ANGSTRÖM, A. Solar and terrestrial radiation. **Quarterly Journal of the Royal Meteorological Society,** v. 50, p. 121-125, 1924.

BARBOSA, R.R.; CARVALHO, M. Dimensionamento de um sistema de aquecimento solar de água para aplicações industriais. **Engevista**, v. 20, n. 2, p. 214-238, abr., 2018.

BASSO, L. H.; SOUZA, S. N. M.; SIQUEIRA, J. A. C.; NOGUEIRA, C. E. C.; SANTOS, R. F. Análise de um sistema de aquecimento de água para residências rurais, utilizando energia solar. **Engenharia Agrícola**, Jaboticabal, v. 30, n. 1, p.14-21, jan./fev. 2010.

BECKMAN, W. A.; KLEIN, S. A.; DUFFIE, J. A. **Solar heating design by the f-Chart Method**. New York: Wiley-Interscience, 1977.

BIERHALS, E. E.; PEREIRA, F.; BRAZIL, C.; ROSSINI, E. Solar radiation projections of Cmip5 models for South of Brazil. **Contemporary Urban Affairs**, v. 1, n. 3, p. 1-6, 2017.

BRASIL. Ministério de Minas e Energia. Empresa de Pesquisa Energética. **Plano Nacional de Energia 2030.**Brasília: EPE, 2007.

BRISTOW, K.L; CAMPBELL, G.S. On the relationship between incoming solar radiation and daily maximum and minimum temperature. **Agricultural and Forest Meteorology,** v. 31, p. 159–166, 1984.

BURIOL, G.A.; ESTEFANEL, V.; HELDWEIN, A.B.; PRESTES, S.D.; HORN, J.F.C. Estimativa da radiação solar global a partir dos dados de insolação, para Santa Maria-RS, **Ciência Rural**, v. 42, n. 9, p.1563-1567, set, 2012.

CAMARGO, A.P.; SENTELHAS, P.C. Avaliação do desempenho de diferentes métodos de estimativa da evapotranspiração potencial no estado de São Paulo. **Revista Brasileira de Agrometeorologia**, Santa Maria, v. 5, n. 1, p. 89-97, 1997.

CAMPOS, H.M.; MANRIQUE, A.K.R.; KOBISKI, B.V.; CASAGRANDE JÚNIOR, E.F.; URBANETZ JÚNIOR, J. Study of technical feasibility and the payback period of the invested capital for the installation of a grid-connected photovoltaic system at the library of the Technological Federal University of Paraná. **International Journal of Energy and Environment** (print), v.5, n.6, p.643-654, 2014.

CARDEMIL, J.M.; STARKE, A.R.; COLLE, S. Multi-objective optimization for reducing the auxiliary electric energy peak in lowcost solar domestic hot-water heating systems in Brazil. **Solar Energy**, v. 163, p. 486-496, 2018.

CELUPPI, R.; SCAPINELLO, J.; ANDRADE, F. G. D.; REVELLO, J. H. P.; MAGRO, J. D. Solar energy use for water pre-heating in boilers of agro-industries. **Engenharia Agrícola**, Jaboticabal, v. 34, n. 3, p. 451-460, maio/jun. 2014.

CHEN, R.; ERSI, K.; YANG, J.; LU, S.; ZHAO, W. Validation of five global radiation models with measured daily data in China. **Energy Conversion and Management,** v. 45, p. 1759-1769, 2004.

COLLE, S.; STARKE, A.R.; PASSOS, L.A.A.; VEIGA, C.E. Uma análise de sistemas de aquecimento solar de água para uso doméstico no Brasil. In: Congresso Brasileiro de Energia Solar, 3, 2010, Belém. **Anais...** Belém: 2010.

COMGAS; ABRINSTAL. **Sistemas de aquecimento de água para edifícios através da associação energia solar e gás natural**: manual técnico para projeto e construção de sistemas de aquecimento solar & gás natural. Mar, 2011.

CRESESB. Centro de referência para energia solar e eólica Sérgio de Salvo Brito. **Energia solar:** princípios e aplicações. 2006.Disponível em: <http://www.cresesb.cepel.br/download/tutorial/tutorial_solar_2006.pdf>. Acesso em: 12 set 2017.

DAUT, I.; IRWANTO, M.; IRWAN, Y. M.; GOMESH, N.; AHMAD, N. S. Combination of Hargreaves method and linear regression as a new method to estimate solar radiation in Perlis, Northern Malaysia. **Solar Energy**, v. 85, p. 2871-2880, 2011.

DELAČ, B.; PAVKOVIĆ, B.; LENIĆ, K. Design, monitoring and dynamic model development of a solar heating and cooling system. **Applied Thermal Engineering**, v. 142, p. 489–501, 2018.

DHARUMAN, C.; ARAKERI, J. H.; SRINIVASAN, K. Performance evaluation of an integrated solar waterheater as an option for building energy conservation. **Energy and Buildings**, v. 38, p. 214–219, 2006.

DONATELLI, M.; CAMPBELL, G.S. A simple model to estimate global solar radiation. In: European Society of Agronomy Congress, 5, 1998, Nitra. **Proceedings...** Nitra, 1998.

DUFFIE, J. A.; BECKMAN, W. A. **Solar Engineering of Thermal Processes.** Hoboken: Wiley, 1974.

EHNBERG, J.; BOLLEN, M. Simulation of global solar radiation based on cloud observations. **Solar Energy**, v. 78, n. 2, p. 157-162, 2004.

ELETROBRAS. **Pesquisa de posse de equipamentos e hábitos de uso, ano base 2005:** classe residencial relatório Sul. Rio de Janeiro: Eletrobras/Procel, 2007.

EPE. Empresa de Pesquisa Energética. **Balanço energético nacional 2017:** ano base 2016. Rio de Janeiro: EPE, 2017.

FEDRIGO, N.S.; GHISI, E.; LAMBERTS, R. Usos finais de energia elétrica no setor residencial brasileiro. In: Encontro Latino Americano de Conforto no Ambiente Construído, 6, 2009, Natal. **Anais...** Natal: 2009, p. 1076-1085.

FRAIDENRAICH, N. **Tecnologia solar no Brasil. Os próximos 20 anos**. 2014. Disponível em: <http://www.feagri.unicamp.br/energia/energia2002/jdownloads/pdf/papers/paper_Fraidenraich.pdf> Acesso em: 18 out 2017.

FRANK, T.H. Climate change impacts on building heating and cooling energy demand in Switzerland. **Energy and Buildings**, v. 37, p. 1175-1185, 2005.

FREITAS, C.H.; SIMÕES, J.; MARTINS, F.B. Modelos para estimativa da radiação solar incidente mensal em Belo Horizonte, Minas Gerais, usando dados de temperatura do ar. In: Workshop Brasileiro de Micrometeorologia, 9, 2015, Santa Maria. **Anais…** Santa Maria, 2015.

GIGLIO, T.; SANTOS, V.; LAMBERTS, R. Analyzing the impact of small solar water heating systems on peak demand and on emissions in the Brazilian context. **Renewable Energy**, 2018, https://doi.org/10.1016/j.renene.2018.08.104.

GNOATTO, E.; DALLACORT, R.; RICIERI, R. P.; SILVA, S. L.; FERRUZI, Y. Eficiência de um conjunto fotovoltaico em condições reais de trabalho na região de Cascavel. **Acta Scientiarum Technology**, Maringá, v. 30, n. 2, p. 215-219, 2008.

HAMADA, Y.; NAKAMURA, M.; SAITOH, H.; KUBOTA, H. Field performance of an energy pile system for space heating. **Energy and Buildings**, v. 39, n.5, p.517-524, 2007.

HARGREAVES, G.H. Responding to tropical climates. In: The Food and Climate Forum, 1981, Boulder. **Proceedings…** Boulder, 1981.

HOFFMAN, L.A.; NGO, T.T. Affordable solar thermal water heating solution for rural Dominican Republic. **Renewable Energy**, v. 115, p. 1220-1230, 2018.

HU, A.; LEVIS, S.; MEEHL, G. A.; HAN, W.; WASHINGTON, W. M.; OLESON, K. W.; RUIJVEN, B. J. V.; HE, M.; STRAND, W. G. Impact of solar panels on global climate. **Nature Climate Change**, v. 6, p. 290-294, 2016.

HUBER, I.; BUGLIARO, L.; PONATER, M.; GARNY, H.; EMDE, C.; MAYER, B. Do climate models project changes in solar resources? **Solar Energy**, v. 129, p. 65-84, 2016.

HUNT, L.A. Estimation of solar radiation for use in crop modeling. **Agricultural and Forest Meteorology**, v. 91, n. 3, p. 293-300, 1998.

IAPAR. Instituto Agronômico do Paraná. **Cartas climáticas do Paraná**. Disponível em <http://www.iapar.br/modules/conteudo/conteudo.php?conteudo=863>. Acesso em nov. 2018.

IPCC. **Climate Change 2014:** Synthesis Report. Contribution of Working Groups I, II and III to the Fifth Assessment Report of the Intergovernmental Panel on Climate Change. Genebra: IPCC, 2014.

JARDIM, C.S.; RÜTHER, R.; SALAMONI, I.T.; VIANA, T.S.; REBECHI, S.H.; KNOB, P.J. The strategic siting and the roofing area requirements of building-integrated photovoltaic solar energy generators in urban areas in Brazil. **Energy and Buildings**, v.40, p. 365-370, 2008.

JERSZURKI, D.; SOUZA, J. L. M. Parametrização das equações de Hargreaves & Samani e Angström-Prescott para estimativa da radiação solar na região de Telêmaco Borba, Estado do Paraná. **Ciência Rural**, Santa Maria, v.43, n.3, p.383-389, mar, 2013.

KALOGIROU, S. A. Solar thermal collectors and applications. **Progress in Energy and Combustion Science**, v. 30, p. 231–295, 2004.

KOPP, G.; LEAN, J. L. A new, lower value of total solar irradiance: evidence and climate significance. **Geophysical Research Letters**, v. 38, p. 1-7, 2011.

KREITH, F.; KREIDER, J.F. **Principles of Solar Engineering**. Washington: Hemisphere, 1978.

LENZ, A.M.; SOUZA, S.N.M.; NOGUEIRA, C.E.C.; GURGACZ, F.; PRIOR, M.; PAZUCH, F.A. Analysis of absorbed energy and efficiency of a solar flat plate collector. **Acta Scientiarum Technology**, Maringá, v. 39, n. 3, p. 279-284, jul./set. 2017.

LI, J.; LI, X.; WANG, N.; HU, Y.; FENG, R. Experimental research on indoor thermal environment of new rural residence with active solar water heating system and external wall insulation. **Applied Thermal Engineering**, v. 95, p. 35–41, 2016.

LIU, X.; MEI, X.; LI, Y.; WANG, Q.; JENSEN, J.R.; ZHANG, Y.; PORTER, J.R. Evaluation of temperature-based global solar radiation models in China. **Agriculture and Forest Meteorology**, v. 149, p. 1433-1446, 2009.

MA, Z.; BAO, H.; ROSKILLY, A.P. Feasibility study of seasonal solar thermal energy storage in domestic dwellings in the UK. **Solar Energy**, v. 162, p. 489–499, 2018.

MARENGO, J.A. Mudanças climáticas globais e regionais: avaliação do clima atual do Brasil e projeções de cenários climáticos do futuro. **Revista Brasileira de Meteorologia**, São Paulo, v. 16, n. 1, p. 01-18, 2001.

MARENGO, J.A.; CAMARGO, C.C. Surface air temperature trends in Southern Brazil for 1960–2002. **International Journal of Climatology**, v. 28, p. 893-904, 2008.

MARQUES, D.D.; BRITO, A.U.; CUNHA, A.C.; SOUZA, L.R. Variação da radiação solar no Estado do Amapá: estudo de caso em Macapá, Pacuí, Serra do Navio e Oiapoque no período de 2006 a 2008. **Revista Brasileira de Meteorologia**, v. 27, n. 2, p. 127-138, 2012.

MARTINAZZO, C.A. **Modelos de estimativa de radiação solar para elaboração de mapas solarimétricos**. 2004, 209 f. Dissertação (Mestrado em Engenharia Mecânica) – Universidade Federal do Rio Grande do Sul, Porto Alegre, 2004.

MARTINS, F. R.; ABREU, S. L.; PEREIRA, E. B. Scenarios for solar thermalenergyapplications in Brazil. **Energy Policy,** v. 48, p. 640–649, 2012.

MARTINS, R.D.; FERREIRA, L.C. Oportunidades e barreiras para políticas locais e subnacionais de enfrentamento das mudanças climáticas em áreas urbanas: evidências de diferentes contextos. **Ambiente & Sociedade**, Campinas, v. 13, n. 2, p. 223-242 jul./dez. 2010.

MAVROMATIS, T.; JAGTAP, S. S. Estimating solar radiation for crop modeling using temperature data from urban and rural stations. **Climate Research**, v. 29, p. 233-243, 2005.

MEDEIROS, J.M.; FÉLIX, W.M.; SILVA, M.G.; MEDEIROS, M.J.; BRAGA, A.H.G. Avaliação técnica e viabilidade econômica de um sistema de aquecimento solar em um edifício residencial. **Revista Principia**, João Pessoa, n. 24, p. 57-71, 2014.

MEZA, F.; VARAS, E. Estimation of mean monthly solar global radiation as a function of temperature. **Agricultural and Forest Meteorology**, v. 100, p. 231-241, 2000.

MICHELS, R. N.; GNOATTO, E.; SANTOS, J. A. A.; KAVANAGH, E.; HALMEMAN, M. C. A influência da temperatura na eficiência de painéis fotovoltaicos em diferentes níveis de incidência da radiância solar. **Revista Agrogeoambiental,** dez. 2010.

MINUZZI, R.B.; CARAMORI, P.H.; BORROZINO E. Tendências na variabilidade climática sazonal e anual das temperaturas máxima e mínima do ar no Estado do Paraná. **Bragantia**, Campinas, v. 70, n. 2, p.471-479, 2011.

MOGAWER, T.; SOUZA, T. M. Sistema solar de aquecimento de água para residências populares. In: Encontro de Energia no Meio Rural e Geração Distribuída, 5, 2004, Campinas. **Proceedings...** Campinas, 2004.

MONTEIRO, N.S.C.; MONTEIRO, R.A.B.; MARIANO, J.D.A.; URBANETZ JUNIOR, J.; ROMANO, C.A. Brazil market outlook for photovoltaic solar energy: A survey study. **British Journal of Applied Science & Technology**, v. 21, n. 5, p. 1-11, 2017.

MORADI, I.; MUELLER, R.; PEREZ, R. Retrieving daily global solar radiation from routine climate variables. **Theoretical and Applied Climatology**, v. 116, p. 661-669, 2014.

NASPOLINI, H. F.; MILITÃO, H. S. G.; RUTHER, R. The role and benefits of solar water heating in the energy demands of low-income dwellings in Brazil. **Energy Conversionand Management**, v. 51, p. 2835-2845, 2010.

NASPOLINI, H.F.; RÜTHER, R. Impacts of Domestic Solar Water Heating (DSWH) systems on the cost of a hot shower in low-income dwellings in Brazil. **Renewable Energy**, v. 111, p. 124-130, 2017.

NIELSEN, L.B.; PRAHM, L.P.; BERKOWICZ, R.; CONRADSEN, K. Net incoming radiation estimated from hourly global radiation and/or cloud observations. **Royal Meteorological Society**, v. 1, n. 3, p. 255-272, jul./sep. 1981.

NOGUEIRA, P. H. O. **Simulação do desempenho de sistemas solares fotovoltaicos para a geração de eletricidade:** um estudo de caso do sistema fotovoltaico da embaixada da Itália. 2014, 110 f. Monografia (Graduação em Engenharia de Energia) – Universidade de Brasília, Brasília, 2014.

OHUNAKIN, O.S.; ADARAMOLA, M. S.; OYEWOLA, O. M.; MATTHEW, O. J.; FAGBENLE, R. O. The effect of climate change on solar radiation in Nigeria. **Solar Energy**, v. 116, p. 272-286, 2015.

OLIVEIRA, L. F. C.; FERREIRA, R. C.; ALMEIDA, R. A. A.; LOBATO, E. J. V.; MEDEIROS, A. M. M. Potencial de redução do consumo de energia elétrica pela utilização de aquecedores solares no Estado de Goiás. **Engenharia Agrícola**, Jaboticabal, v. 28, n. 3, p. 406-416, jul./set. 2008.

PARKER, D.S.Research highlights from a large scale residential monitoring study in a hot climate. **Energy andBuildings**, v. 35, n. 9, p. 863-876, 2003.

PBMC, 2013: **Contribuição do Grupo de Trabalho 2 ao Primeiro Relatório de Avaliação Nacional do Painel Brasileiro de Mudanças Climáticas**. Sumário Executivo do GT2. PBMC, Rio de Janeiro, Brasil. 28 p.

PEREIRA, E.B.; MARTINS, F.R.; GONÇALVES, A.R.; COSTA, R.S.; LIMA, F.J.L.; RÜTHER, R.; ABREU, S.L.; TIEPOLO, S.M.; PEREIRA, S.V.; SOUZA, J.G. **Atlas brasileiro de energia solar**. 2.ed. São José dos Campos: INPE, 2017.

PEREIRA, R.W.L. **Economia de energia na perspectiva do plano nacional de energia 2030:** o papel do aquecimento solar. 2010, 231 f. Dissertação (Mestrado em Desenvolvimento Sustentável) – Centro de Desenvolvimento Sustentável, Universidade de Brasília, Brasília, 2010.

PINHO, J.T.; GALDINO, M.A. **Manual de engenharia para sistemas fotovoltaicos**. Rio de Janeiro: CRESESB, 2014.

PODESTÁ, G.P.; NÚÑEZ, L.; VILLANUEVA, C.A.; SKANSI, M.A. Estimating daily solar radiation in the Argentine Pampas. **Agricultural and Forest Meteorology**, v. 123, p. 41-53, 2004.

PRESCOTT, J.A. Evaporation from a water surface in relation to solar radiation. **Transactions of the Royal Society Science Australian**, Adelaide, v.64, p.114-118, 1940.

PRIETO, J.I.; MARTÍNEZ-GARCÍA, J.C.; GARCÍA, D. Correlation between global solar irradiation and air temperature in Asturias, Spain. **Solar Energy**, v. 83, p. 1076–1085, 2009.

RIBEIRO, W. C. Impacto das mudanças climáticas em cidades no Brasil. **Parcerias Estratégicas**, Brasília, n. 27, p. 297-321, dez. 2008.

RICHARDSON, C.W. Weather simulation for crop management models. **Transactions of the American Society of Agricultural Engineers**, v. 28, n. 5, p. 1602-1606, 1985.

RÜTHER, R.; KNOB, P.J.; JARDIM, C.S.; REBECHI, S.H. Potential of building integrated photovoltaic solar energy generators in assisting daytime peaking feeders in urban areas in Brazil. **Energy Conversion & Management**, v. 49, p. 1074-1079, 2008.

RÜTHER, R.; SALAMONI, I. O potencial dos setores urbanos brasileiros para a geração de energia solar fotovoltaica de forma integrada às edificações. **Fórum Patrimônio,** Belo Horizonte, v. 4, n. 2, p. 84-94, 2011.

RÜTHER, R; ZILLES, R. Making the case for grid-connected photovoltaics in Brazil. **Energy policy,** v. 39, n. 3, p. 1027-1030, 2011.

SALAMONI, I.; DOS SANTOS, I.; ZOMERO, C.; RÜTHER, R. Estudo do potencial de contribuição da energia solar fotovoltaica integrada a prédios públicos e interligada à rede elétrica na Região Sul do Brasil em períodos quentes. In: Encontro Nacional de Tecnologia do Ambiente Construído, 15, 2014, Maceió. **Anais...** Maceió, 2014.

SANTOS, E.C.M. dos. **Viabilidade técnica e econômica do uso da energia solar térmica em condominios horizontais com habitações populares.** 2015, 96 f. Dissertação (Mestrado em Engenharia Mecânica) – Faculdade de Engenharia, Universidade Estadual Paulista, Guaratinguetá, 2015.

SANTOS, G.H.S.S. **Análise numérica de um sistema integrado coletor solar/armazenador térmico.** 2007, 138 f. Dissertação (Mestrado em Engenharia Mecânica) – Faculdade de Engenharia, Universidade Estadual Paulista, Bauru, 2007.

SIEBERT, C. 2012. Resiliência urbana: planejando as cidades para conviver com fenômenos climáticos extremos. In: Encontro Nacional da Associação Nacional de Pós-Graduação e Pesquisa em Ambiente e Sociedade, 06, 2012, Belém. **Anais...** Belém, 2008.

SILVA, C.R.; SILVA, V.J.; ALVES JÚNIOR, J.; CARVALHO, H.P. Radiação solar estimada com base na temperatura do ar para três regiões de Minas Gerais. **Revista Brasileira de Engenharia Agrícola e Ambiental**, Campina Grande, v. 16, n. 3, p. 281–288, 2012.

SILVA, V.J.; SILVA, C.R.; FINZI, R.R.; DIAS, N.S. Métodos para estimar radiação solar na região noroeste de Minas Gerais. **Ciência Rural**, Santa Maria, v.42, n.2, p.276-282, fev, 2012.

SILVA, W. L.; DERECZYNSKI, C.; CHANG, M.; FREITAS, M.; MACHADO, B. J.; TRISTÃO, L.; RUGGERI, J. Tendências observadas em indicadores de extremos climáticos de temperatura e precipitação no Estado do Paraná. **Revista Brasileira de Meteorologia**, v.30, n.2, p. 181-194, 2015.

SINGH, R.; BANERJEE, R. Estimation of rooftop solar photovoltaic potential of a city. **Solar Energy**, v. 115, p. 589-602, 2015.

SINIGAGLIA, T.; SEIBOTH, T.R.; MICHELS, A.; LOVATO, A.; JAHN, S.L. Dimensionamento da produção energética de um coletor solar plano para aquecimento de água. **Revista GEINTEC**, v. 6, n. 4, p.3487-3498, 2016.

SUPIT, I.; VAN KAPPEL, R.R. A simple method to estimate global radiation. **Solar Energy**, v. 63, n. 3, p. 147-160, sep. 1998.

TIEPOLO, G.M.; URBANETZ JUNIOR, J.; CANCIGLIERI JUNIOR, O.; VIANA, T. Photovoltaic generation potential of Paraná State, Brazil – a comparative analysis with European countries. **Energy Procedia**, v. 57, p. 725-734, 2014.

TIEPOLO, G.M.; URBANETZ JUNIOR, J.; PEREIRA, E.B.; PEREIRA, S.V.; ALVES, A.R. Comparação do potencial fotovoltaico do Estado do Paraná com outros Estados e Europa – Resultados parciais. In: Congresso Brasileiro de Energia Solar, 6, 2016, Belo Horizonte. **Anais...** Belo Horizonte, 2016.

URBANETZ, J.; ZOMER, C.D.; RÜTHER, R. Compromises between form and function in grid-connected, building-integrated photovoltaics (BIPV) at low-latitude sites. **Building and Environment,** v. 46, p. 2107-2113, 2011.

VERA, L. H. **Programa computacional para dimensionamento e simulação de sistemas fotovoltaicos autônomos.** 2004, 189 f. Dissertação (Mestrado em Engenharia Mecânica) – Universidade Federal do Rio Grande do Sul, Porto Alegre, 2004.

VIRGENS FILHO, J.S.; OLIVEIRA, R.B.; LEITE, M.L.; TSUKAHARA, R.Y. Desempenho dos modelos CLIGEN, LARS-WG e PGECLIMA_R na simulação de

séries diárias de temperatura máxima do ar para localidades do estado do Paraná. **Engenharia Agrícola**, Jaboticabal, v. 33, n. 3, p. 538-547, maio/jun. 2013.

WEISS, A. HAYS, C.J. Simulation of daily solar irradiance. **Agricultural and Forest meteorology**, v.123, p.187-199, 2004.

WREGE, M.S.; STEINMETZ, S.; REISSER JÚNIOR, C.; ALMEIDA, I.R. **Atlas climático da região Sul do Brasil**: Estados do Paraná, Santa Catarina e Rio Grande do Sul. Brasília: EMBRAPA, 2012.

YANG, K.; KOIKE, T.; YE, B. Improving estimation of hourly, daily, and monthly solar radiation by importing global data sets. **Agricultural and Forest Meteorology**, v. 137, p. 43–55, 2006.

ZIREBWA, F.S.; KAPENZI, A.; MAKUVARO, V.; SAMMIE, B.; MADANZI, T. An evaluation of the performances and subsequent calibration of three solar radiation estimation models for semi arid climates in Mildlands Zimbabwe. **Midlands State University Journal of Science, Agriculture and Technology**, Special Edition, p. 44-55, 2015.